

**TWO-DIMENSIONAL POLYANILINE NANOSTRUCTURES FOR THE
DEVELOPMENT OF ULTRASENSITIVE FLEXIBLE BIOSENSORS**

by

Pei Liu

B.S. in Material Physics, Nanjing University, 2011

Submitted to the Graduate Faculty of
The Swanson School of Engineering in partial fulfillment
of the requirements for the degree of
Doctor of Philosophy

University of Pittsburgh

2017

UNIVERSITY OF PITTSBURGH
SWANSON SCHOOL OF ENGINEERING

This dissertation was presented

by

Pei Liu

It was defended on

July 10th, 2017

and approved by

William Stanchina, Ph.D., Professor
Department of Electrical and Computer Engineering

Kevin Chen, Ph.D., Professor
Department of Electrical and Computer Engineering

Zhihong Mao, Ph.D., Associate Professor
Department of Electrical and Computer Engineering

Sung Kwon Cho, Ph.D., Associate Professor
Department of Mechanical Engineering & Materials Science

Dissertation Director: Minhee Yun, Ph.D., Associate Professor
Department of Electrical and Computer Engineering

Copyright © by Pei Liu

2017

TWO-DIMENSIONAL POLYANILINE NANOSTRUCTURES FOR THE DEVELOPMENT OF ULTRASENSITIVE FLEXIBLE BIOSENSORS

Pei Liu, PhD

University of Pittsburgh, 2017

The demand for ultrasensitive, inexpensive and wearable biosensors is always strong due to the increasing healthcare related concerns. In this work, field-effect-transistor (FET) biosensors based on two-dimensional (2-D) polyaniline (PANI) nanostructures were developed on both nonflexible (SiO_2) and flexible substrates (polyethylene terephthalate and polyimide). The biosensor devices were fabricated through a facile and inexpensive method that combines top-down and bottom-up processes. A low-temperature bilayer process was developed that vastly improved the yield of flexible devices. The chemically synthesized PANI nanostructures showed excellent p-type semiconductor properties as well as good compatibility with flexible designs. With the 2-D PANI nanostructure being as thin as 80 nm and its extremely large surface-area-to-volume (SA/V) ratio due to the intrinsic properties of PANI chemical synthesis, the developed biosensors exhibited outstanding sensing performance in detecting B-type natriuretic peptide (BNP) biomarkers. Excellent reproducibility, and high specificity with the limit of detection as low as 100 pg/mL were achieved for both designs. PANI nanostructure under bending condition was also investigated and showed controllable conductance changes being less than 20% with good restorability which may open up the possibility for wearable applications.

In addition, a facile and template-free method is demonstrated to synthesize a new two-dimensional thin film structure: PANI film/nanotubes hybrid. The hybrid is a 100 nm thick PANI film embedded with PANI nanotubes. This well controlled method requires no surfactant or

organic acid as well as relatively low concentration of reagents. Synthesis condition studies reveal that aniline oligomers with certain structures are responsible for guiding the growth of the nanotubes. Electrical characterization also indicates that the hybrid nanostructure possesses similar FET characteristics to bare PANI film. With its 20% increased SA/V ratio contributed by surface embedded nanotubes and the excellent p-type semiconducting characteristic, PANI film/nanotubes hybrid shows clear superiority compared with bare PANI film. Such advantages guarantee the hybrid a promising future towards the development of ultra-high sensitivity and low cost biosensors.

TABLE OF CONTENTS

TABLE OF CONTENTS	VI
LIST OF TABLES	X
LIST OF FIGURES	XI
PREFACE.....	XV
1.0 INTRODUCTION.....	1
1.1 BIOSENSORS.....	2
1.1.1 Biosensor and its Categories	2
1.1.2 FET Biosensor Working Principle	7
1.1.3 Recent Progress in Flexible Sensors.....	10
1.2 FLEXIBLE SUBSTRATES	12
1.2.1 General Requirements for Flexible Substrates	12
1.2.2 PET & PEN	14
1.2.3 PI	16
1.2.4 PDMS	18
1.2.5 Other Flexible Substrates	19
1.3 CONDUCTIVE POLYMER AND POLYANILINE.....	20
1.3.1 Conductive Polymer	20
1.3.2 Polyaniline (PANI).....	21

1.3.3	Synthesis of PANI	23
1.3.4	PANI Nanostructures	25
2.0	BIOMOLECULES IMMOBILIZATION	27
2.1	IMMOBILIZATION METHODS	27
2.1.1	Physical Absorption.....	27
2.1.2	Entrapment	28
2.1.3	Covalent Attachment.....	28
2.2	IMMOBILIZATION ON PANI.....	29
2.2.1	Immobilization of Antibodies and Enzymes on PANI	29
2.2.2	Immobilization of PNAs and Aptamers on PANI.....	31
2.2.3	Prevent Nonspecific Absorption.....	33
3.0	DEVELOPMENT OF 2-D PANI BIOSENSORS ON SILICON OXIDE SUBSTRATE.....	34
3.1	INTRODUCTION	34
3.2	EXPERIMENTAL.....	36
3.2.1	Chemicals	36
3.2.2	Development of 2-D PANI Layers.....	37
3.2.3	Surface Functionalization of PANI.....	42
3.2.4	Integration of Microfluidic Channels	42
3.3	RESULTS AND DISCUSSION.....	44
3.3.1	Surface Morphology Study of 2-D PANI Layers.....	44
3.3.2	PANI FET Measurement	45
3.3.3	Fluorescence Test of Functionalized PANI	46

3.3.4	BNP Biomarker Detections.....	47
3.3.5	Debye Length Investigation	49
3.3.6	Sensing Performances Using PANI in Different Oxidation States.....	50
3.4	CONCLUSIONS	51
4.0	DEVELOPMENT OF 2-D PANI BIOSENSORS ON FLEXIBLE SUBSTRATES	
	53	
4.1	INTRODUCTION	53
4.2	EXPERIMENTAL.....	54
4.2.1	Chemicals	55
4.2.2	Optimization of Electrodes Patterning on PET Substrates	55
4.2.3	Patterning of 2-D PANI Layers	59
4.2.4	Preparation and Optimization of PI Substrates	59
4.2.5	Surface Functionalization of PANI.....	63
4.2.6	Integration of Microfluidic Channels	63
4.3	RESULTS AND DISCUSSION	64
4.3.1	Surface Morphology Study of 2-D PANI Layers on Flexible Substrates ..	65
4.3.2	Electrical Characteristics of Bendable 2-D PANI Layers.....	68
4.3.3	Fluorescence Tests of Functionalized PANI.....	70
4.3.4	BNP Biomarker Detections.....	71
4.4	CONCLUSIONS	76
5.0	DEVELOPMENT OF PANI FILM/NANOTUBES HYBRID	
	NANOSTRUCTURES	78
5.1	INTRODUCTION	78

5.2	EXPERIMENTAL.....	80
5.2.1	Chemical and Substrates Preparation.....	80
5.2.2	Synthesis Method.....	81
5.3	RESULTS AND DISCUSSION.....	82
5.3.1	Characterization of PANI Nanotubes.....	82
5.3.2	Investigation of Synthesis Time in Step A.....	86
5.3.3	Importance of Protonated Aniline.....	89
5.3.4	Synthesis of the PANI Film/Nanotubes Hybrid Nanostructures on Substrates.....	91
5.3.5	PANI Film/Nanotubes Hybrid FET.....	93
5.3.6	Quantitatively Evaluating SA/V Ratio of the Hybrid Nanostructure.....	94
5.3.7	FET Characterizations.....	98
5.4	CONCLUSIONS.....	100
6.0	SUMMARY.....	101
6.1	LIST OF PUBLICATIONS.....	102
7.0	FUTURE WORK.....	104
	BIBLIOGRAPHY.....	106

LIST OF TABLES

Table 1. Physical and chemical properties of PET (Melinex) and PEN (Teonex).	15
Table 2. Physical and chemical properties of PI (Kapton).	17

LIST OF FIGURES

Figure 1. Illustration of the gating effect of FET biosensor.	8
Figure 2. Illustration of PANI FET biosensor working in different ion strength environments. The Debye length corresponding to PBS 1X, PBS 0.1X and PBS 0.01X are 0.7 nm, 2.3 nm and 7.3 nm.....	9
Figure 3. (a) Molecule structure of PANI. (b) Hopping mechanism in PANI.....	22
Figure 4. Reaction mechanism of using EDC and NHS to covalently bind an antibody on PANI film.....	30
Figure 5. Reaction mechanism of using Glu as cross-linker to covalently bind an antibody on PANI film.....	31
Figure 6. Reaction mechanism of using Glu as cross-linker to covalently bind a PNA on PANI film.....	32
Figure 7. Reaction mechanism of cross-link a PNA on PANI film with fluorescent unit.....	33
Figure 8. Illustration of the fabrication processes to develop PANI FETs.....	37
Figure 9. The chemical reactions of PANI synthesis.....	38
Figure 10. Estimation of PANI film thickness and oxidation state over synthesis time.	40
Figure 11. Microscope images of PANI film synthesized under the same conditions with different synthesis time: 1.5 hours (top), over 4 hours (bottom).	41
Figure 12. (a) Illustration of microfluidic design and microfluidic integration. (b) Image of a biosensor device with microfluidic integrated.....	43
Figure 13. (a) SEM image of PANI surface. (b) High magnification AFM image of PANI surface.	44
Figure 14. FET measurement of PANI film. V_d was fixed at different value from 0 to 0.4V while sweeping V_g from 1.0V to -2.5V.	45

Figure 15. Fluorescent test of functionalized PANI.	47
Figure 16. Testing system including a potentiostat, syringe pump, test circuit, multiple inlets and a power supply.	47
Figure 17. Sensing results with nonspecific targets (IgG and BSA) and different concentration of BNP biomarkers.....	49
Figure 18. BNP biomarker detections performed under different buffer concentration (Debye Length).....	50
Figure 19. BNP biomarker detections performed with PANI films in different oxidation states.	51
Figure 20. Electrodes patterned on PET substrate. (a) Au/PET (b) Au/Ti/PET (c) Au/Cr/PET. .	57
Figure 21. Optimization of electrodes patterning with bilayer structure. (a) Illustration of the bilayer process. (b) Microscope image of bilayer developed electrodes on PET substrate.	58
Figure 22. Molecular structure of poly(amic acid) and the imidization mechanism.	60
Figure 23. (a) Single layer PI flexible devices before debonding. (b) Single layer PI flexible devices after debonding.	61
Figure 24. Three-layer PI flexible devices with sufficient mechanical strength after debonding. .	62
Figure 25. Integration of a microfluidic to the device. (a) The microfluidic channel is located right on top of a 2-D PANI nanostructure array. (b) A microfluidic integrated PET biosensor. (c) A microfluidic integrated PI biosensor. The device shows good flexibility due to the flexible nature of PET, PI and PDMS.....	64
Figure 26. Different dimensions of 2-D PANI films on PET substrate.....	65
Figure 27. PANI surface characterizations. (a) An SEM image of the 2-D PANI nanostructure surface. The PANI surface was formed by nanogranular structures. (b) AFM result that shows the detail surface morphology of the 2-D PANI nanostructure. The average diameter of the nanogranular structures is around 100nm which dramatically increases the surface area by over 50% compared with flat surface	66
Figure 28. (a) 3D view of AFM results of clean PET and silicon oxide surface. (b) Illustration on how surface roughness increases the sensitivity of the PANI FET biosensor.	67
Figure 29. Device resistance measurements under bending conditions. (a) Illustration of the bending test sequence: first, the device was fixed at the edge of a step and measured under no bending condition; then the device was bent and measured with the bending radius around 5cm and 1cm, respectively; finally the device was released from bending. (b) V_d - I_d responses corresponding to four bending condition. V_g was fixed at 0V, and I_d was obtained by sweeping V_d from 0V to 0.4V. The current changes were small and	

proportional to the bending degree. This result proves the good compatibility of 2-D PANI nanostructure with flexible designs	68
Figure 30. Fluorescent images taken by optical microscope under same exposure conditions. (a) Functionalized area using the correct filter, clear green light corresponding to the fluorescent wavelength was observed. (b) Functionalized area using the control filter, no notable fluorescent light observed (c) Unfunctionalized area using the correct filter, no notable fluorescent light observed	71
Figure 31. Device biomarker sensing results using PI (a) and PET (b). Biomarker and specificity test result of a 2-D PANI nanostructure on detection different concentration level of BNP among nonspecific targets (BSA and IgG). PBS buffer solutions that contained high concentration of BSA and IgG showed similar current responses as the PBS background sample. The drain current increased distinctly as sample solutions contained different concentrations of BNP were pumped in. The current changes were consistent with different BNP concentrations.....	73
Figure 32. BNP biomarker statistic test results of 15 2-D PANI nanostructure biosensor devices. All devices showed current increase over the increase of BNP concentration. Useful information such as sensitivity can be extracted from these figures.	74
Figure 33. Illustration of the two-step synthesis process. Step A reaction has a starting pH of 7, while the pH in Step B reaction starts below 1.	81
Figure 34. SEM and TEM images of aniline oligomers and PANI nanotubes grown on gold substrate. (a) SEM image of flake-like aniline oligomers formed in Step A. (b) SEM image of PANI nanotubes with a diameter of 300 nm formed after Step B. (c) TEM image of stripped-off PANI nanotube with inner diameter of 200 nm.....	83
Figure 35. SEM images of PANI nanotubes synthesized in acetic acid (a & b) and perchloric acid (c & d).	85
Figure 36. Optical images of synthesis condition optimization results. (a) 10 min in Step A. Small flake-like oligomers were formed. (b) 30 min in Step A. The density and size of oligomers were getting larger. Some oligomers started to evolve into clusters. (c) 1 hour in Step A. The density and size of oligomers kept increasing and reached to maximum. (d) 4 hours in Step A. All oligomers existed in the form of clusters. (e) 10 min in Step A and 4 hours in Step B. No nanotubes sighted. (f) 30 min in Step A and 4 hours in Step B. Some nanotube was found. (g) 1 hour in Step A and 4 hours in Step B. High density of nanotubes were observed (h) 4 hours in Step A and 4 hours in Step B. No nanotube was found.	86
Figure 37. SEM images of the sample with 4 hours of Step A before and after Step B. (a) Oligomer clusters before Step B. (b) PANI film covered oligomer clusters after Step B.	89
Figure 38. SEM image of the sample after 4 hours of Step A reaction with pH tuned after 1 hour.	90

Figure 39. Optical images of PANI film/nanotubes hybrid on different of substrates. (a) PET after Step A, most oligomers grew vertically to the surface. (b) SiO ₂ after Step A, half of oligomers were vertical while the other half were parallel to the surface. (c) HF-dipped SiO ₂ after Step A, all oligomers were parallel to the surface. (d) PET after Step A and Step B, nanotubes were found. (e) SiO ₂ after Step A and Step B, less density of nanotubes were found compared with it on PET. (f) HF-dipped after Step A and Step B, no nanotube was found.	91
Figure 40. Optical and AFM images of PANI film/nanotubes hybrid FET and bare film FET. (a) Hybrid FET. (b) Bare film FET. (c) Surface topography of the hybrid. (d) High magnification of bare film surface measured by AFM. (e) High magnification of the dark area in (c).	94
Figure 41. (a) TEM picture of a PANI nanotube. (b) Simplified structure of nanotubes and thin film. (c) Cross section view of the hybrid structure.....	95
Figure 42. FET characterization of the hybrid FET (a) and bare film FET (b). The I_d - V_g characteristic was obtained by sweeping V_g from 0 to -4 V while keeping V_d staying at different potential level from 0 to 0.4 V.	98
Figure 43. Preliminary design of microfluidic integrated PANI/QLED biosensor.	104

PREFACE

First, I would like to express my sincere gratitude to my advisor, Professor Minhee Yun, for offering me this great study and research opportunity in University of Pittsburgh. His insightful advices and continuous supports have truly motivated me to become a capable and experienced researcher. Personally, I am also extremely grateful to Professor Yun, without whom, my wife and I could not reunite in the United States.

Second, I want to thank my dissertation committee members: Professor William Stanchina, Professor Zhihong Mao, Professor Kevin Chen and Professor Sung Kwon Cho, for their continued supports and valuable suggestions. I would also like to thank my colleagues: Jiyong Huang, Donald Volland and Jorge Torres. It was my privilege and pleasure to work with them.

Finally, I would like to thank my parents and family for their unconditional supports and love. A special thanks to my wife, Yisi, for her optimistic personality and exceptional cooking skills. Accompanied by her, I never feel lonely.

1.0 INTRODUCTION

Flexible electronics, also known as flexible circuits, describes circuits that are able to bend or stretch without losing their functions. This feature can enable significant versatility in designs and applications as well as offer advantages such as low cost and large area compatibility. From the last decade, extensive efforts from both industries and research institutions have been done to design and create new flexible and bendable devices. With the advances in thin-film materials being complemented with the development of new integration processes, the combination of flexible substrates with wafer-scale processes has been achieved. Thus, flexible electronics has recently become a rapidly emerging field that attracts researchers from both science and industry. In the past few years, flexible thin film transistors (TFTs) and circuits have been widely reported.¹⁻⁵ Numerous efforts have also been made in fields such as flexible displays⁶⁻⁸ and photovoltaic.⁹

Addressing basic questions such as early diagnoses and novel therapies has always been of great significance in current healthcare research. Flexibility in electrical materials is also highly desired in medical and bioengineering, not only for its low cost and excellent biocompatibility, but also because of the fact that living organisms are naturally malleable and flexible. Therefore, flexible designs in health care such as biosensors are preferred to achieve integration into human body or being worn without causing any discomfort. Recently, electronics integrated into human bodies have been reported to continuously monitor physiological indexes

such as skin temperature, blood pressure and heart rate.¹⁰⁻¹³ However, flexible immunoassay based biosensor designed is seldom reported. With such motivation in mind, this thesis focuses on the development and optimization of flexible immunoassay based biosensors.

In this chapter, different types of biosensors that are categorized by their sensing mechanisms, and the recent progress in flexible sensors are reviewed firstly. Physical and chemical properties of several possible flexible substrates candidates are then introduced. Last but not least, the reviews of the synthesis methods and nanostructures of polyaniline (PANI) are presented.

1.1 BIOSENSORS

1.1.1 Biosensor and its Categories

Biosensors are analytical devices that are able to perform specific quantitative or semi-quantitative analysis based on a biological recognition element and a transduction element. Therefore, a typical biosensor consists of two main components: a bioreceptor and a transducer. The function of a bioreceptor is to recognize and immobilize certain target while a transducer converts this binding event into measurable signal. According to this working principle, many of the performance characteristics of a biosensor such as sensitivity, detection limit and signal stability are directly determined by the transduction efficiency provided by the transducer. Therefore, biosensors are generally categorized by types of transducers. Three most representative types are introduced in this section.

Optical Transducer

The principle of optical detection is to measure the changes of a certain optical property when light wave interacts with nanomaterials. The sensing performance is highly dependent on the optical phenomena being utilized and the optical property being measured. Surface plasmon resonance (SPR) is so far one of the most successful optical detection methods. When light illuminates on thin metal film, at certain condition, the collective oscillation of surface electrons, which is named as surface plasmon waves (SPW), can be excited.¹⁴ SPR detection monitors resonant angle or wavelength shift when surface property is altered due to the target bindings. Limits of detection at about 25 ng/mL and a dynamic range of 2 logs were achieved with the most recent method.¹⁵ However, SPR usually has poor resolution and specificity because of bulk solution interference and lacks of sensitivity when monitoring targets with low molecule weight.

An improvement for SPR was brought up and developed during recent years which takes advantage of a unique SPW that only exists when light interacts with a metal nanoparticle. This confined plasmon oscillation is known as localized surface plasmon resonance (LSPR). LSPR sensors based on this principle are sensitive to the surface environment of metal nanoparticles when their local refractive index changes.¹⁶ With the electrical field around the nanoparticle surface being enhanced by LSPR, local refractive index changes caused by biomarker molecule recognition can trigger changes in the extinction spectra of the incident light. So far, many LSPR nanosensors were demonstrated and a multi-arrayed LSPR biochip with detection limits of 100 pg/mL have been reported.¹⁷

Surface-enhanced Raman scattering (SERS) is another optical detection method that can achieve single molecule detection due to large Raman scattering enhancement factors ($\sim 10^{10}$) generated by metal or core-shell nanoparticles. Works by Nie *et al.* have demonstrated SERS in field of nanotechnology.¹⁸ Utilizations of SERS for vivo cancer detection were also reported.^{19, 20}

A major obstacle of optical transducer based biosensors is system miniaturization since they generally require sophisticated instruments and large volume to create space for necessary light paths. Also, no position changing or device deformation is tolerable while conducting tests. These shortcomings limit their applications in flexible and wearable biosensor designs.

Mechanical Transducer

The principle of mechanical detection is based on the ultrasensitive detection of extremely small mechanical forces existed on the molecular scale. The mass resolution of mechanical devices tremendously increases as the sizes of mechanical sensors decrease to the nanoscale since mass resolution is proportional to the total mass of the device. This feature grants nanomechanical sensors the ability of measuring molecular scale transport and affinity as well as forces, displacements and mass changes. So far, both detections of biomolecules in vacuum²¹ and in fluid²² have been demonstrated.

The most commonly used device design in mechanical nanosensors is the microcantilever. The displacement can be measured by using two responses generated by the cantilever when the analyte molecules bind with the immobilized receptors on the surface of a cantilever. First, the targets/receptors association or dissociation creates shifts of the cantilever resonance frequency. Second, surface stress by target molecules binding also physically bends the cantilever. The quantitative measurements of resonance frequency shifts and bending can be achieved with the help of established techniques such as optical beam deflection, piezoelectricity and capacitance.²³ Biomarker molecule detection in fluid has been reported with suspended cantilever resonators, because particles can be weighed in real time as they flow through the channel.²² However, detection in fluid, which is an ideal condition for biomolecular, is still a

major challenge for mechanical nanosensors. The sensitivity and specificity of the mechanical sensors are greatly reduced due to the viscous damping in fluid.

Mechanical nanosensors so far are still limited for clinical applications and flexible design. The sensing components are extremely delicate, thus cannot survive from any deformation when fabricated on flexible substrates. And the sensitivity and selectivity of nanomechanical sensors are highly dependent on the uniformity of cantilevers as well as surface functionalization efficiency. In addition, high cost instruments are required for efficient mechanical sensing.

Electrical Transducer

Detection using electrical transducer is a rapidly emerging field due to the development of simple and low-cost fabrication techniques. Electrical nanosensors such as field-effect transistors (FETs) based nanosensors can achieve simple and real-time measurements as well as portability. FET-based electrochemical nanosensors measure the change in conductance or resistance yielded when the target molecule binds to the receptor with the utilization of nanowires, nanoribbons, and nanotubes.^{24, 25}

Silicon nanowires are commonly utilized for FET nanosensors because of their high sensitivity and excellent semiconductor properties. Lieber *et al.* demonstrated the first use of Si nanowires for direct, real-time and sensitive detection in aqueous solution in 2001.²⁶ This proof-of-concept Si nanowire FET sensor has performed the detection of protein concentrations as low as 10 pM.^{27, 28} Zheng *et al.* developed a Si nanowire FET based multiplexed electrochemical biosensor.²⁸ The nanowire arrays of about 200 individual sensors are functionalized to detect multiple protein biomarkers in undiluted serum. When the binding events take place, the conductance change of one specific nanowire is detected. Both arrays of p-type and n-type Si

nanowires were employed to distinguish protein binding signals from noise and reduce false-positive signals. This was the first demonstrated high sensitive Si nanowire arrays based electrical nanosensors.

Carbon nanomaterials such as carbon nanotubes (CNTs) have also been utilized for FET nanosensors.²⁴ High sensitivity (\sim pM) has been reported using CNTs for DNA detection.²⁹ Cai *et al.* developed a CNTs array with a molecular imprinted polymer (polyphenol) coating on the CNT tips to detect proteins.³⁰ Specifically, the target protein was first trapped in the polyphenol and then removed, leaving an imprint of the protein on the CNT surface and change the local electrical property. Then this change in permittivity and resistivity in response to protein capture can be measured using electrochemical impedance spectroscopy (EIS). The sensitivity was found to be the highest when target protein was trapped at the CNT tips than other scenarios due to the fast electron transfer along the CNT tip. This method can achieve high specificity due to this confined area, and it can be applied for detecting different conformations of proteins.

A significant limitation of electrochemical biosensors is the incapable of detecting molecules in high salt concentration solutions such as body fluid.^{22, 28} High salt concentration buffers can screen out charges that contribute to signal change, thus affect the sensitivity of biosensors. For instance, a typical nanowire FET requires a salt concentration less than 1 mM to prevent signal screening. One approach to circumvent this signal screening is to lower the salt concentration upstream of the nanosensors. Stern *et al.* developed a microfluidic purification system and demonstrated its feasibility with the detection of two cancer antigens from a whole blood sample with the response time less than 20 minutes.³¹ The decisive component in this device is the purification chip that captures biomarkers from blood and release them back to purified buffer. The detection is then carried out without interference from high salt

concentration. Though progresses have been made, the signal screening still remains a big challenge in electrical biosensor design.

1.1.2 FET Biosensor Working Principle

In past decades, various of electrical-transducer based biosensing architectures have been demonstrated such as amperometric, potentiometric, and field-effect transistor (FET) biosensors. Among them, FET biosensor has become the most intriguing one since it was initially reported in 1970s^{32, 33} due to its ability of offering rapid and sensitive detection of the binding events between the target biological molecules and the receptors on biosensor surface.²⁶ A typical FET configuration contains three components: a drain, a source and a gate. A semiconductor channel is connecting drain and source, in which current can flow and be tuned by the voltage applied on gate. For a traditional metal-oxide-semiconductor field-effect transistor (MOSFET) with an n-channel (p-type semiconductor), the turning on condition is that a large enough positive voltage is applied on the gate which causes electrons to accumulate on the channel surface and form an induced n-type region. This layer is also known as inversion layer. Oppositely, a negative voltage is required to turn on a p-channel (n-type semiconductor) transistor.

Typical FET biosensors usually work in form of ion-selective field-effect transistor (ISFET). A major difference is that ISFET has an ion-selective electrode, an electrolyte solution and a reference electrode.³⁴ The working principle of FET biosensor can be explained by the gating effects (figure 1). For some of the ISFET designs, unlike traditional MOSFET, the semiconductor channel (sensing component) in a FET biosensor works in “accumulation” region, and the “gate voltage” that affects the channel’s conductivity is replaced by the surface charges carried by the target molecules. More specifically, when a p-type sensing component such as

polyaniline (PANI) film is in contact with analyte that contains target molecules, the pre-functionalized bioreceptors on top of PANI surface such as antibodies, enzymes or DNAs can bind with specific target molecules. By presetting the pH of the analyte accordingly to the isoelectric point (PI value) of the target molecules, the bound target molecules can be negatively charged which induces the accumulation of holes on PANI surface. Thus the conductivity of PANI increases which leads to an increase in drain-source current output. Because of the high transduction efficiency of FET and short time for molecule binding, FET biosensor exhibits high sensitivity, low detection limit and fast response.

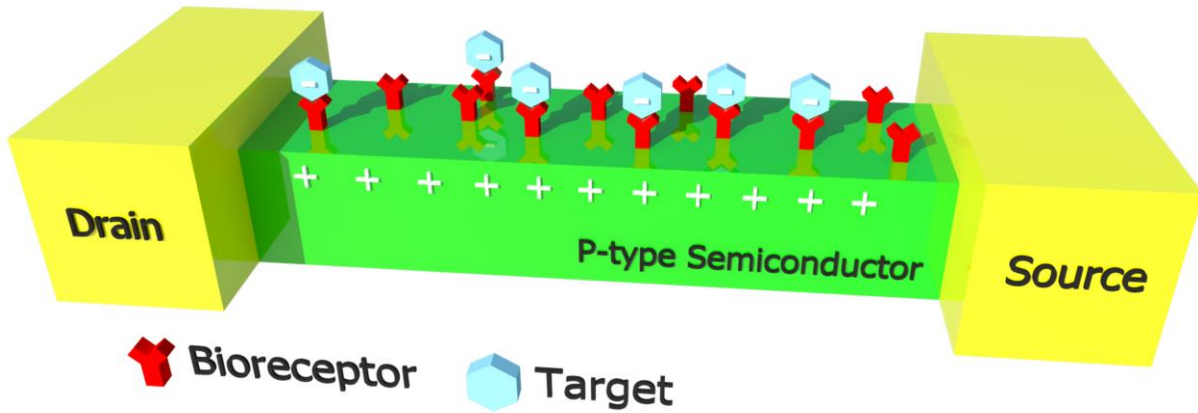


Figure 1. Illustration of the gating effect of FET biosensor.

There are many factors that affect the sensing performance of an FET biosensor. One of the most significant factors is Debye screening³⁵ on a certain length scale, termed as Debye length (λ_D). Debye length characterizes the distance within which charges introduced by the captured molecules on the surface of PANI layer can contribute to the current change while those charges beyond the Debye length will be screened out. For aqueous solutions, λ_D is expressed by the equation:

$$\lambda_D = \sqrt{\frac{\epsilon_0 \epsilon_r k_B T}{\sum \rho_i z_i^2}}$$

ϵ_0 and ϵ_r are the dielectric constant of vacuum and the relative permittivity; k_B and T are the Boltzmann's constant and the temperature in Kelvin; and ρ_i and Z_i are the density and the valence of the i -th ionic species. The equation can be further simplified when at room temperature (25°C):

$$\lambda_D = \frac{2.15 \times 10^{-10}}{\sqrt{I_s}}$$

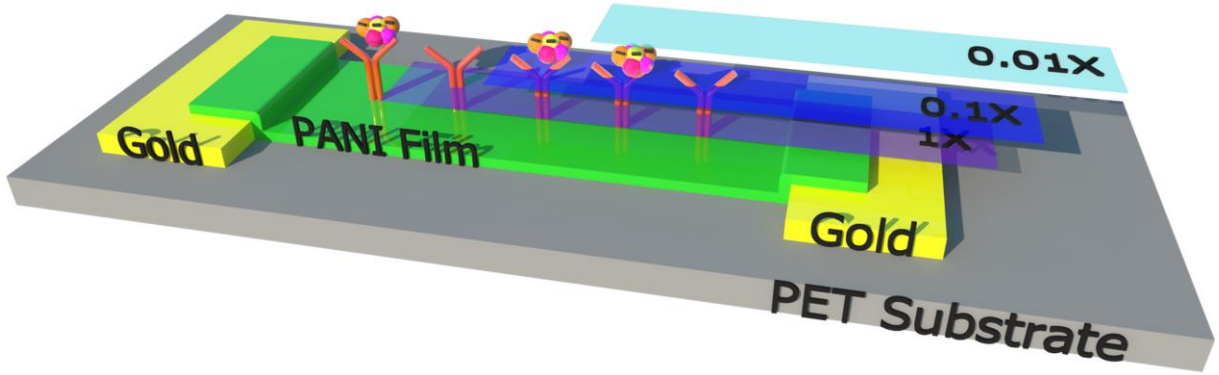


Figure 2. Illustration of PANI FET biosensor working in different ion strength environments. The Debye length corresponding to PBS 1X, PBS 0.1X and PBS 0.01X are 0.7 nm, 2.3 nm and 7.3 nm.

I_s here represents the ionic strength of the solution. Thus, it is evident that biosensor devices working in lower ionic strength environment should have longer Debye length, which has lower detection limit as illustrated in figure 2. This optimal protocol was demonstrated by Stern *et al.*³⁵

Another approach to optimize FET biosensor sensing performance is by tuning the potential on the reference electrode. According to Gao *et al.*,³⁶ optimal sensitivity for nanowire FET biosensor can be obtained by making the nanowire to work in subthreshold regime. Though the general current signals detected are getting weaker due to the subthreshold depletion, the ratio of current signal change over current ($\Delta I/I$) is greatly enhanced. Therefore, the sensitivity and resolution are significantly improved. This phenomenon can be explained by the Debye length of semiconductor which is also known as Thomas-Fermi screening length:

$$\lambda_d = \sqrt{\frac{\epsilon K_B T}{q^2 N_d}}$$

Where ϵ is the dielectric constant, K_B is the Boltzmann's constant, T is the temperature, q is the elementary charge, and N_d is the density of dopants. Thomas-Fermi screening length characterizes the penetration depth of the electrical field that is generated by the surface charges. And the higher portion of semiconductor that is affected by the surface charges, the higher sensitivity it can achieve. When a device is working under subthreshold regime, a smaller N_d gives a relatively larger λ_d , thus enhances the sensitivity.

1.1.3 Recent Progress in Flexible Sensors

Flexible designs always require devices to be tolerable for physical deformations such as rolling, folding or stretching. More advanced designs for wearable applications also need devices to be as small as possible in terms of both size and weight. Sensors based on mechanical transducers can be small and light, since device sensitivity is inverse proportional to its size. However, the mechanical nanosensors are vulnerable to even a tiny shape change. Optical sensors usually

require sophisticated instruments and large volume to create enough space for light paths thus are difficult to be miniaturized. Therefore, up to now, most flexible or wearable sensors are designed based on electrical transducers.

In 2006, Kudo *et al.* developed a flexible and wearable glucose sensor based on functional polymer.³⁷ Hydrophilic 2-methacryloyloxyethyl phosphorylcholine (MPC) copolymerized with dodecyl methacrylate (DMA) was utilized as the sensing material and hydrophobic polydimethyl siloxane (PDMS) was used as substrate. The device was able to detect glucose level over a range of 0.06-2.00 mmol/L and it was also capable to work when released after being expanded to 120% longer than the normal length which shows great flexibility and stretch ability. In the subsequent work, the flexible glucose sensor was used to detect rabbit tear glucose by direct attaching the device on the rabbit eye.³⁸ The device was sufficiently stable and sensitive as well as harmless to the subject.

Park and co-workers demonstrated an ultrasensitive flexible FET olfactory system in the year of 2012.³⁹ The electrodes were fabricated on polyethylene terephthalate (PET) substrate and both oxygen (p-type) and ammonia (n-type) plasma treated bilayer graphene were used as the semiconductor sensing components. Minimum detection limit of 0.04 fM for amyl butyrate (AB) was achieved with the signal-to-noise ratio of 4.2. The bending and relaxing test showed that the device can maintain the same detection limit after 100 bending/relaxing cycles due to its great flexibility.

Advanced wearable sensor designs require highly integration and flexibility from the whole system including sensing and data acquisition components. In 2014, Xu et al. developed a soft microfluidic assembly of sensors, circuits and radios for wirelessly physiological monitoring.⁴⁰ The system can be mounted on skin without causing any discomfort. Components

such as sensors, amps, ICs and radios were sealed in elastomeric superstrate and substrate. Microfluidic was then injected into the device, creating free-floating interconnects that can support bending, twisting, and stretching. The whole system was able to expand 100% in two dimensions. Electrocardiography (ECG), electroencephalogram (EEG) and electromyography (EMG) tests were demonstrated and the wirelessly acquired results were verified by wired commercial devices.

1.2 FLEXIBLE SUBSTRATES

In flexible sensor designs, flexible substrates play an essential role in creating basic device mechanical properties such as flexibility and elasticity. Once the substrate is chosen, further device fabrication processes should be optimized to be compatible with the physical and chemical properties of the substrate. In this section, general requirements for flexible substrate selection are explained and several commonly utilized substrates such as polyethylene terephthalate (PET), polyethylene naphthalate (PEN), polyimide (PI) and polydimethylsiloxane (PDMS) are introduced.

1.2.1 General Requirements for Flexible Substrates

Numerous materials are naturally flexible when they are below certain thickness. Nevertheless, not all of them are suitable for flexible electronics applications. Several requirements need to be fulfilled with respect to their applications. Such rules include meeting the basic requirements of mechanical, chemical, thermal, electrical and optical properties:

Mechanical properties – Young’s modulus of the substrate film needs to be low to create necessary flexibility and elasticity. A hard but not brittle surface is also desired in order to support the device under impact.

Chemical properties – The substrate should be inert against fabrication process chemicals and no contaminants should be release from it. Commonly used chemicals are organic solvents such as acetone and isopropyl alcohol (IPA), and alkaline solutions such as developer (mainly TMAH). It is also ideal for substrates to be good barriers against gas permeation.

Thermal properties – For a polymer substrate, the glass transition temperature is one of the most important factors that decides its application scope. The working temperature and the maximum fabrication-process temperature of a substrate need to be compatible with its glass transition temperature. Low coefficient of thermal expansion (CTE) is also highly desirable. Substrate with high CTE will easily expand during heat processes, thus cause thermal mismatch between substrate and device films. It may be of advantage to substrates to be high thermal conductive.

Electrical properties – In most flexible designs especially for electrical sensor applications, the substrates are acting as the insulating layers. Therefore, the materials should possess large volume and surface resistivity. Most polymers meet this requirement. For conductive substrates like metal foil, they may serve as a node or electromagnetic shield.

Optical properties – Optical clear and colorless are imperative for flexible designs in applications such as transmissive displays, bottom emission OLED displays and photovoltaic solar cells.

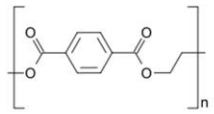
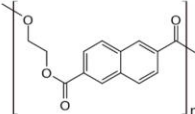
Furthermore, surface roughness is a factor that is worth paying attention to. Larger surface roughness may benefit the adhesion between substrate and the patterns on top. However,

too much roughness can affect the devices' electrical function. Therefore, proper surface roughness is desired. Substrates, whose surface roughness can be physically or chemically modified, show better applicability due to the versatility in designs.

1.2.2 PET & PEN

Polyethylene Terephthalate (PET) and Polyethylene naphthalate (PEN) are commonly used thermoplastic polymer resins from polyester family. PET was first patented in 1941,⁴¹ and has been used for making bottles since 1973. PEN was developed afterwards and was intended to be the replacement of PET. Some of the physical properties of PET and PEN are listed in the table. 1 below.

Table 1. Physical and chemical properties of PET (Melinex) and PEN (Teonex).

	PET (Melinex)	PEN (Teonex)
Molecule structure		
T_g , °C	78	121
CTE (-55 to 85 °C), ppm/°C	15	13
Transmission (400-700 nm), %	89	87
Moisture absorption, %	0.14	0.14
Young's modulus, Gpa	5.3	6.1
Tensile strength, Mpa	225	275
Density, gcm ⁻³	1.4	1.36
Resistivity, Ohmcm	>10 ¹⁴	>10 ¹⁴
Refractive index	1.66	1.5-1.75
Resistance to acids	Good	Good
Resistance to alkalis	Fair	Good

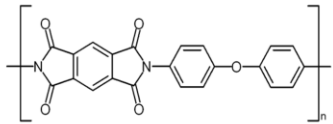
According to table 1, PET and PEN have very similar physical properties. The high transmission in visible spectrum makes them good candidates for photovoltaics,^{42, 43} OLED displays⁴⁴ and flexible transparent electrodes.⁴⁵ Excellent electric insulating property also makes them ideal as substrates for flexible thin film transistor (TFT).⁴⁶ Compared with PET, PEN has much higher glass transition temperature (T_g) which allows it to survive in higher process temperature. The two condensed aromatic rings of PEN also endow PEN with large tensile strength as well as better chemical and hydrolytic resistance. Some of the significant limitations of PET and PEN generated from their thermo properties include limited process temperature

capability, lack of dimensional stability, and observable differences in the linear TCE between the substrate and patterns on top.⁴⁷ A low adhesion with metal also brings additional difficulty in device fabrications. However, despite of these limitations, PET and PEN are still considered as good candidates in both researches and applications due to their low cost in comparison with more thermo stable substrates like thin metal films. In 2004, Nomura *et al.* fabricated a transparent flexible thin-film transistor in room temperature on PET substrate that exhibits excellent FET behavior.⁴⁶ Biosensors fabricated on top of PET have also been reported: Zhang *et al.* demonstrated an ultrasensitive and low-cost graphene sensor based on layer-by-layer nano self-assembly;⁴⁸ Park *et al.* reported an ultrasensitive flexible graphene based FET bioelectronic nose.³⁹

1.2.3 PI

Polyimide (PI) is a polymer of imide monomer. According to the chemical composition of their main chain, PIs can be subdivided into several categories such as aliphatic, aromatic and semi-aromatic. Among them, aromatic polyimides became the most commonly used ones due to their thermo stability since aromatic polyimides were first produced in 1908⁴⁹ and have been in mass production since 1955. A classic commercialized polyimide is named Kapton, which was developed by DuPont in the late 1960s, and has been utilized in flexible printed circuits, displays and even the outside layer of space suits. Some of the properties of Kapton PI are listed below in table 2.

Table 2. Physical and chemical properties of PI (Kapton).

	PI (Kapton)
Molecule structure	
T _g , °C	410
CTE (-55 to 85 °C), ppm/°C	30-60
Transmission (400-700 nm), %	Yellow
Moisture absorption, %	1.8
Young's modulus, Gpa	2.5
Tensile strength, Mpa	231
Density, gcm ⁻³	1.43
Resistivity, Ohmcm	>10 ¹⁷
Refractive index	1.70
Resistance to acids	Good
Resistance to alkalis	Fair

Notably, the key features of Kapton polyimide are the very high glass transition temperature and the ability to sustain stable across a wide range of temperatures from -269 to +400 °C. This feature makes PI capable of being used in some fabrication processes such as low temperature chemical vapor deposition (LTCVD) where other organic flexible films cannot survive. Additional large resistivity and excellent flexibility makes it the ideal substrate for thin-film-transistor. Kapton PI typically shows yellow color due to the absorption of blue light, which limits its applications. To improve this, colorless transparent PI was developed and applied in solar cell applications.⁵⁰

Another superiority of PIs over other polymer films is that they can be easily synthesized in lab and staying on a wafer during the entire fabrication processes. This feature enables the using of CMOS-compatible fabrication processes on PI films as well as brings versatility in PI film designs in terms of film thickness, surface roughness and other physical properties. The synthesis of Kapton PI involves a “ring closure” process in which poly(amic acid), the intermediate, is cured in high temperature. Intermediates for other types of PIs are also commercialized.

1.2.4 PDMS

Polydimethylsiloxane (PDMS) is from a group that is often referred to as silicones. The repeated unit monomer is composed of one oxygen and silicon atom and two methyls. Since microfluidics was first emerged in 1980s, PDMS has become one of the most frequently used materials in microfluidics designs. Same as other polymer flexible substrates, PDMS also has excellent properties such as optical transparency, biocompatibility, gas permeability and electrical insulation.⁵¹ However, unique from polymers like PET or PI, the most amazing characteristic PDMS has is its unusual rheological property. This property grants cured PDMS with mechanically elasticity, which makes it superior in stretchable and wearable electronics applications.^{52, 53}

Similar with PI, PDMS can also been synthesized easily in lab. The most commonly used approach is to mix PDMS base monomer together with PDMS curing agent at the weight ratio of 10:1. The mixture behaves like a viscous liquid which is able to cover the whole surface and mold to any shape if given with enough time. After curing, PDMS becomes elastic solid. This curing method can be utilized to design PDMS with a variety of structures for microfluidics use.

More excitingly, it also allows devices to be built inside the cured or uncured PDMS instead of just on top of it since the curing temperature is only 80 °C. In 2014, Xu *et al.* developed a soft microfluidic assembly of sensors, circuits and radios for wirelessly physiological monitoring. The injected PDMS can provide sufficient flexibility, stretchability as well as protection to the sensing components.⁴⁰ The disadvantage of the cured PDMS is that it lacks of tensile strength when the film is thin.

1.2.5 Other Flexible Substrates

Glass plates, due to its high optical transmittance and similar behaviors as SiO₂ wafer, are commonly used as the substrates for transparent electrodes such as ITO or the control samples for fabrication optimization. Flexibility can be obtained with glass plates when its thickness is reduced to several hundred microns.⁵⁴ Much thinner glass foils (30 µm) can be achieved by the overflow downdraw method, which retains all the advantages of glass plates such as optical transmittance of >90% in the visible region, temperature tolerance of up to 600 °C, high dimensional stability, low coefficient of thermal expansion (CTE), impermeability against oxygen and water, electrical insulation and smooth surface.⁴⁷ However, thin flexible glasses are usually fragile.

Another commonly used inorganic substrate is metal foil such as stainless steel. With the thickness below 125 µm, it possesses good flexibility as well as excellent properties such as temperature tolerance as high as 1000 °C while remaining dimensional stable, perfect permeation barrier against oxygen and moisture, good resistance to corrosion and process chemicals and ability to provide electromagnetic shielding. With the help of these features, stainless steel has long been utilized in flexible solar cells designs.^{55, 56} However, though stainless steel substrates

are more durable than plastic and glass foils, its lacking of electrical resistivity makes it impossible to be a good insulating substrate in flexible electronic applications.

1.3 CONDUCTIVE POLYMER AND POLYANILINE

Polyaniline (PANI) is one outstanding member of conductive polymer family that has acquired numerous attentions from researchers because of its remarkable semiconducting properties. Further excellent chemistry property allows simple biomolecule immobilization which makes PANI an ideal candidate for biosensor applications. The combination of PANI and FET has been reported for cardiac biomarkers detection.⁵⁷ Furthermore, PANI is also one of a few conductive polymers that are capable of forming numerous of nanostructures. In this section, introductions of conductive polymer, PANI as well as chemical synthesis and nanostructures of PANI are provided.

1.3.1 Conductive Polymer

Conductive polymers (CPs) or intrinsically conducting polymers (ICPs) are organic polymers that conduct electricity.⁵⁸ Since doped polyacetylene was first discovered to have large conductivity in 1977,⁵⁹ new exciting applications for ICPs in fields including analytical chemistry and biosensing devices have been opened up. Some widely studied examples of ICPs are polyacetylene (PA), polypyrrole (PPy), polythiophene (PT) and polyaniline (PANI). The reason for ICPs to exhibit exceptional conductivity is that they have single and double bonds alternatively (π -conjugated system) along the molecule chain, which is also responsible for

properties such as low energy optical transitions, low ionization potential and high electron affinity.⁶⁰ From the biochemical perspective, ICPs are known to be compatible with biological molecules as well as suitable for biomolecule entrapment, and their flexible chemical structures also grant ICPs the potential to acquire desired electrical properties via modification. In addition, ICPs are capable of efficiently transferring electrons produced by biochemical reactions. Therefore, with these features, ICPs have been extensively utilized in biochemical sensors in the form of transducers. Some related works are introduced as follows.

Ekanayake and co-workers developed PPy nanotube arrays enzymatic biosensor for detection of glucose.⁶¹ PPy was electro polymerized on a platinum plated nano-porous alumina substrate. This structure was believed to both enhance the adsorption of the enzyme-glucose oxidase and increase surface area for the reaction sensing. A sensitivity of $7.4 \text{ mA cm}^{-2} \text{ M}^{-1}$ for glucose detection was observed. In 2012, Lee *et al.* demonstrated the detection of cardiac biomarkers with single PANI nanowire.⁵⁷ The PANI nanowire was fabricated in a nanochannel between two metal electrodes by electrochemical deposition. Microfluidic channel was integrated to miniaturize the system and enhance the sensing performance. Four different cardiac biomarkers (Myo, cTnI, CK-MB and BNP) were detected with the lowest detection limit at 50 fg/mL.

1.3.2 Polyaniline (PANI)

PANI is an ICP of semi-flexible polymer family, which is known as a mixed oxidation state polymer with both reduced benzoid units and oxidized quinoid units.⁶² Since it was discovered with high electrical conductivity in the early 1980s, PANI has recaptured the attentions of scientific community and researchers are continuously exploring its applications in fields like

biosensors due to a number of useful features such as 1) low cost, 2) direct and easy deposition on the sensor electrode, 3) control of thickness, 4) redox conductivity and polyelectrolyte characteristics, 5) high surface area, 6) chemical specificities, 7) long term environmental stability and 8) tunable properties.⁶³

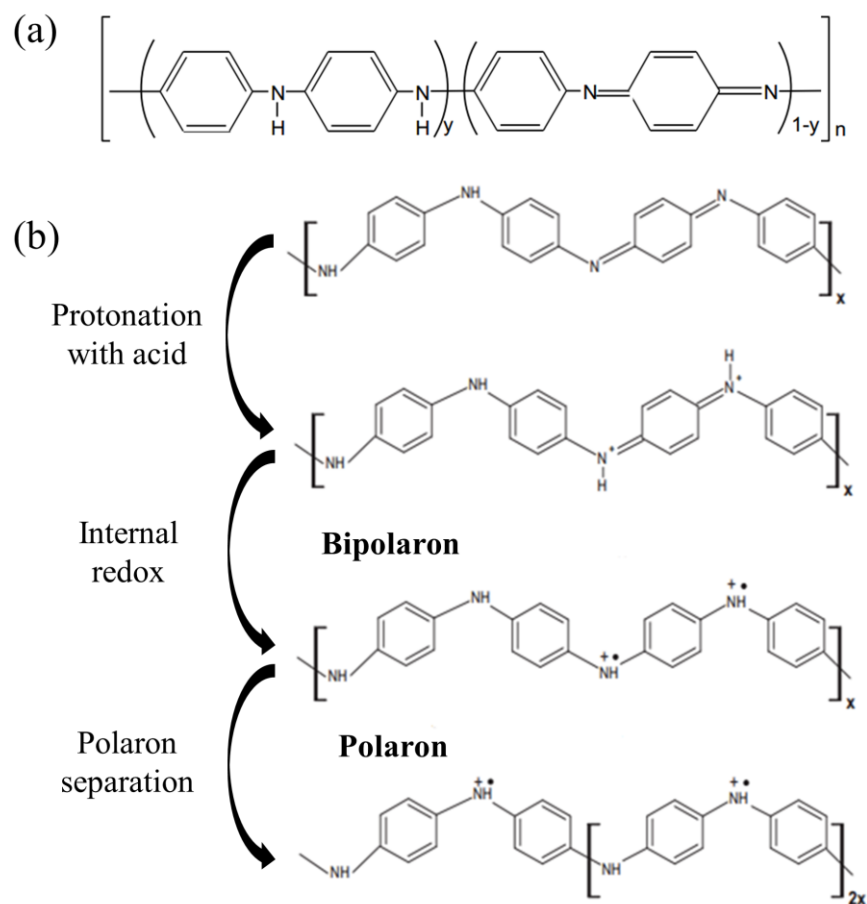


Figure 3. (a) Molecule structure of PANI. (b) Hopping mechanism in PANI.

The molecule structure of PANI is shown in figure 3a, which illustrates three distinct PANI oxidation states.⁶² The three oxidation states are determined by the value of x , and $1-x$ indicates PANI's average oxidation state. When $1-x=0$, PANI exists as the fully reduced form known as leucoemeraldine (LE), whereas when $1-x=1$, PANI stays in its fully oxidized form

known as pernigraniline (PE). The most useful form of PANI, however, exists when $1-x=0.5$, which is called half oxidized emeraldine base (EB). EB exhibits great semiconductor property owing to its alternative structure of two benzoid units and one quinoid unit, and it is the most stable form in room temperature. Moreover, EB has the potential to be the most conductive form through protonic acid doping.⁶⁴

PANI is a p-type semiconductor due to the delocalized π -bonds available in this system, thus the majority carriers are holes.⁶⁵ When EB PANI is doped with a protonic acid, a polaron structure is formed through the formation of a series of intermediate products that are shown in figure 3b. The hopping mechanism that is responsible for PANI's electrical conduction can take place in this polaron structure and this hopping may happen in both intra-chain and inter-chain.⁶⁶ To be specific, a cation radical of one nitrogen acts as a hole which acts as charge carriers. This hole starts to move when the electron from the adjacent nitrogen (neutral) jumps to this hole and turns it to electrically neutral. However, the electron hopping is not possible in bipolaron structure since two holes are adjacently located.

1.3.3 Synthesis of PANI

Electrochemical oxidation of monomer and chemical synthesis are two mostly used methods to synthesize PANI film.⁶⁷ Other methods such as photochemically-initiated polymerization and enzyme-catalyzed polymerization have also been demonstrated.⁶⁸ Essentially, at the initial stage of the polymerization, low molecular weight oligomers are formed from aniline monomers under acid environment. These low molecular weight oligomers are further oxidized to form polyaniline chain molecules at the potential that is lower than that at which the monomers are oxidized.⁶⁷

A three electrode assembly including a counter electrode, a reference electrode and a working electrode is required for conducting electrochemical polymerization. The aniline monomers are oxidized by cycling between a potential window, and the synthesized polymer is directly deposited onto the working electrode which may be anything that is conductive such as gold or transparent indium tin oxide (ITO). During polymerization, either 1) a constant voltage (potentiostatic), 2) a variable current and voltage (potentiodynamic) or 3) a constant current (galvanostatic) is employed to the aniline monomer solution.⁶⁸ A sufficient low pH environment is also necessary to protonate the aniline monomer in order to avoid undesired products.⁶⁹ Though electrochemical polymerization can precisely control the thickness and growing rate of the deposited film, the requirement of a conductive substrate greatly narrows down its applications.

Chemical polymerization, on the other hand, can deposit PANI films on insulating surfaces as well as conductive surfaces without the help of any template. Chemicals that exhibit oxidation potentials such as $(\text{NH}_4)_2\text{S}_2\text{O}_8$ ($E_0 = 1.94 \text{ V}$), FeCl_3 ($E_0 = 0.77 \text{ V}$) and H_2O_2 ($E_0 = 1.78 \text{ V}$) are commonly utilized for oxidizing monomers instead of using electrical instruments.⁷⁰ The chemical polymerization rate is very sensitive to the solution temperature. Therefore, ice bath is sometimes needed in order to gain better control of PANI film thickness and growing rate since the reaction is much slower in lower temperature. Similar with electrochemical polymerization, low pH condition ($\text{pH} < 3$) is also required for chemical polymerization to obtain desired products.⁷¹

1.3.4 PANI Nanostructures

Recently, nanostructured materials have been a rapidly growing field of research due to the realization that well-studied materials can exhibit new and sometimes surprising properties at the nanoscale.^{72, 73} The high surface-area-to-volume (S/V) ratio, which is the fundamental characteristic of nanomaterials, enables a number of unique physical and chemical properties such as high molecular adsorption, large surface tension force, enhanced chemical and biological activities, and large catalytic effects.⁷⁴ Interestingly, PANI is one of the few polymers that have the ability to adopt numerous different nanoscale shapes. Because of this, synthesis and characterizations of different PANI nanostructures have been continuously studied in recent years.

The most commonly observed PANI nanostructure morphology is the nanofiber. It was first observed by Huang and co-workers in 1986, when they electrochemically grew emeraldine PANI film on an indium tin oxide glass.⁷⁵ Later studies showed that the dopant used during oxidation directly affects the entangled dendritic degree of PANI nanofibers and the diameter of the nanofibers can be controlled by changing the sweep rate during polymerization.^{76, 77} Nanofibers fabricated via chemical oxidation were also demonstrated with the help of surfactants such as cetyltrimethylammonium bromide (CTAB) or hexadecyltrimethylammonium (C16TMA).⁷⁸⁻⁸⁰ The use of surfactants makes it possible to generate nanostructures without using traditional “hard-templates”, and it can be used for other conducting polymers.⁷⁸

Another intriguing nanostructure that appeals to researchers is the hollow sphere due to its potential usefulness in applications such as drug delivery and encapsulation.⁸¹ In 2006, MacDiarmid *et al.* obtained nano/micro self-assembled hollow spheres using a “falling pH method”. Aniline, ammonium peroxydisulfate (APS) and hydrochloric acid were mixed with

molar ratio 1:1:1 and started at pH = 4.2. As the process went on, APS degraded into sulfuric acid which resulted in the falling of pH value. The diameter of the hollow spheres obtained by this method is in microscale while the walls of the hollow spheres are on the order of tens of nanometers. As for nanosize spheres, chemical polymerization of aniline in the presence of sufficiently high concentration of a steric stabilizer, poly(N-vinylpyrrolidone) (PVP) were recently studied.^{82, 83}

Nanotubes of many different materials have been utilized in various applications.⁸⁴ Old PANI nanotube synthesis methods usually require hard templates such as porous alumina.⁸⁵ In recent years, efforts on synthesis PANI nanotubes with soft templates or no template have been made. For example, functional dopants such as propionic acid and lactic acid were reported to be utilized as soft template to generate polyaniline nanotubes.⁸⁶ In 2008, Stejskal et al. proposed a hypothesis that explains the mechanism of the forming of PANI nanotube. Due to the hydrophobicity, the phenazine-like moieties formed from *ortho*-coupled aniline in high pH environment are believed to aggregate into a template-like structure which generates nanotube afterwards.⁸⁷

Beyond these commonly observed nanostructures, other complex structures such as flower-like⁸⁸ and brain-like⁸⁹ structures have also been reported. However, the detailed mechanisms behind most of the reactions still remain unclear, and more works need to be done to utilize these nanostructures in practical applications.

2.0 BIOMOLECULES IMMOBILIZATION

Immobilization of biomolecules such as antibodies, enzymes and DNAs on the functioning materials, also called surface functionalization or modification, plays a decisive role in most biosensor designs. Different methods of the immobilization not only directly affect the sensing performances including sensitivity and limit of detection, but also have a great impact on the reproducibility and reusability. Based upon the mechanisms, immobilization techniques can be briefly categorized as physical methods and chemical methods. In this chapter, physical immobilization methods such as physical absorption and entrapment, and chemical methods that include covalent attachment are introduced, and methods for the immobilizations of biomolecules including antibodies, aptamers, enzymes and peptide nucleic acids on PANI surface are reviewed for our biosensor project as well as possible future biosensor designs.

2.1 IMMOBILIZATION METHODS

2.1.1 Physical Absorption

Physical absorption is one of the most straightforward methods for the immobilization of biomolecules, especially for enzymes. The absorptions are usually established through weak and non-specific interactions such as van der Waals, hydrophobic surface and hydrogen bonds.⁹⁰⁻⁹²

Though such weak forces make the biosensors liable to condition changes such as temperature, pH and ionic strength,⁹²⁻⁹⁴ it benefits the reusability of the supporting materials since the immobilized biomolecules can be reversibly removed under gentle conditions. In addition, better biomolecular activity can be retained using this method due to the chemical free process. There are two approaches to achieve physical absorptions: one is to soak the supporting materials into a solution that contains functioning biomolecules and incubate for enough time; another is to wait for the solution to dry on the supporting materials and rinse with buffer to remove the biomolecules that are not absorbed.

2.1.2 Entrapment

Different from physical absorption, entrapment is an irreversible method to immobilize biomolecules, where the biomolecules are physically restricted within a confined networks such as inside fibers, material with lattice structures or polymer membranes.⁹⁵⁻⁹⁷ Based on this working principle, the immobilizations are done during the synthesis of the supporting materials. The most significant advantages of entrapment are that it can minimize biomolecules leaching and improve mechanical stability.⁹⁸ However, it usually requires specific materials such as polyacrylamide gels or alginate to create matrixes.

2.1.3 Covalent Attachment

Covalent attachment is a method that utilizes chemical reactions to form covalent bonds between biomolecules and the supporting materials. The bonds are strong and irreversible, which make covalent bonding one of the most widely used immobilization methods. Depending on what

supporting materials and biomolecules are being used, the biomolecules can be immobilized directly on the supporting materials with the help of certain crosslink chemicals, or via cross-linkers. The most commonly used crosslink chemical is 1-ethyl-3-(3-dimethylaminopropyl) carbodiimide (EDC). With the presence of EDC, peptide bonds (-CO-NH-) can be formed through a dehydration condensation reaction from carboxyl groups (-COOH) and amines (-NH₂). N-Hydroxysuccinimide (NHS) is usually used together with EDC to speed up the process. When the supporting material and the biomolecule do not “match”, cross-linkers with two terminals that can covalently bind with either of them can be applied. For example, glutaraldehyde (GLu) molecule has two aldehyde groups (-CHO) at the end of each terminal, which makes it a good cross-linker to connect supporting materials and biomolecules that both have amines.

2.2 IMMOBILIZATION ON PANI

2.2.1 Immobilization of Antibodies and Enzymes on PANI

For a conducting polymer substrate, chemical immobilization post polymerization and entrapment during chemical synthesis are two most widely used approaches. Though entrapment method has relatively wider applicability, better protection of bound biomolecules and less cost, the severe condition of polymer synthesis and inaccessibility of target biomolecules dramatically lower its feasibility. On the other hand, not only does covalent attachment have great binding and less running problems, but also PANI has been widely known as an excellent material for biomolecule covalent immobilization. Both the secondary amine linkages in the PANI chains and primary amines at the end of the molecules are supposed to react with carboxyl groups and

aldehyde groups which can be commonly found in proteins (antibodies, enzymes) as well as linker molecules.

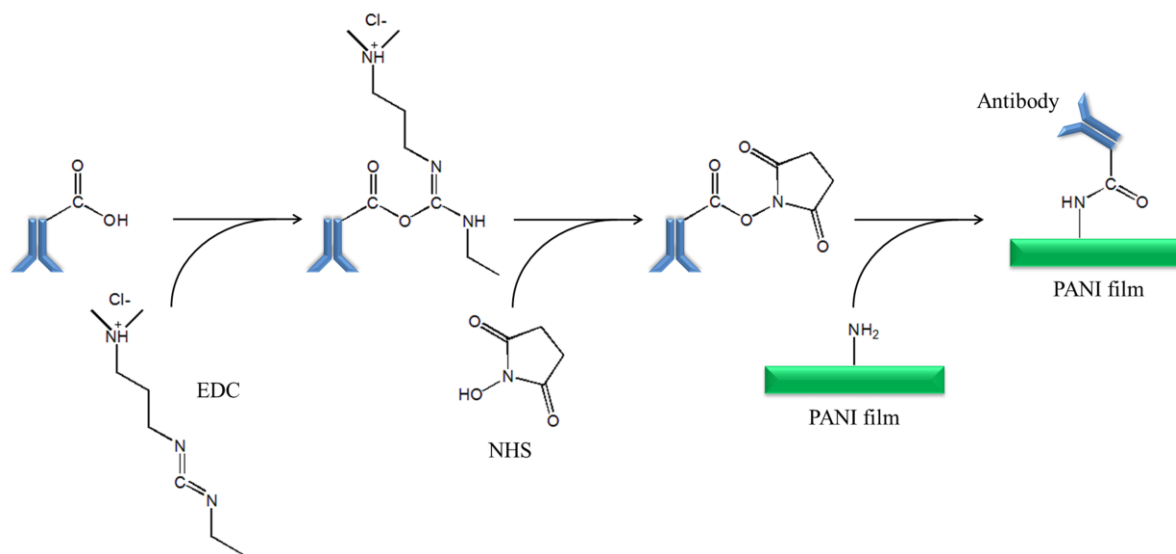


Figure 4. Reaction mechanism of using EDC and NHS to covalently bind an antibody on PANI film.

To implement covalent binding antibodies or enzymes onto N-terminus substrate (contains amine groups) such as PANI, two methods have been reported and widely employed. One is to use EDC and NHS as intermediates to link carboxyl groups on protein molecules with the primary amines at the end of PANI molecules. The reaction mechanism is illustrated in figure 4. Briefly, the carboxyl group first reacts with EDC/NHS to form a semi-stable amine-reactive NHS ester. Then it reacts with primary amines to form a stable amide. The major advantage of this method is its water solubility. The chemical and electrical properties of PANI can mostly be preserved during immobilization. In addition, this method can also be utilized for immobilization of proteins or other biomolecules with primary amines on substrates with carboxyl groups.

Another method is to use GLu as a cross-linker to connect both amines on the N-terminus of protein molecule and the substrate. The aldehyde groups on the linker react with primary or

secondary amines to form imine or enamine bonds, respectively. Figure 5 shows the reaction mechanism.

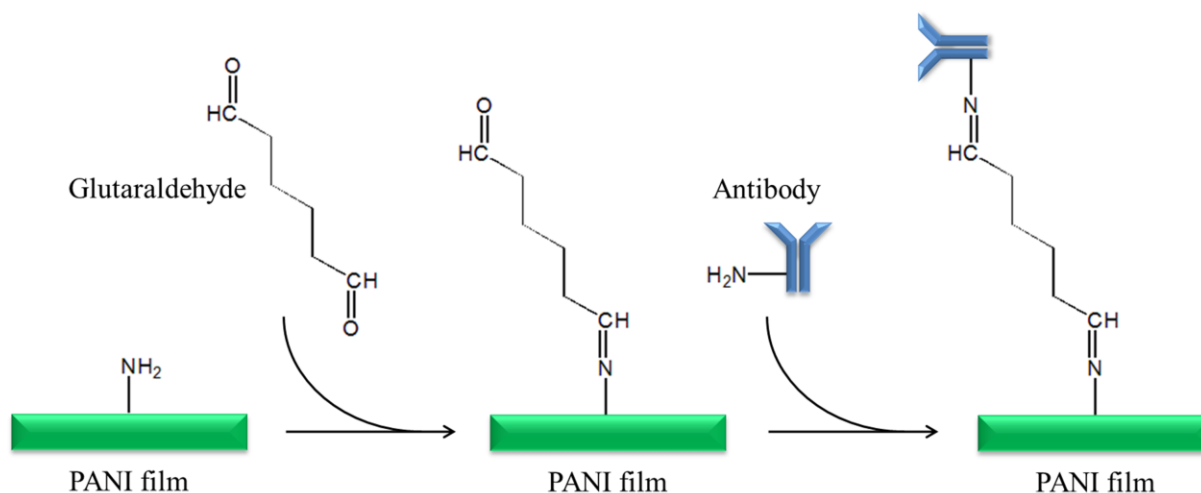


Figure 5. Reaction mechanism of using Glu as cross-linker to covalently bind an antibody on PANI film.

2.2.2 Immobilization of PNAs and Aptamers on PANI

Peptide nucleic acids (PNAs) are artificially synthesized polymers that are similar to DNA, which can be used as DNA or RNA probes. Aptamers are oligonucleotide or peptide molecules that are capable of binding specific molecules. Chemical methods are also the better choices here for the immobilization of PNAs and aptamers on PANI. Different from proteins, PNAs and aptamers do not have the carboxyl groups. Nevertheless, the primary amines at the end of PNAs and aptamers can be connected with the amines on PANI in the presence of cross-linkers. Figure 6 illustrates a method of using Glu as the cross-linker for PNA immobilization, which is similar to figure 5. To be specific, substrate with PANI film is kept in 1% glutaraldehyde for 4h at 25 °C.⁹⁹ The aldehyde groups in GLu will react with primary amines and secondary amines to

form imine and enamine bonds, respectively. After Glu treated, PANI film is washed, added with PNA and incubated for about 12 h.⁹⁹ The N-terminus of PNA will also bind with aldehyde in Glu molecules. This method can also be used for aptamers.

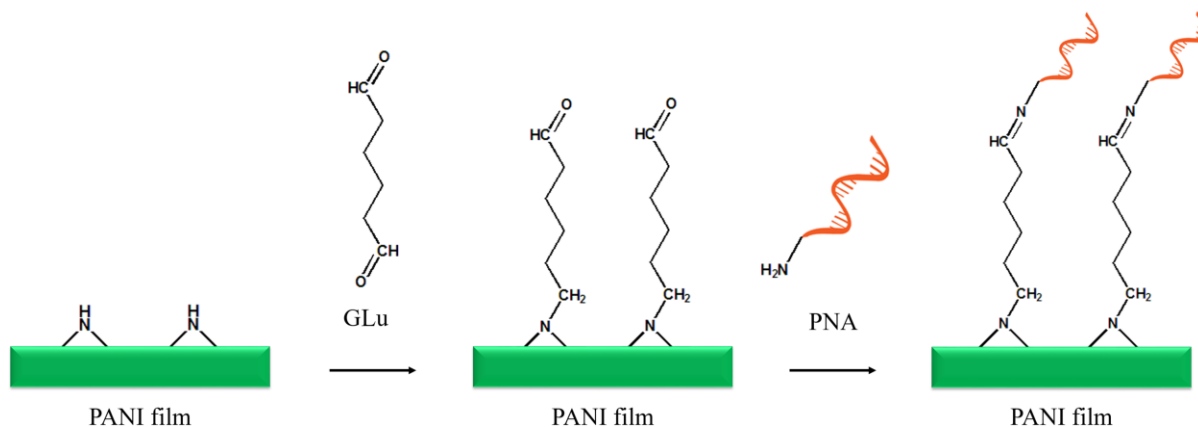


Figure 6. Reaction mechanism of using Glu as cross-linker to covalently bind a PNA on PANI film.

Another interesting PNA immobilization approach developed by Hyun Gyu Park *et al.* is more complicated, since it involves more chemical reactions.¹⁰⁰ However, the linker that connects PANI and PNA has fluorescence, which makes it easier to identify whether the immobilization is successful or not. The reaction is shown in figure 7. PANI substrate is first incubated in dimethylformamide (DMF) solution of [(4-ethynylphenylcarbonyl)-methoxy]-acetic acid (4EPA) for 12 h at 37 °C¹⁰⁰ together with coupling agents O-benzotriazolyl-N,N,N',N'-tetramethyluronium hexafluorophosphate (HBTU) and N,N-diisopropylethylamine (DIEA).^{101,102} After that (3-azido-2-oxo-2H-chromen-7-yloxy)-acetic acid (AZCO)-linked PNA is added to finish the immobilization.

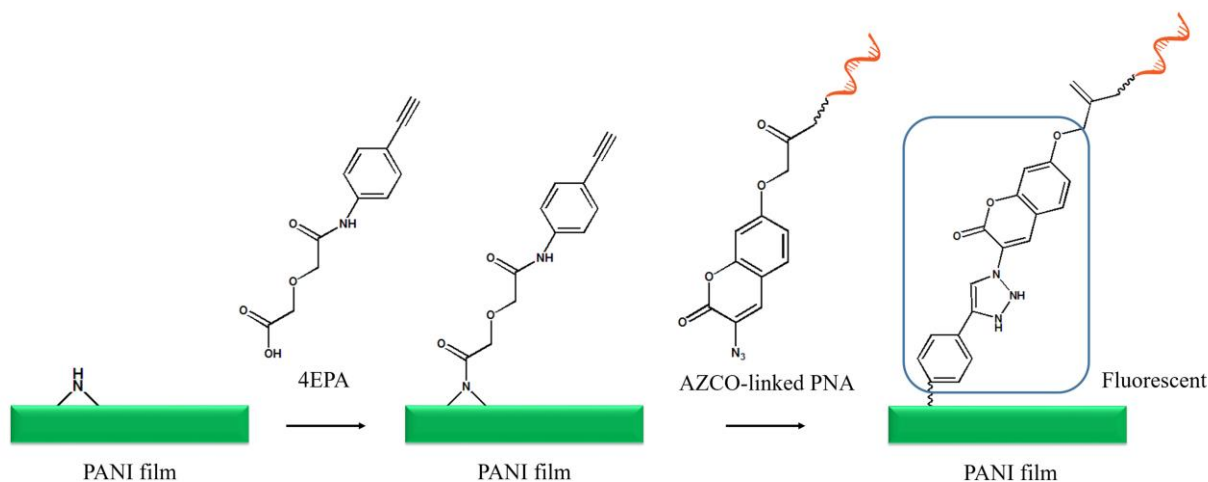


Figure 7. Reaction mechanism of cross-link a PNA on PANI film with fluorescent unit.

2.2.3 Prevent Nonspecific Absorption

Physical absorption not only is a specific method for biomolecule immobilization, but also happens every time during chemical immobilization and biosensor testing. Charged nonspecific target molecules that are absorbed on PANI's surface can cause false detection signals. To prevent this, a commonly used method is to drop high concentration of blocking agents such as bovine serum albumin (BSA) on the functioning materials (PANI) after immobilization. BSAs will absorb on the surface and cover the free-sites where no immobilized biomolecules exist. This "thin film" of BSA will prevent nonspecific targets from attaching to the surface.

3.0 DEVELOPMENT OF 2-D PANI BIOSENSORS ON SILICON OXIDE SUBSTRATE

3.1 INTRODUCTION

The rapid growth of biosensors is being continuously driven by the increasing health-related concerns. Medical biosensors for blood monitoring and real-time point-of-care testing are highly demanded. Ongoing researches have been focusing on improving existing models in terms of accuracy, sensitivity, reduced size, and increased portability. To achieve this, efforts are directed towards combining nanotechnology, material science, and miniaturization of devices in biosensors field.

Nanostructure materials, with at least one dimension in nano scale, have enabled numerous unique physical and chemical properties such as high molecular adsorption, enhanced chemical and biological activities, and large catalytic effects.⁷⁴ Based on the dimensions, nanostructures can be roughly categorized into zero-dimensional (0-D nanoparticle), one-dimensional (1-D nanowire) and two-dimensional (2-D nanolayer) structures. One common feature for nanostructure materials is that they all possess much larger surface-area-to-volume (SA/V) ratio compared with bulk materials, which drives the development of nanotechnology. Such a property is also highly desired in bioelectronics, resulting in the fast growing interests in sensor related researches. Polyaniline (PANI) nanostructures have been extensively utilized in

developing of low cost and reliable biochemical sensors due to their controllable electrical and chemical properties, thermal and electrochemical stability, and suitable nature for biomolecules functionalization.⁶⁰ Among all forms of PANI nanostructures, the 1-D PANI nanowire has proved its superiority in terms of sensitivity and limit of detection.^{103,104} The excellent sensing performance is believed to be attributed to its extremely large SA/V ratio and good FET behavior. However, the fabrication complexity of 1-D structures strongly impedes the realization of highly uniform and reliable PANI nanowires, resulting in low yield and high fabrication costs. To circumvent this, one alternative is to scale up the 1-D nanowire to 2-D nanostructure with only thickness that is in nano scale. This change is favorable mainly for two reasons. First, from fabrication perspective, it is much easier to create thin film structures with nano scale thickness than defining nano sizes on length or width dimension. This feature can endow the 2-D nanostructure with much better controllability, higher uniformity, and volume production¹⁰⁵⁻¹⁰⁷ due to the much simpler and lower cost processes. Moreover, though this change loses one nano scale dimension which often suggests the dropping of the total SA/V ratio, 2-D nanostructures can still exhibit comparable SA/V ratio to 1-D nanowire structure. This can be achieved by reducing the film thickness or increasing the surface roughness.

In this chapter, microfluidics integrated biosensors based on 2-D PANI layers were developed. B-type natriuretic peptide (BNP), an important cardiac marker, was used as the target for characterizing the sensing performance of the 2-D PANI layer biosensors. The common BNP concentration in a healthy person is ~100 pg/mL, and may increase to over 2 ng/mL in patients with severe heart failure.¹⁰⁸ BNP biomarker tests were first conducted under constant Debye length environment to obtain the sensitivity and specificity of the PANI layer biosensors over detection of BNP. Debye length investigation was then carried out with constant BNP target

concentration under different Debye length environment to verify the impact of Debye screening on FET sensing performance. Sensing performances of PANI layers at different oxidation states were also compared for optimization purpose.

3.2 EXPERIMENTAL

In this section, fabrication processes to develop 2-D PANI layer biosensors including PANI layers patterning, PANI synthesis, surface functionalization and microfluidics integration are thoroughly explained.

3.2.1 Chemicals

1-ethyl-3-(3-dimethylaminopropyl) carbodiimide (EDC), N-Hydroxysuccinimide (NHS), aniline monomer, bovine serum albumin (BSA), perchloric acid (70%), ammonium persulfate ((NH₄)₂S₂O₈) were purchased from Sigma Aldrich. Fluorescent-dye-labeled aptamer (5'-GGGGCACGTTTATCCGTCCCTCCTAGTGGCGTGCCCC-3') was synthesized by Integrated DNA Technologies. Mouse anti- B-type natriuretic peptide (BNP) monoclonal antibodies were purchased from Abcam. Phosphate buffer solution (PBS, pH 7.4) was used to prepare the BSA, EDC, NHS, and BNP solutions with different concentrations.

3.2.2 Development of 2-D PANI Layers

The fabrication of the devices started with a typical electrodes patterning processes including lithography, e-beam evaporator deposition and lift-off as illustrated in figure 8. The micron size PANI layers were then defined and patterned by applying a bilayer lithography/lift-off process on top of the wafer with electrodes. The patterns were aligned using Qunitel mask aligner Q4000. Benefits of using bilayer structure here are that it can significantly increase the PANI lift-off uniformity as well as prevent undesirable current signals.

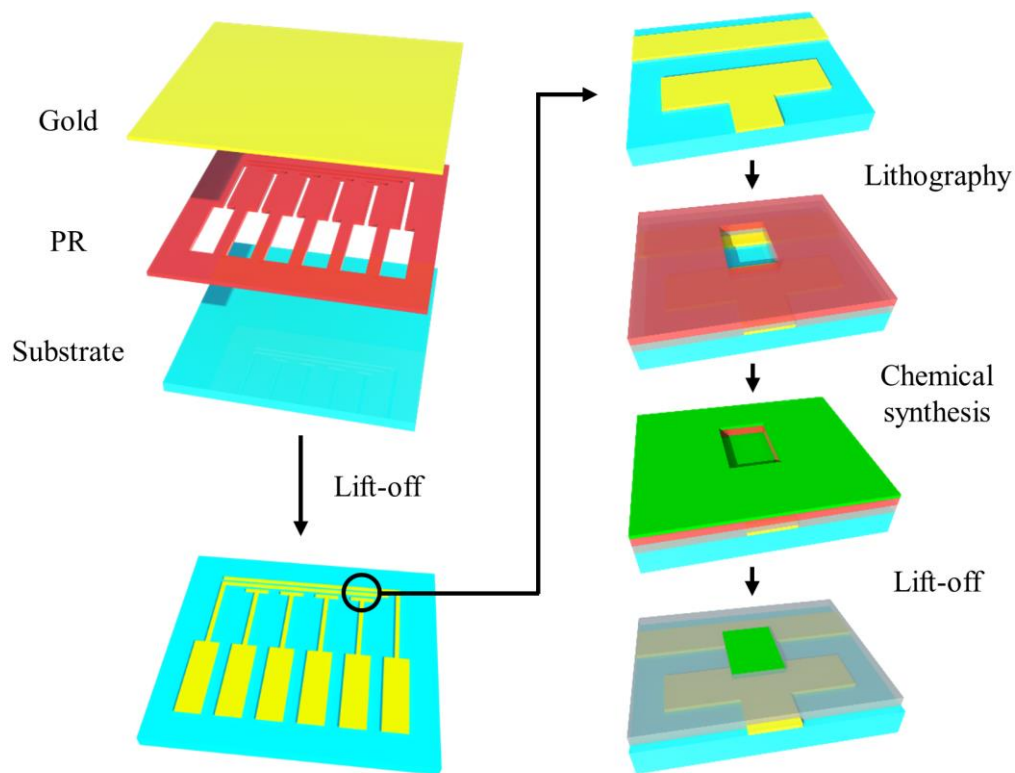


Figure 8. Illustration of the fabrication processes to develop PANI FETs.

PANI chain molecules are typically formed by the oxidation of aniline monomer. This reaction requires three elements: aniline, acid to protonate aniline and an oxidation potential. Based on this mechanism, electrochemical oxidation of monomers and chemical synthesis are the two most commonly used approaches to polymerize PANI films.⁶⁷ Electrochemical polymerization utilizes a working electrode to offer the required oxidation potential which makes the PANI film directly deposited on top of it. Though this method can precisely control the thickness and growing rate of the deposited film, the requirement of a conductive substrate greatly narrows its applications. Chemical synthesis, on the other hand, can polymerize PANI film on any solid surface. In addition, the nucleation of PANI molecules taking place both in the bulk solution and on the substrate results in a much rougher surface morphology,¹⁰⁹ which potentially increases its sensitivity. Therefore, chemical synthesis was utilized in this work to deposit high sensing performance PANI film.

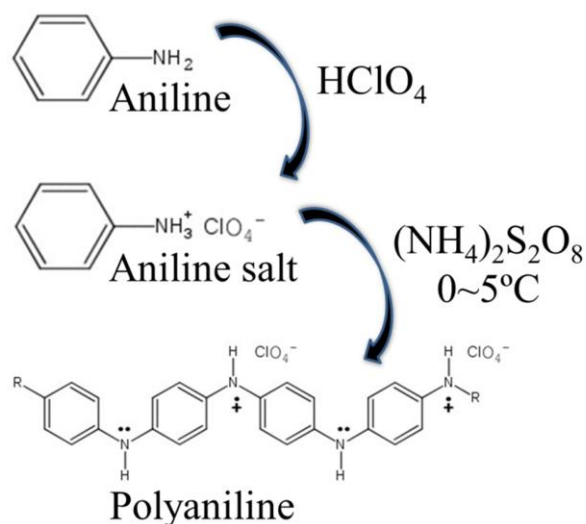


Figure 9. The chemical reactions of PANI synthesis.

After bilayer process was done, a dilute chemical polymerization method^{110,111} was utilized to deposit a uniform PANI thin film on electrode patterned wafer surface. In a typical procedure, the prefabricated wafer was immersed in 180 mL of 0.35 mol/L aqueous HClO₄ solution. 0.91 mL of aniline monomer was then added into the HClO₄ solution, and the whole solution was kept stirring at 400 rpm for 30 min in ice bath to form a uniform mixture. In a different beaker, 0.6845g of oxidant (NH₄)₂S₂O₈ (APS) (the molar ratio of aniline to APS is 3 to 1) was dissolved in 20 mL of aqueous HClO₄ solution and cooled to ~0-5 °C in a freezer. The polymerization was initiated by combining the two solutions. The mixture was kept stirring in ice bath during the whole reaction to accomplish the formation of PANI thin film. The detailed reactions are shown in figure 9. After the polymerization, the wafer was taken out from the solution and rinsed with DI water to remove adhering PANI precipitate. The dark green or blue color (depends on polymerization time) shown on the wafer indicates that a thin layer of PANI film was successfully coated on its surface. Then the PANI coated wafer was dried and immersed in acetone for 5 min to lift-off the photoresist layer together with undesired PANI film. The finished wafer was covered with both LOR and PANI with no electrode exposed to air. After rinsing it with deionized water 3 times, the samples with PANI patterns were cut from the wafer and stored for future use.

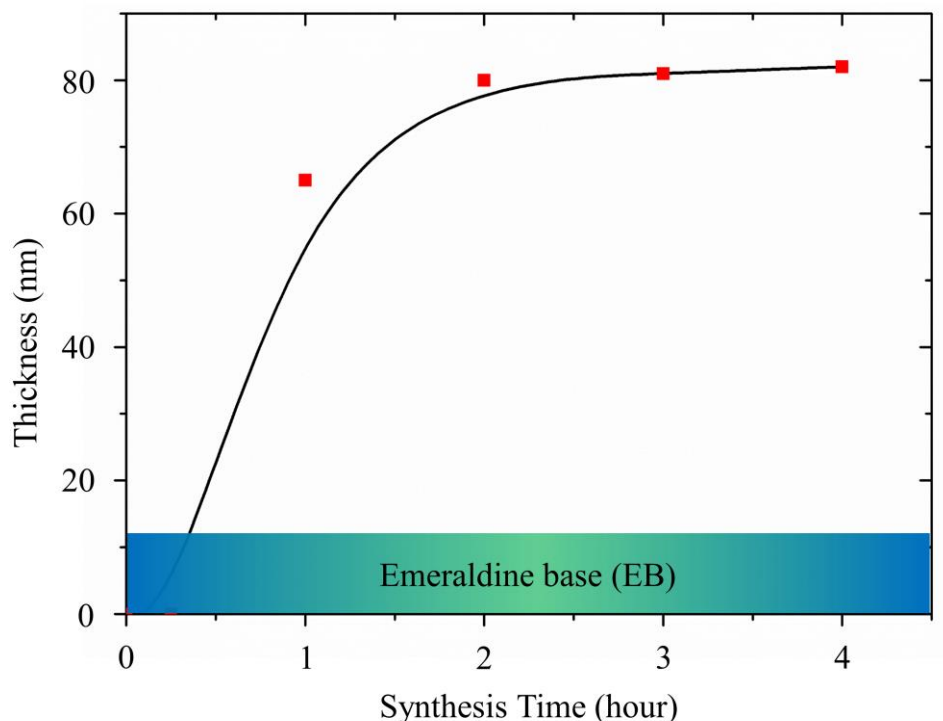


Figure 10. Estimation of PANI film thickness and oxidation state over synthesis time.

The thickness and oxidation state (indicates conductivity) of PANI film over polymerization time were investigated and shown in figure 10. The introduction period of the reaction took around 15 minutes, during which most of the aniline monomers got protonated in the low pH environment. Oxidative polymerization started to speed up after introduction period when the solution turned from clean colorless to dark black. This color change is due to PANI nucleation took place in the bulk solution. Thickness of PANI films were measured by atomic force microscope (AFM). The results showed that after 1.5 hours of polymerization, the film thickness remained constant around 80 nm, which indicates the end of polymerization. The oxidation state can be roughly acquired by observing the color of PANI films. At half an hour time, the film showed blue, which corresponds to a relatively high oxidation state. The conductivity is as low as insulators. One hour after the reaction was initiated, the film displayed

green color which corresponds to the most useful acid-doped emeraldine salt (ES) form. However, given more oxidation time (over 4 hours), the PANI films change back to dark blue-violet (per)nigraniline form. A comparison of 2-D PANI films with different oxidation states is shown in figure 11. The green emeraldine salt form exhibits much larger conductivity than blue-violet (per)nigraniline form.

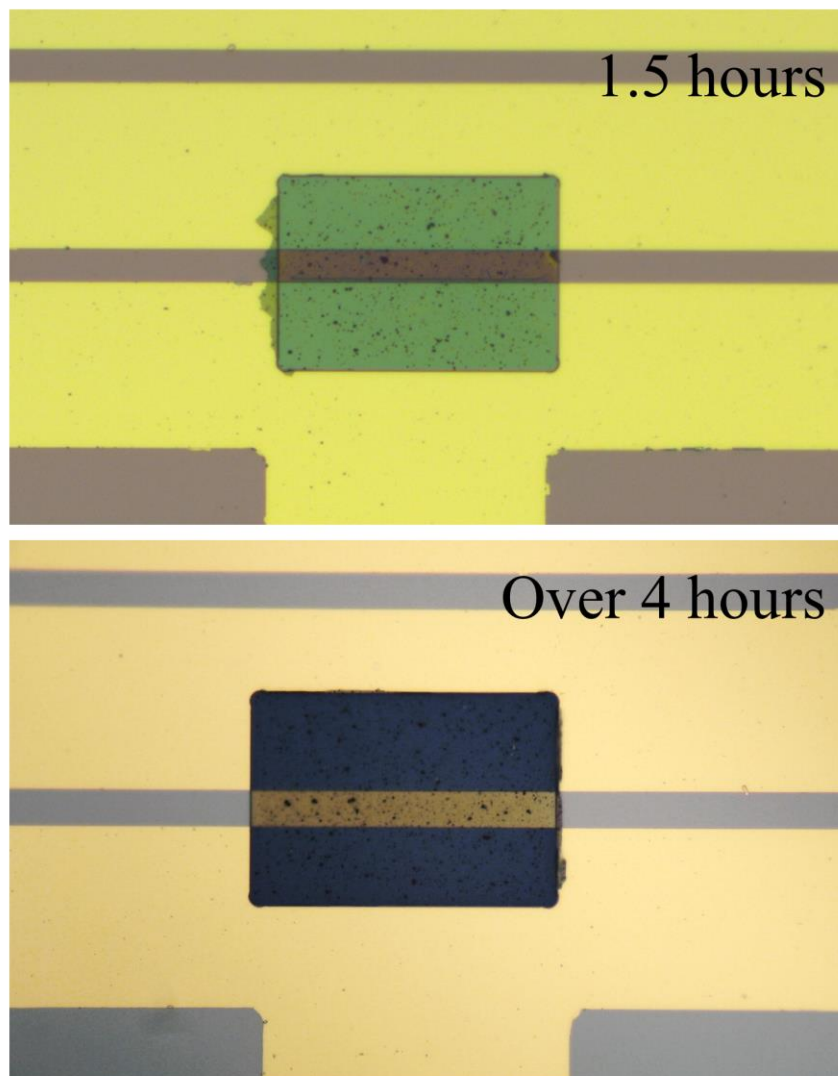


Figure 11. Microscope images of PANI film synthesized under the same conditions with different synthesis time:

1.5 hours (top), over 4 hours (bottom).

3.2.3 Surface Functionalization of PANI

In this project, EDC and NHS were used to functionalize PANI with monoclonal antibodies (mAbs). 2 μ L of PBS solution contains 100 μ g/mL of B-type natriuretic peptide (BNP) antibody was first added into a micro tube. 49 μ L of both PBS solutions with 0.1M EDC and NHS were added into the same micro tube. The solution was then shaken for 15 seconds to form a uniform mixture, and added onto PANI layers at room temperature. After 4 hours, the functionalized PANI layers were then thoroughly rinsed with DI water to remove physically adsorbed antibodies. To prevent possible nonspecific adsorption of other biomolecules to the PANI layers, PBS solution contains 200 μ g/mL bovine serum albumin (BSA) was then dropped onto PANI layers for 30 minutes to block the free sites on their surfaces.

3.2.4 Integration of Microfluidic Channels

Recently, microfluidics has been an increasing attraction to researches due to its ability of integrating advanced biosensors into lab-on-a-chip systems.¹¹² The lab-on-chip systems with microfluidics have several advantages including low consumption of costly reagents, minimal handling of hazardous materials, short reaction time required for analysis, multiple sample detection in parallel, portability, and versatility in design.¹¹³ Microfluidics designs for whole blood separation in clinical applications were also demonstrated using different techniques and platforms.¹¹⁴⁻¹¹⁷

A PDMS microfluidics device with a micron-thick channel (1 cm \times 1 mm \times 100 μ m) connecting inlet and outlet was fabricated through a replica molding process. Silicon elastomer base and curing reagent were mixed in a 10:1 ratio, stirred for 10 minutes and degassed for 30

minutes. After all the bubbles were gone, the mixture was poured in a box with prefabricated mask (to create channels, inlets and outlets) located on the bottom. The box was then put in oven and cured at 85 °C for 3 hours. The single microfluidic device was cut off and stuck onto the device with the channel right on top of the PANI layers as shown in figure 12a. Microtubes were used as both inlet and outlet. The finished device with microfluidic is shown in figure 12b.

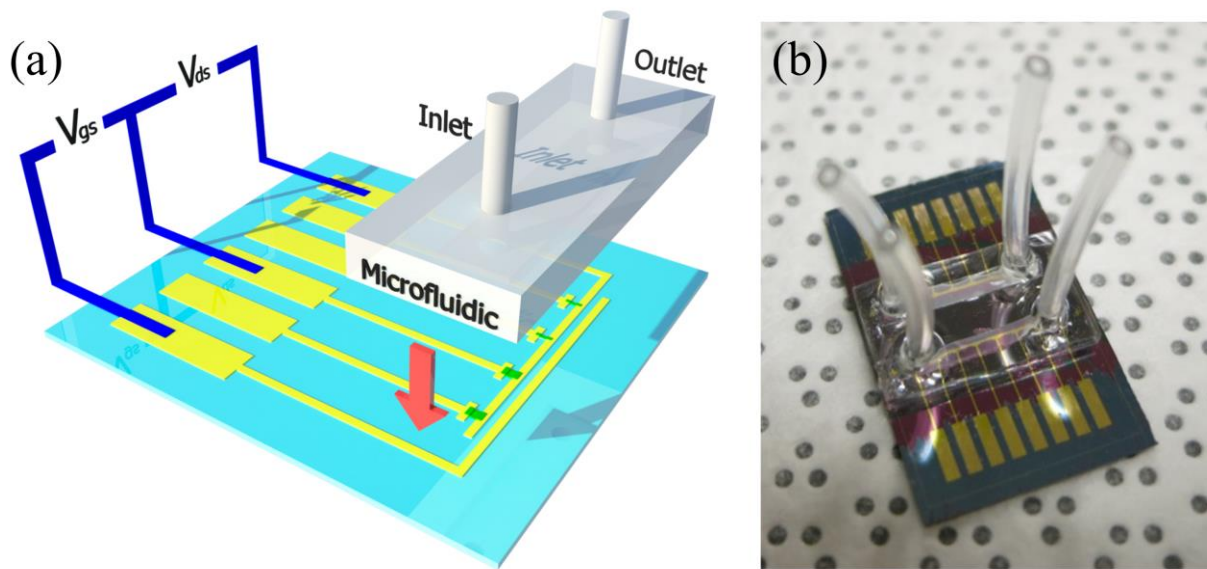


Figure 12. (a) Illustration of microfluidic design and microfluidic integration. (b) Image of a biosensor device with microfluidic integrated

3.3 RESULTS AND DISCUSSION

3.3.1 Surface Morphology Study of 2-D PANI Layers

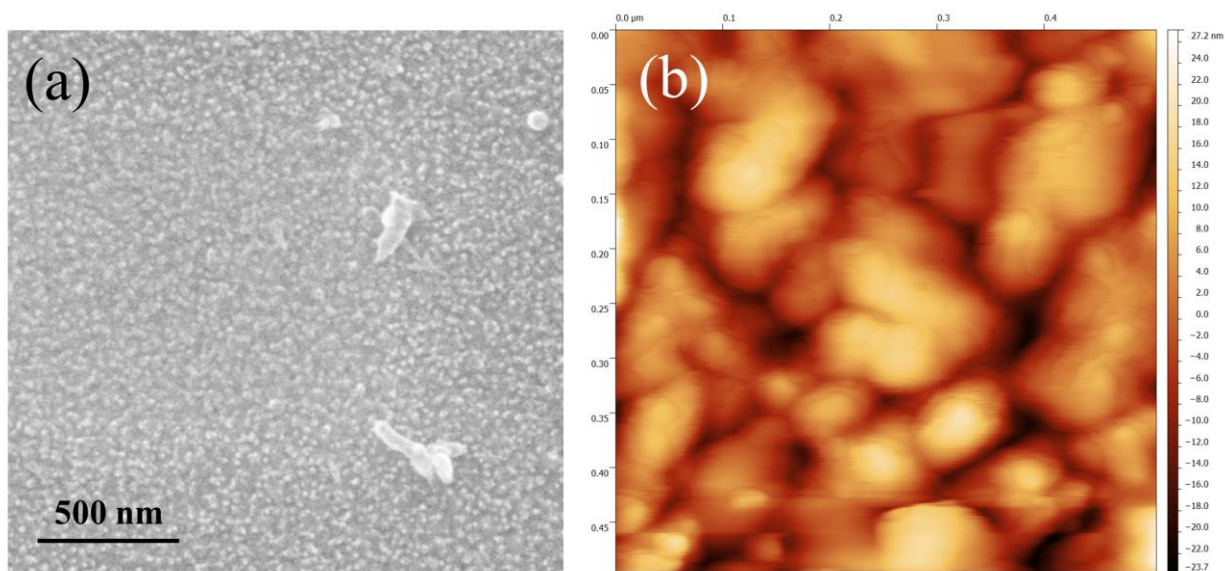


Figure 13. (a) SEM image of PANI surface. (b) High magnification AFM image of PANI surface.

The surface morphology of 2-D PANI nanostructures was studied by scanning electron microscope (SEM) (Quanta 600 FE-SEM) and atomic force microscopy (AFM) (PSIA XE-100 & Solver Next AFM). From the SEM image shown in figure 13a, a rough surface with nanogranular structures can be observed. This observation was confirmed by the topography investigation using the AFM in non-contact mode. A $0.5\mu\text{m}$ by $0.5\mu\text{m}$ image with Z scale (color range) from 0 nm (dark) to 55nm (bright) was shown in figure 13b. The nanogranular structures have an average diameter of 100 nm and height difference around 30 nm. Two factors have been proposed to be responsible for the formation of these structures.¹⁰⁹ First, the secondary nucleation centers occurred and started growing on the surface of preformed PANI film. Second,

the PANI molecules nucleated in the bulk solution precipitated and incorporated with PANI nucleated on the surface. The average size of the nanogranular structures was also demonstrated to increase with reaction temperature.¹¹⁸ This result indicates that the surface morphology of PANI can be easily controlled by tuning the temperature. Same high magnification AFM images were taken at two other random spots, and the results revealed that the surface area of PANI film was increased averagely by 46% compared with flat surface due to this unique morphology. With the film thickness below 100 nm, extremely large SA/V ratio was achieved, which is believed to contribute to its excellent sensing performance.

3.3.2 PANI FET Measurement

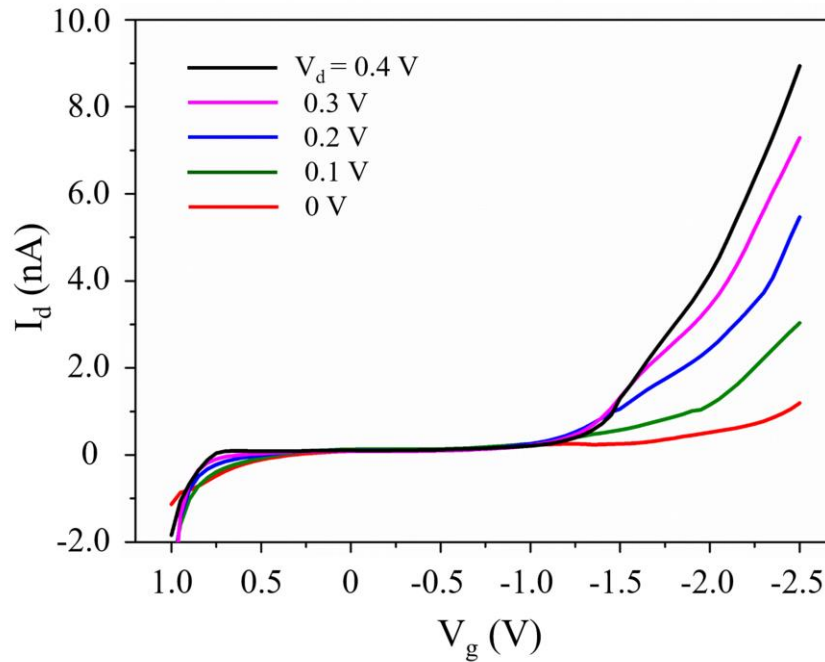


Figure 14. FET measurement of PANI film. V_d was fixed at different value from 0 to 0.4V while sweeping V_g from 1.0V to -2.5V.

Field-effective transistor measurements of 2-D PANI layers were conducted by using the probe station (Signatone s-1160). Figure 14 shows the drain current (I_d) versus gate voltage (V_g) characteristics, while keeping V_d fixed from 0 to 0.4V. I_d stays low when V_g is from 0.5V to -1.0V no matter what V_d is applied, which indicates the depletion region of the PANI film. After V_g passes below -1.2V, I_d begins to rise sharply. Since PANI is well-known p-type semiconductor material, this negative V_g induced regime should correspond to the carrier accumulation due to the increase of hole concentration on the PANI surface. The significance of this figure is that it can help us determine the working condition for our PANI biosensors. According to Gao *et al.*,³⁶ optimal sensitivity can be achieved when the FET sensing component is working in subthreshold regime. Therefore, from figure 14, we can infer that the best working condition for our PANI FET biosensor is when V_g is around -1.0V. Though the magnitude of drain current change upon targets binding is much smaller than the device that is working in accumulation regime, the current increase over current ($\Delta I_d/I_d$), which represents the sensitivity of the biosensor, is vastly enhanced.

3.3.3 Fluorescence Test of Functionalized PANI

Alexa Fluor™ 488 Conjugate aptamers with excitation wavelength peak at 495 nm and emission wavelength peak at 519 nm were functionalized on the surface of PANI in the presence of EDC and NHS. Figure 15 shows the result of the fluorescent test. Clear green light was observed on the PANI film area which verifies the successful functionalization of the aptamers. Thus confirms the viability of our surface functionalization method.

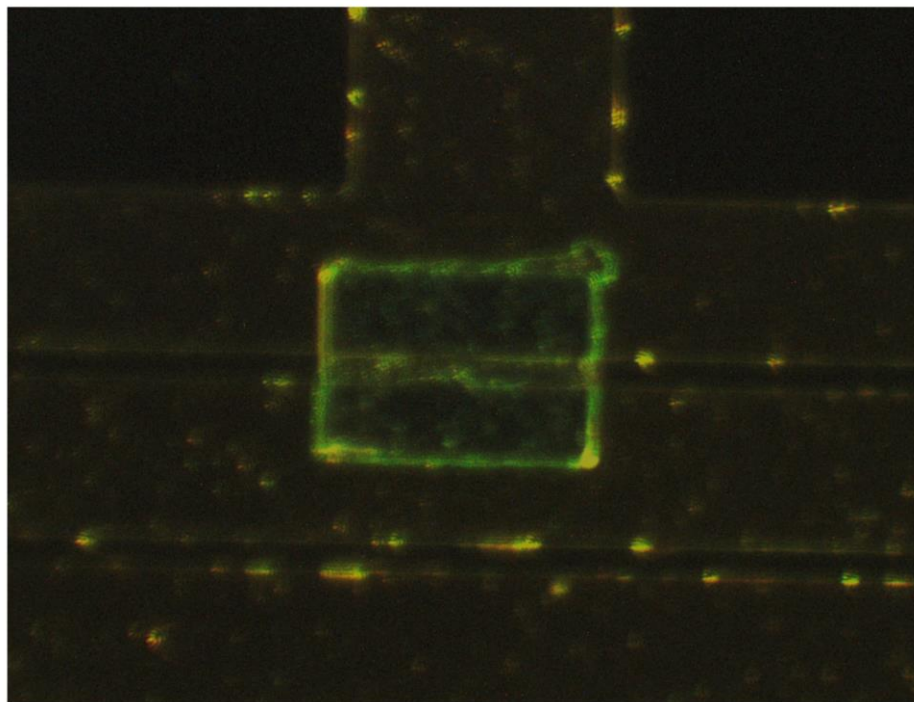


Figure 15. Fluorescent test of functionalized PANI.

3.3.4 BNP Biomarker Detections

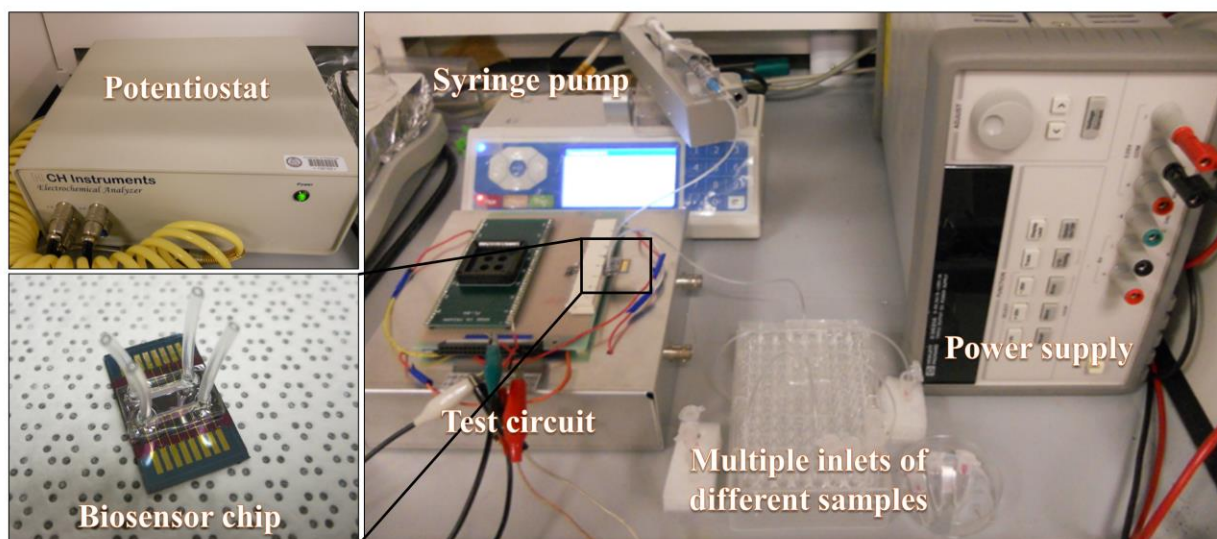


Figure 16. Testing system including a potentiostat, syringe pump, test circuit, multiple inlets and a power supply.

The testing system shown in figure 16 contains a testing circuit with a memory socket for device connection, a syringe pump, and a potentiostat (CHI 1000C). The microfluidic integrated device can be inserted into a memory socket without using any wire-bonding steps. The memory socket is connected to the testing circuit. During the test, different sample solutions can be selectively pumped into the microfluidic channel from the multiple inlets by the syringe pump. The current signals flowing through 2-D PANI films can then be obtained by the potentiostat using linear sweeping method that sweeps the drain-source voltage from 0V to 0.25V (sweeping rate: 0.1V/s, sample interval: 0.005V) at fixed gate voltage condition. In particular, -1.0V gate voltage was chosen according to the FET measurement.

The tests were started with pumping in PBS 0.01X solution by using a syringe pump. When the microfluidic channel was filled with PBS solution, the pump was stopped and I_d - V_d measurement was read three times by sweeping V_d from 0V to 0.25V. After stable current signal was obtained, PBS 0.01X solution samples that contain high concentrations of nonspecific targets such as IgG and BSA, and different concentrations of BNP targets (ranging from 100 pg/mL to 1000 pg/mL) were pumped into the microfluidic channel successively. Linear sweep I_d - V_d measurements were performed each time when the microfluidic channel was filled with new sample solution. As shown in figure 17, nonspecific biomarkers IgG and BSA show similar current outputs to the PBS background signal despite their high concentrations. On the contrary, samples with different BNP biomarker concentrations show clear current increase with the increasing of concentration. These current changes can be explained by the gating effect from charged target molecules. BNP molecules, with an isoelectric point (pI) of 5.4¹¹⁹ are negatively charged in the neutral (pH=7.20) solution. When BNP molecules are bound on the surface, negative charges start gating the p-type PANI film, causing the accumulation of carriers, thus

increasing the conductivity. These results not only indicate that the 2-D PANI layer biosensor is able to specifically recognize BNP biomarker, but also show its excellent sensitivity.

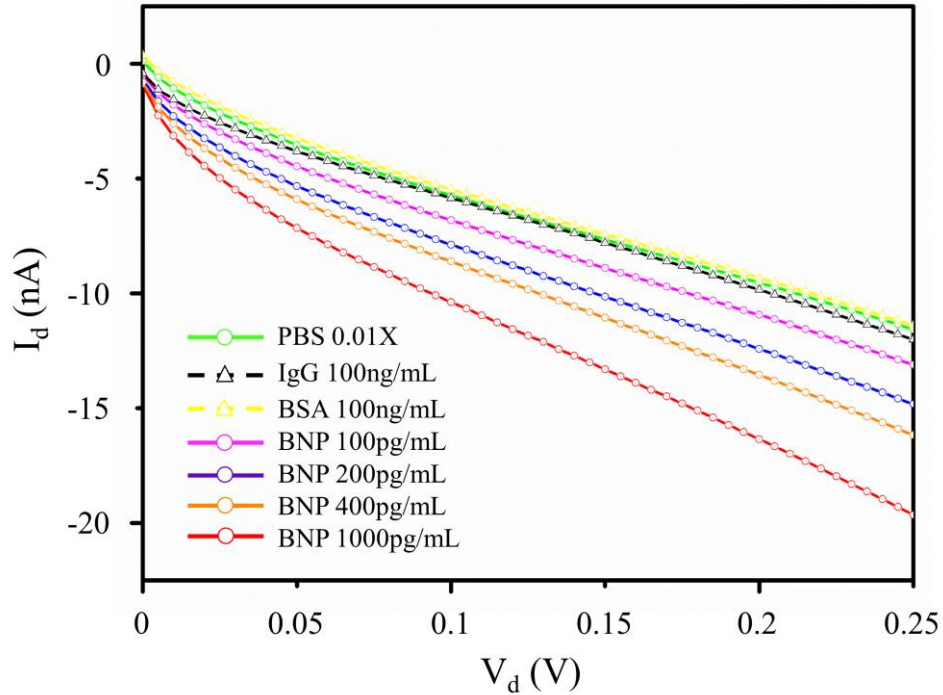


Figure 17. Sensing results with nonspecific targets (IgG and BSA) and different concentration of BNP biomarkers.

3.3.5 Debye Length Investigation

Debye length, as introduced in chapter 1, is well-known as one of the most significant factors that affect FET biosensor's performance. To investigate this, two biomarker tests were carried out. The BNP biomarker samples in these two tests were made out of different concentrations of PBS solutions (0.1X and 0.01X), which correspond to different Debye length environments. As we can see from the sensing results shown in figure 18, biosensor that was tested with solutions based on 0.01X PBS shows more distinguishable current increases over the increases of target concentration. This difference is consistent with the theory, and it is mainly because of some of

the antibody-antigen complexes formed on PANI surface being screened out due to the relatively small Debye length (2.3 nm) in 0.1X PBS environment compared with it (7.3 nm) in 0.01X PBS.

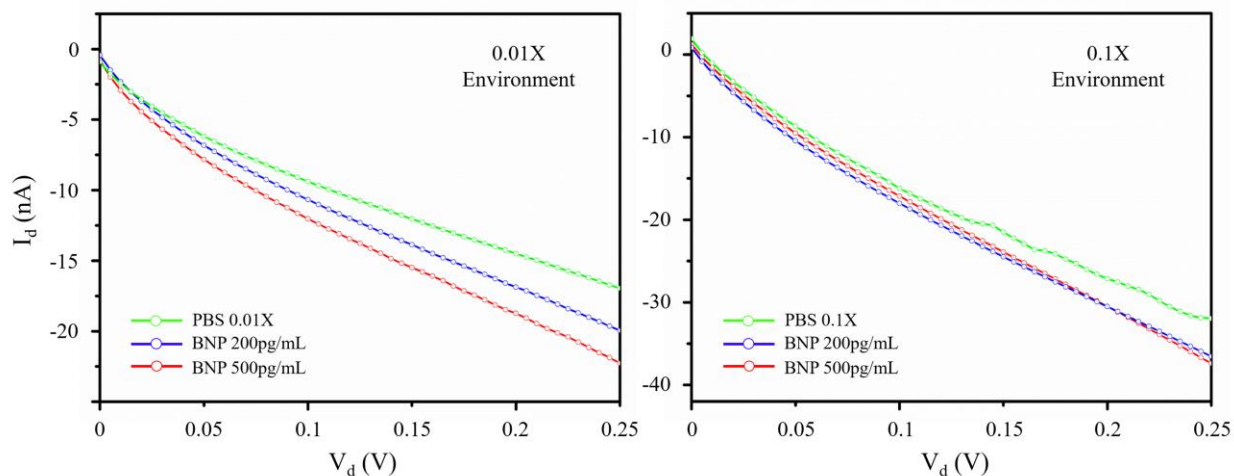


Figure 18. BNP biomarker detections performed under different buffer concentration (Debye Length).

3.3.6 Sensing Performances Using PANI in Different Oxidation States

The chemically synthesized PANI films have different oxidation states due to different synthesis time. For optimization purpose, PANI layers that are in emeraldine form and near (per)nigraniline form (not fully oxidized) were tested with BNP biomarkers. The emeraldine form PANI layers was synthesized for 1.5 hours, while the near (per)nigraniline form was synthesized for over 4 hours. The tests were conducted with only PBS and BNP (200 pg/mL and 500 pg/mL). Figure 19 shows the comparison of both microscope images of the PANI layers and their sensing results. The green emeraldine form PANI shows 2 orders of magnitude larger current with less noise. The current differences are also easier to identify. Such superiorities are believed to be attributed by both the natural high conductivity of emeraldine form and the fact that emeraldine form is better for antibodies immobilization.

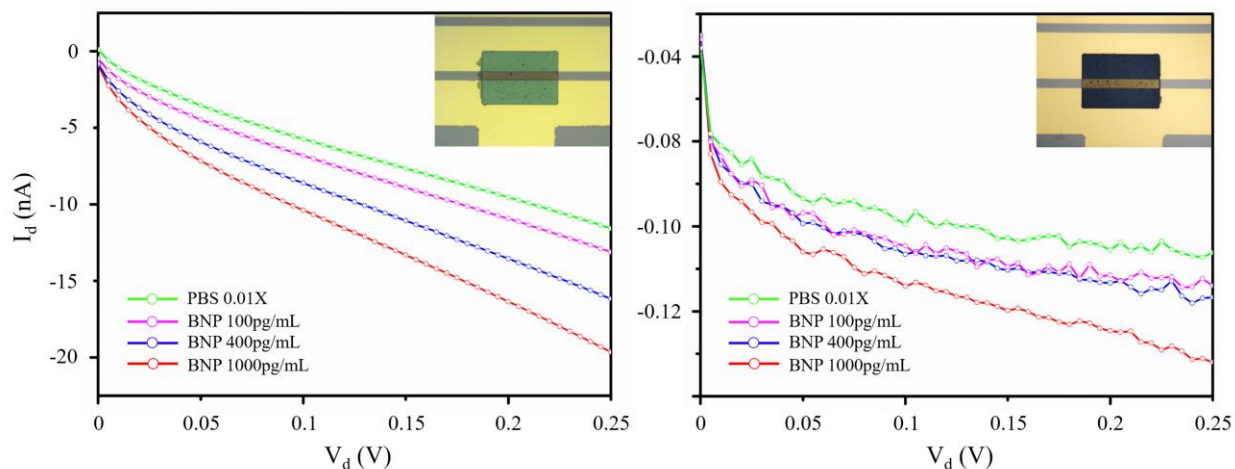


Figure 19. BNP biomarker detections performed with PANI films in different oxidation states.

3.4 CONCLUSIONS

We have established a facile way to develop 2-D PANI layer biosensors on SiO_2 substrates that combines both top-down and bottom-up processes. The chemically synthesized 2-D PANI nanostructures exhibit extremely large surface roughness which is attributed by the well-controlled low temperature synthesis condition. Such structures assure the biosensors to have outstanding sensitivity. With the help of microfluidics channels, a detection limit as low as 100 pg/mL was achieved for detecting BNP biomarkers. Biomarker tests conducted in different ionic strength environment verified that larger Debye length can, in some degree, enhance the sensing performance. In addition, sensing performances of PANI layers at different oxidation states were also compared and evaluated. The half oxidized emeraldine form showed better sensing performance due to its higher conductivity and better chance for antibodies immobilization.

Based on this biosensor design, two major improvements were investigated in this dissertation: one is to use flexible substrates such as PET and PI to replace current nonflexible

SiO₂ substrate; the other is to develop 2-D PANI film/nanotubes hybrid nanostructures as the substitutes for 2-D PANI layers (bare films). The details will be explained in the following two chapters.

4.0 DEVELOPMENT OF 2-D PANI BIOSENSORS ON FLEXIBLE SUBSTRATES

4.1 INTRODUCTION

Nowadays, electronic devices tend to get smaller and more highly integrated due to the ceaseless development of micro and nano fabrication techniques. With the device thickness down to the micron scale, flexible design becomes an excellent alternative for devices to maintain basic mechanical stability as well as offering versatility in designs and large area compatibility. As a result, the rapid development of flexible electronics in recent years has inspired and fueled numerous applications in fields such as radio-frequency identification (RFIDs) tagging,¹²⁰ flexible displays,^{121,122} and flexible solar cells.^{123,124} Such “evolution” is also highly desired in healthcare applications. This emerging trend has driven the growing of point of care (POC) biosensor market, resulting in plenty of low cost and portable flexible biosensor designs.^{48,125} More importantly, flexibility and stretchability are necessary features for designing wearable and implantable devices for the fact that living organisms are naturally curvilinear, soft, and flexible.

The realization of 2-D PANI nanostructures as biosensors has been successfully demonstrated in the second chapter of this thesis. It is noteworthy that another advantage of using 2-D PANI nanostructure over 1-D nanowire is its better compatibility with flexible designs associated with its thin film nature. Flexible substrates, as an essential part in flexible designs, provide the basic mechanical strength and flexibility for the devices. The device developing

procedures are also highly dependent on the physical and chemical properties of the flexible substrates. Commonly used flexible substrates such as polyimide (PI), polyethylene terephthalate (PET), and cured polydimethylsiloxane (PDMS) are suitable for FET based electrical biosensor designs due to their excellent electrical resistivity, mechanical flexibility and sufficient chemical stability. In particular, their good resistance to acid makes them compatible with constructing 2-D PANI nanostructures using chemical synthesis. In light of this, in this chapter, the development of 2-D PANI nanostructure based flexible field-effect-transistor (FET) biosensors are presented. Thermally imidized PI films were chosen as the flexible substrate because of its high glass transition temperature (T_g) and easy-to-handle feature compared to other flexible substrates. PET films were also used due to their easy-to-get feature. The 2-D PANI nanostructures were prepared through a combination of conventional CMOS (Complementary Metal–Oxide–Semiconductor) compatible microfabrication techniques with a well-controlled chemical synthesis method.^{126,127} The PANI nanostructure features small size, high reproducibility, large surface roughness, and good compatibility with flexible design. B-type natriuretic peptide (BNP), an important cardiac marker was used to determine the sensing performance such as limit of detection and specificity of the devices.

4.2 EXPERIMENTAL

In this section, fabrication processes of PI and PET based PANI layer biosensor devices including PI film synthesis, electrodes and PANI layers patterning, surface functionalization and microfluidics integration are described. Issues such as, PET/metal adhesion, PI film thickness, lift-off and chemical polymerization are reviewed and optimized.

4.2.1 Chemicals

Polyethylene terephthalate (PET) film (100 μ m thickness), silicon elastomer base and curing reagent were purchased from Fisher scientific. Polyamic acid, adhesion, 1-ethyl-3-(3-dimethylaminopropyl) carbodiimide (EDC), N-Hydroxysuccinimide (NHS), aniline monomer, bovine serum albumin (BSA), perchloric acid (70%), ammonium persulfate ((NH₄)₂S₂O₈) were purchased from Sigma Aldrich. Fluorescent-dye-labeled aptamer (5'-GGGGCACGTTTATCCGTCCCTCCTAGTGGCGTGCCCC-3') was synthesized by Integrated DNA Technologies. Mouse anti- B-type natriuretic peptide (BNP) monoclonal antibodies were purchased from Abcam. Phosphate buffer solution (PBS, pH 7.4) was used to prepare the BSA, EDC, NHS, and BNP solutions with different concentrations.

4.2.2 Optimization of Electrodes Patterning on PET Substrates

The electrodes were patterned onto PET substrates through a standard lithography/lift-off process. To be specific, a PET film was cut (smaller than 4 inch wafer) and fixed onto a four-inch holder wafer. SC1827 photoresist was first employed to accomplish the lithography process. During soft bake, the PET films tend to bend due to their lack of dimensional stability during heating, which dramatically reduces the effect of soft bake. To overcome this, a sandwich-like heating process was applied by putting the PET film in between two four-inch wafers while heating on a hot plate. This method can both assure the heating uniformity as well as keep the PET film flat for future procedures such as lithography alignment. After lithography was done, e-beam evaporator was used to deposit metal on top of the substrate and acetone lift-off was utilized to form the final structure of the electrodes.

The major challenge of electrodes patterning is the low adhesion between PET and metal. Though many flexible devices on PET substrates have been demonstrated, devices with small feature-size (several microns) electrodes patterning on PET are seldom reported. This particular challenge is mostly expected in lift-off process since a lift-off result is highly dependent on the adhesion between metal and substrates. To investigate this, gold only (Au), gold with titanium as adhesion layer (Au/Ti), and gold with chromium as adhesion layer (Au/Cr) were tried separately. The reason for using gold as the electrode material is that gold is known for its great conductivity, stability and biocompatibility. Figure 20 shows the comparison of three different results of 2 hours lift-off followed by 5 seconds of ultrasonic cleaning. It is obvious that Au/Cr/PET possesses much higher adhesion than the other two. However, high magnification microscope image reveals that the uniformity of Au/Cr/PET lift-off was still poor. The gap distance, which are supposed to be 10 microns, showed a large variation with very bad repeatability.

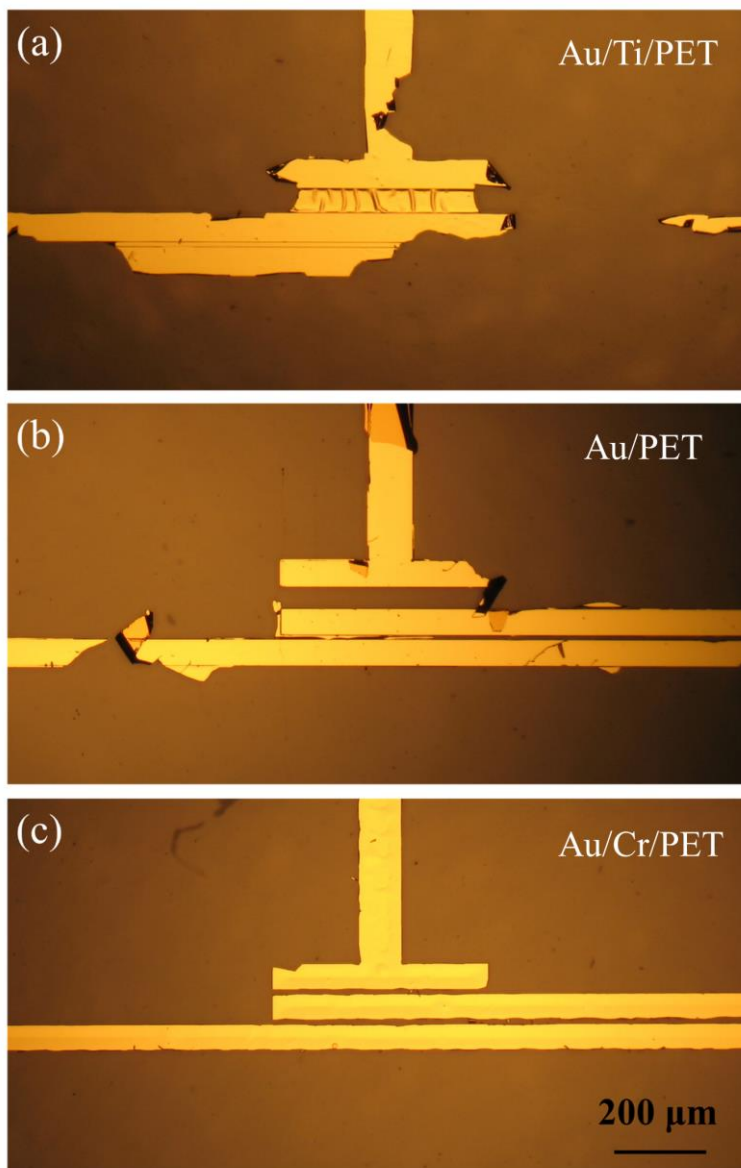


Figure 20. Electrodes patterned on PET substrate. (a) Au/PET (b) Au/Ti/PET (c) Au/Cr/PET.

To further improve the lift-off uniformity and reproducibility, a bilayer lithography process was introduced to replace the single layer standard lithography. Figure 21a explains how bilayer lift-off works. LOR-5B, a resist that is not dissolvable in acetone but dissolvable in developer, was utilized to create the undercut structures together with the photoresist S1805. The difficulty here is to precisely control the size of the undercut which highly depends on the LOR

soft-bake temperature and developing time. Typical soft-bake temperature for LOR-5B is over 170 °C, which is too high for PET to survive, while low temperature baked LOR dissolves much faster in developer compared with that baked in high temperature. After many attempts, a set of highly repeatable parameters for low temperature (115 °C) bilayer lithography process was established. With the help of the undercut structures, the lift-off of wafer-size Au/Cr/PET was able to be completed within one hour without any help of ultrasonic cleaning. An optical microscope image of the highly uniform lift-off result is shown in figure 21b. This method was then verified to be useful for other flexible substrates.

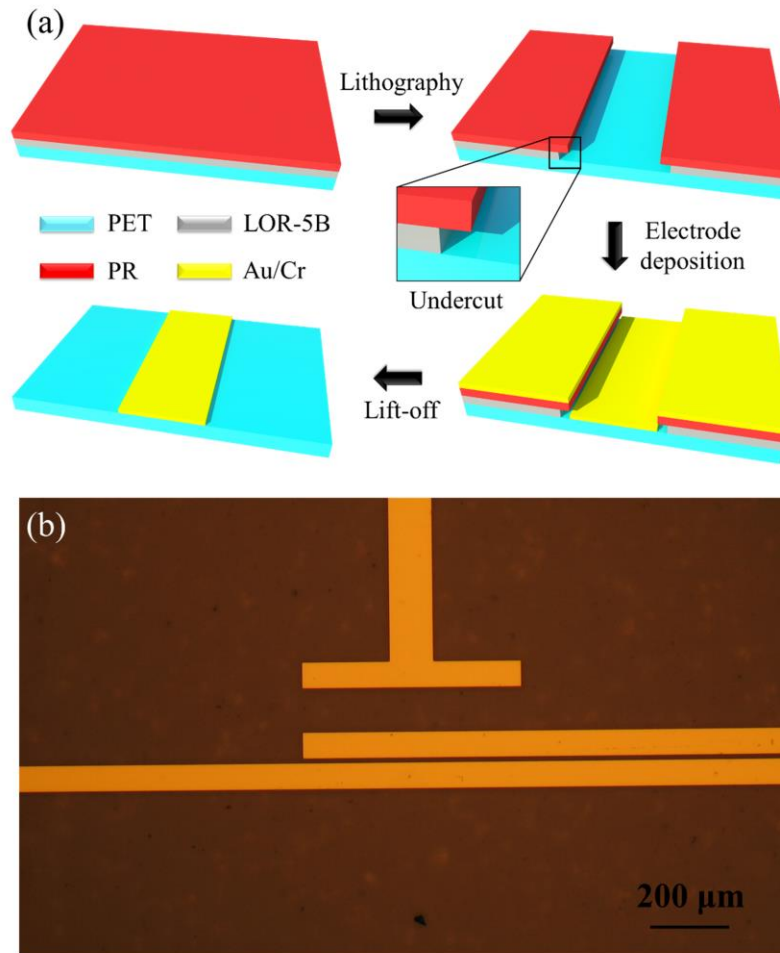


Figure 21. Optimization of electrodes patterning with bilayer structure. (a) Illustration of the bilayer process. (b) Microscope image of bilayer developed electrodes on PET substrate.

4.2.3 Patterning of 2-D PANI Layers

The same method to pattern micro-size 2-D PANI layers for nonflexible devices was utilized here for flexible ones. First, a low temperature bilayer (LOR-5B and S1805) lithography process was performed to define the patterns of PANI layers. The samples were then immersed in 180 mL of 0.35 mol/L aqueous HClO_4 solution. 0.91 mL of aniline monomer was added into the HClO_4 solution, and the whole solution was kept stirring at 400 rpm for 30 min in an ice bath to form a uniform mixture. In a different beaker, 0.6845g of oxidant $(\text{NH}_4)_2\text{S}_2\text{O}_8$ (APS) was dissolved in 20 mL of aqueous HClO_4 solution and cooled to $\sim 0-5^\circ\text{C}$ in a freezer. The polymerization was initiated by combining the two solutions. The synthesis time used is 1.5 hours and the PANI film with thickness around 80 nm can be obtained. The samples were then taken out from the reaction beaker, washed with DI water three times and immersed in acetone for 10 min to lift-off the undesired PANI film.

4.2.4 Preparation and Optimization of PI Substrates

Unlike PET, PI films were prepared through a high temperature imidization process.¹²⁸⁻¹³⁰ The reason for not using prefabricated PI films is that thermal imidized PI will stay on top of a wafer during the whole process which makes device fabrication processes such as alignment much easier compared with PET. Three wafers (marked as 1, 2, 3) with 500nm thick of SiO_2 were cleaned and tried for PI synthesis to investigate the adhesion of poly(amic acid) with different surfaces. Adhesion layer (glycidyl methacrylate) was first coated on the front side of wafer 1. Poly(amic acid) were then spin coated onto both the front side of wafer 1 & 2, and the back side of wafer 3 at 800 rpm. The results showed that clean SiO_2 behaves like a “hydrophobic” surface

to poly(amic acid) which is not suitable for PI synthesis, while poly(amic acid) was able to cover uniformly on wafer 1 and 3 due to the adhesion layer on wafer 1 and the rough Si surface of wafer 3. Wafer 1 & 3 were then put into an oven for thermal imidization. The molecular structure of poly(amic acid) and the imidization mechanism are shown in figure 22. Decisive factors for achieving successful (close to 100%) imidization include a nitrogen environment and a well-controlled temperature. Oxygen can break the long chains of the PI and make the film brittle. To prevent that, the oven was kept flowing with nitrogen in to keep a relatively low-oxygen environment. The utilized thermal cycles contained several steps: the poly(amic acid) mixtures were first heated up to 100 °C with a ramp of 5 °C/min and held for one hour; then the temperature increased from 100 °C to 200 °C and held again for one hour; finally, the mixtures were heated from 200 °C to 300 °C, held for another hour and slowly cooled to room temperature from 300 °C. After curing, thin yellow films were observed on wafer 1 and 3, which indicated that PI films were successfully synthesized. The following steps including electrode patterning and PANI polymerization were the same as PET substrates.

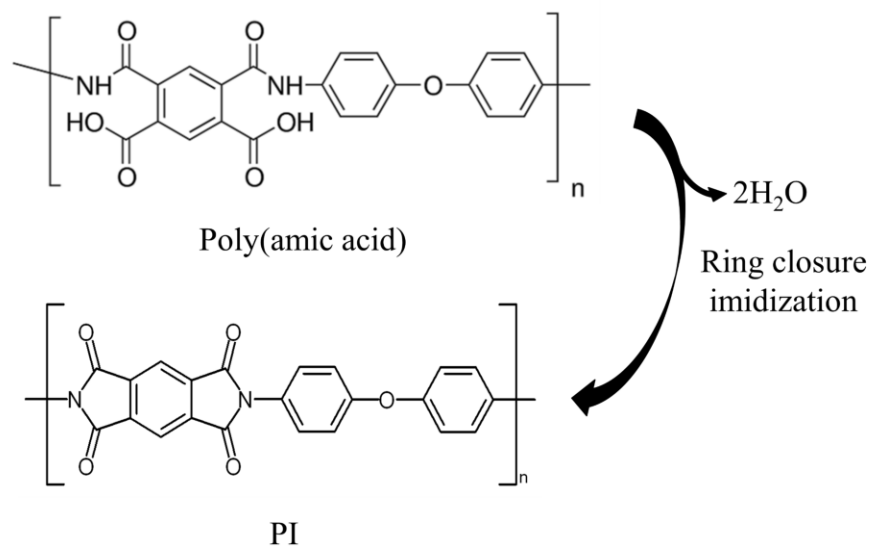


Figure 22. Molecular structure of poly(amic acid) and the imidization mechanism.

One crucial step is to debond PI films from wafers without damaging them and keep reusing the wafers. Some debonding methods such as applying buffer layer have already been demonstrated.¹³¹ In this experiment, wafer 1 showed great bonding with PI film during fabrication processes, however, the additional adhesion layer made it difficult to strip PI film off without damaging it. On the other hand, PI on wafer 3 can be easily stripped off after polymerization without any complex debonding method. Figure 23 shows the PI film on wafer 3 before (figure 23a) and after (figure 23b) debonding.

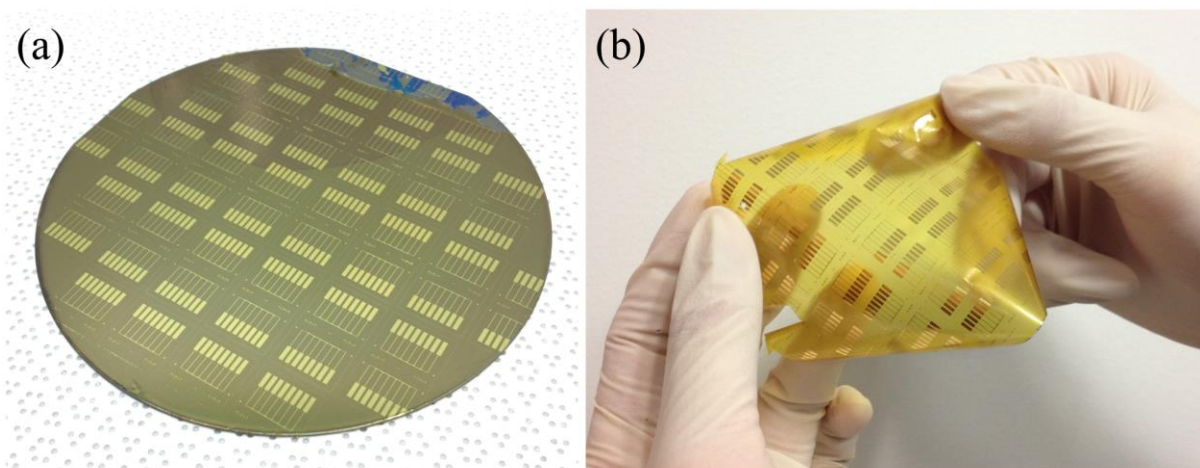


Figure 23. (a) Single layer PI flexible devices before debonding. (b) Single layer PI flexible devices after debonding.

Though electrodes were successfully patterned on PI film, the extremely thin (<10 microns) PI film made it much difficult to be applied in biosensor use. Thickness optimization was then carried out to improve PI film's basic mechanical property. The thickness of PI mostly depends on the viscosity of poly(amic acid) and cannot be significantly increased by changing the spinning rate. Therefore, a three-layer PI synthesis was employed. Specifically, two wafers (marked as A, B) were used as PI holders. Instead of applying adhesion layer, the front side of

wafer A was first etched by using reactive-ion etching (RIE) (pressure at 15 mTorr; RF power at 200 watts; CHF_3 flow at 23 sccm; O_2 flow at 2 sccm; etching time: 1 min) to create a relatively rough SiO_2 surface. The first layer of poly(amic acid) was spin coated on the front side of wafer A and the back side of wafer B at 500 rpm. Thermal curing was introduced afterwards. Different from single-layer PI process, the curing temperature was set up to slowly decrease to room temperature after being held at 200 °C for 1 hour. Then the second layer of poly(amic acid) was spin coated and cured in the same way on top of the first layer. The reason for not using 300 °C is to increase the bonding between the first and second layer since they were not fully imidized. After the third layer was spin coated on, the same thermal curing process as for single-layer PI was conducted to fully imidize all three layers into one thick film. The three-layer PI appeared dark brown and possess excellent mechanical property. The result also showed that wafer A (plasma etched SiO_2) exhibited better adhesion compared with wafer B (rough Si). An image of the three-layer PI film on wafer A is shown in figure 24.

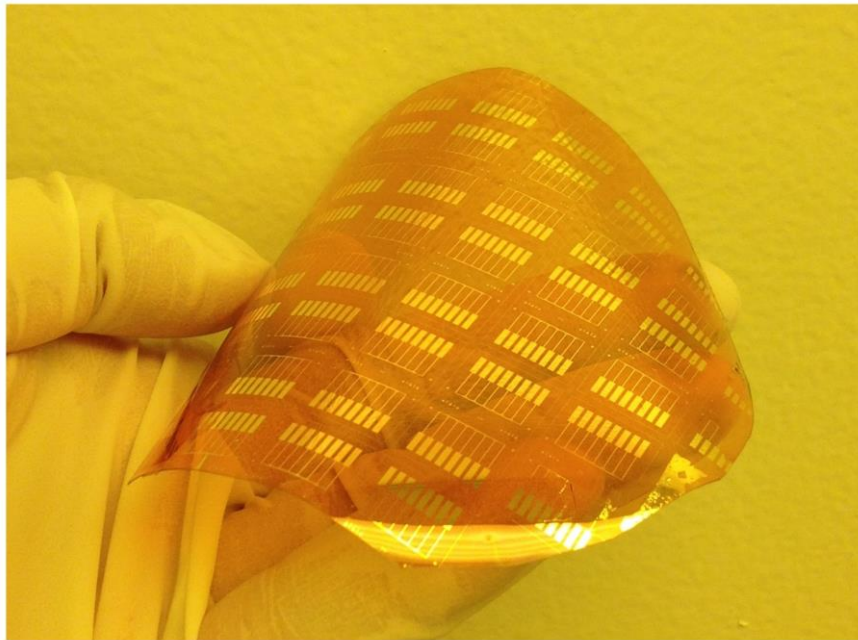


Figure 24. Three-layer PI flexible devices with sufficient mechanical strength after deboding.

4.2.5 Surface Functionalization of PANI

The same functionalization method using EDC and NHS was applied here for flexible devices. 2 μ L of PBS solution containing 100 μ g/mL of B-type natriuretic peptide (BNP) antibody was first added into a micro tube. 49 μ L of both PBS solutions with 0.1M EDC and NHS were added into the same micro tube. The solution was then shaken for 15 seconds to form a uniform mixture, and added onto PANI at room temperature. After 4 hours, the functionalized PANI nanostructures were then thoroughly rinsed with DI water to remove physically adsorbed antibodies. Finally, 200 μ g/mL bovine serum albumin (BSA) was dropped onto PANI nanostructures for 30 minutes to block the free sites in order to prevent possible nonspecific adsorption of other biomolecules.

4.2.6 Integration of Microfluidic Channels

A PDMS microfluidic device with a microns-thick channel (1cm \times 1mm \times 100 μ m) was fabricated using the same method described in 2.3.3. In order to make the microfluidic device sufficiently flexible, the thickness of the mixture of silicon elastomer base and curing reagent was controlled less than 3 mm. The single microfluidic device was adhered to the flexible device with the channel right on top of the PANI films by using glue as illustrated in figure 25a. Each device has an array of 6 individual and identical 2-D PANI nanostructures which can be fully covered by the microfluidic channel. The images of microfluidic integrated flexible devices are shown in figure 25b & c. Microfluidics tubing was used as inlet and outlet. The devices exhibit sufficient flexibility due to the good flexibility of PDMS.

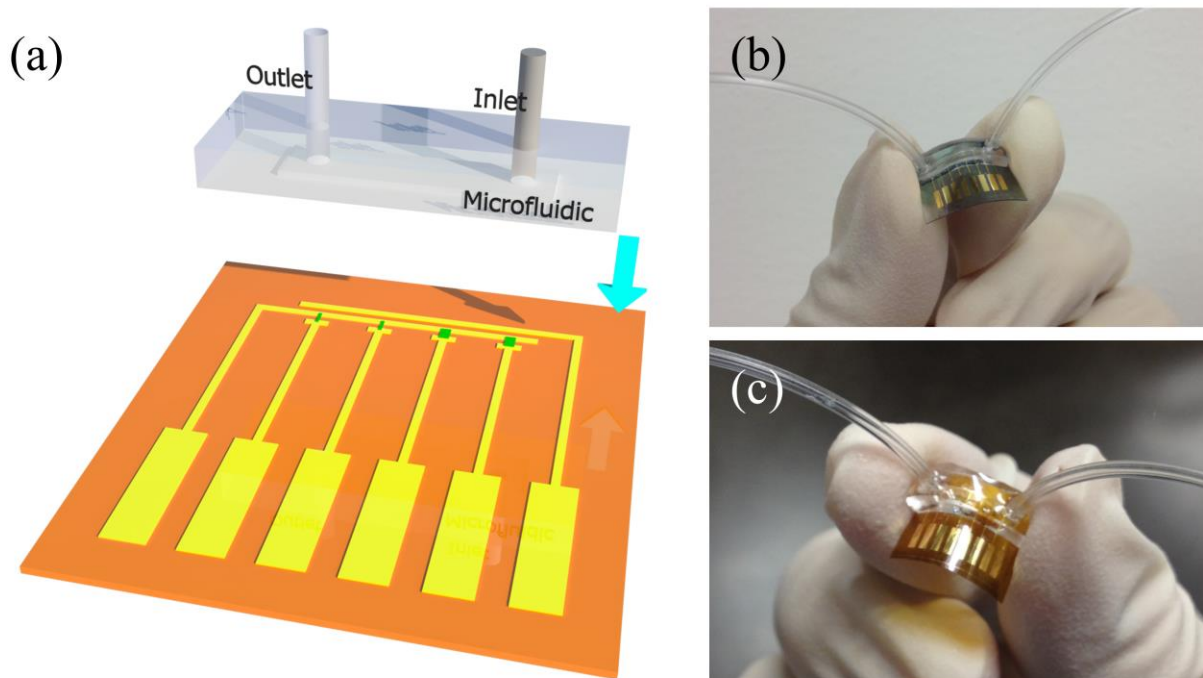


Figure 25. Integration of a microfluidic to the device. (a) The microfluidic channel is located right on top of a 2-D PANI nanostructure array. (b) A microfluidic integrated PET biosensor. (c) A microfluidic integrated PI biosensor.

The device shows good flexibility due to the flexible nature of PET, PI and PDMS.

4.3 RESULTS AND DISCUSSION

In this section, experimental results such as surface morphology study of PANI, electrical characterization of bending device, and BNP biomarker detections were presented. Due to the relatively lower yield of PET devices caused by their significant thermal expansion, PI based flexible devices were used in reproducibility tests.

4.3.1 Surface Morphology Study of 2-D PANI Layers on Flexible Substrates

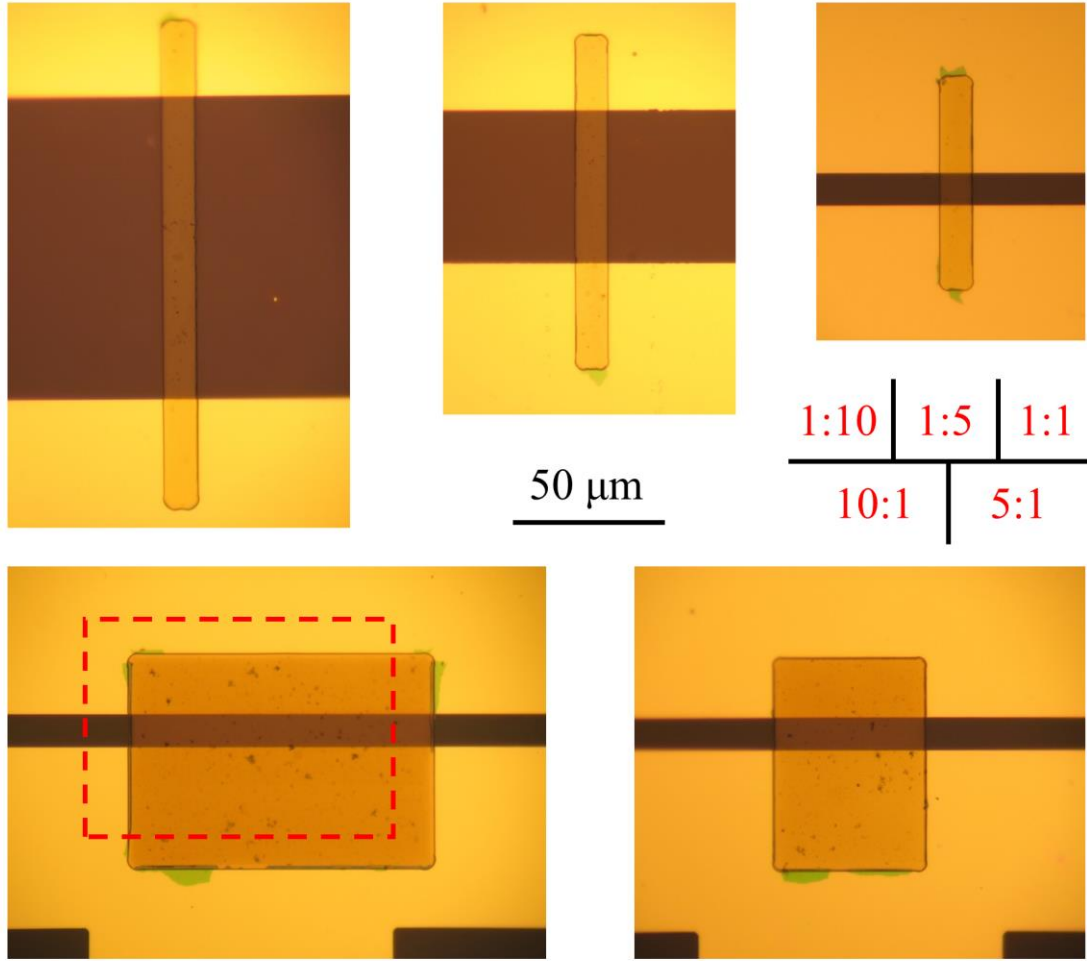


Figure 26. Different dimensions of 2-D PANI films on PET substrate.

Five different dimensions of 2-D PANI films were patterned and the microscope images of those structures on PET substrate are shown in figure 26. The rectangular PANI films cover across the drain and source electrodes while the non-PANI-covered area is all shrouded by LOR-5B, an insulating lift-off resistor. The LOR layer here not only works as an improvement in PANI lift-off procedure which was mentioned before, but also acts as an insulating layer that can prevent ion solution directly connecting drain and source electrode. The ratio shown in figure 26

indicates the length-to-width ratio of the part that does not contact with electrodes. It is noticeable that the 10:1 2-D PANI film shifts a lot from its correct position (red box). When baked over 100 °C, the PET film, due to its low heat resistance and relatively high thermal expansion coefficient, will shrink which can cause the device patterns to shift (misalignment). The farther the pattern is away from the center of the mask, the larger the shift is. PI, on the other hand, does not have such problem due to its good thermal stability.

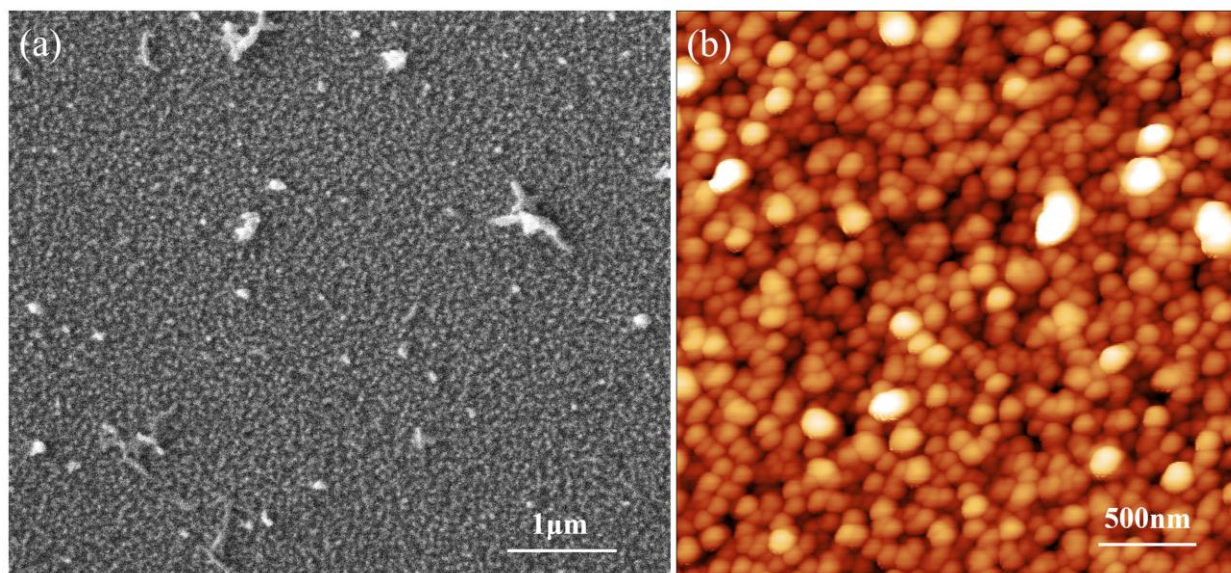


Figure 27. PANI surface characterizations. (a) An SEM image of the 2-D PANI nanostructure surface. The PANI surface was formed by nanogranular structures. (b) AFM result that shows the detail surface morphology of the 2-D PANI nanostructure. The average diameter of the nanogranular structures is around 100nm which dramatically increases the surface area by over 50% compared with flat surface

The morphology of PANI film on flexible substrate was also study by both SEM and AFM measurement. Figure 27a shows the SEM result of PANI film surface morphology. It can be clearly observed that the surface is extremely rough with nano mountain-like structures. Further analysis on higher magnification AFM result (figure 27b) shows that the surface area of the film is averagely increased by 52% compared with smooth surface due to the roughness. This

result is higher than the average PANI surface area increase measured on SiO₂ wafer surface (46%). We believed that the naturally rougher surface of PET and PI is responsible for this improvement. According to our AFM results shown in figure 28a, clean PET substrate shows much rougher surface than silicon oxide. This feature will further increase the surface roughness of PANI synthesized on top of PET, thus increase the surface binding sites (shown in figure 28b). In addition, higher surface roughness also dramatically increase the volume of Debye sphere surrounded the PANI layer even under same Debye length environment (same solution ion strength). The Debye sphere is twisted in 3-dimension because of the extremely rough surface, and may overlap in trenches that are small enough (shown in figure 28b). This may result in much less antibody-antigen binding being screened out. Hence, the sensitivity is again further improved.

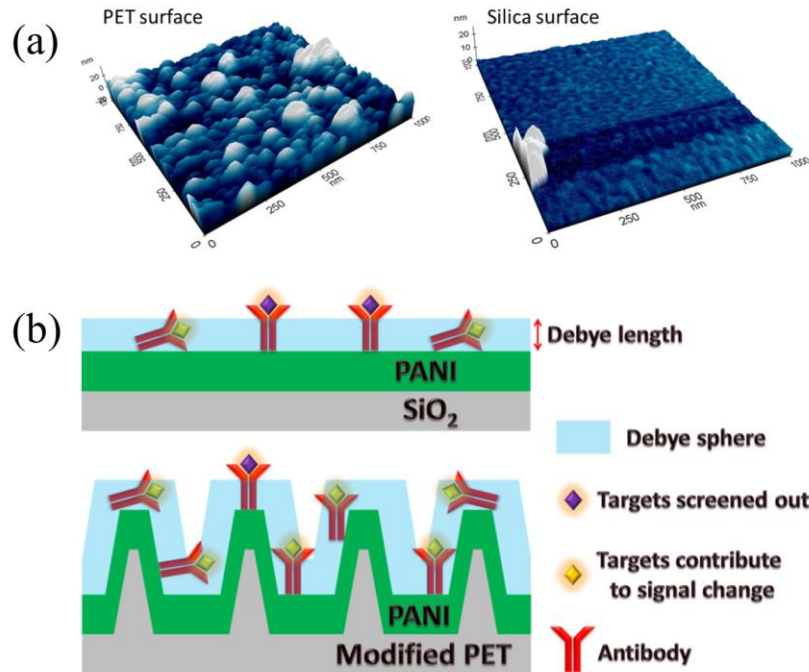


Figure 28. (a) 3D view of AFM results of clean PET and silicon oxide surface. (b) Illustration on how surface roughness increases the sensitivity of the PANI FET biosensor.

4.3.2 Electrical Characteristics of Bendable 2-D PANI Layers

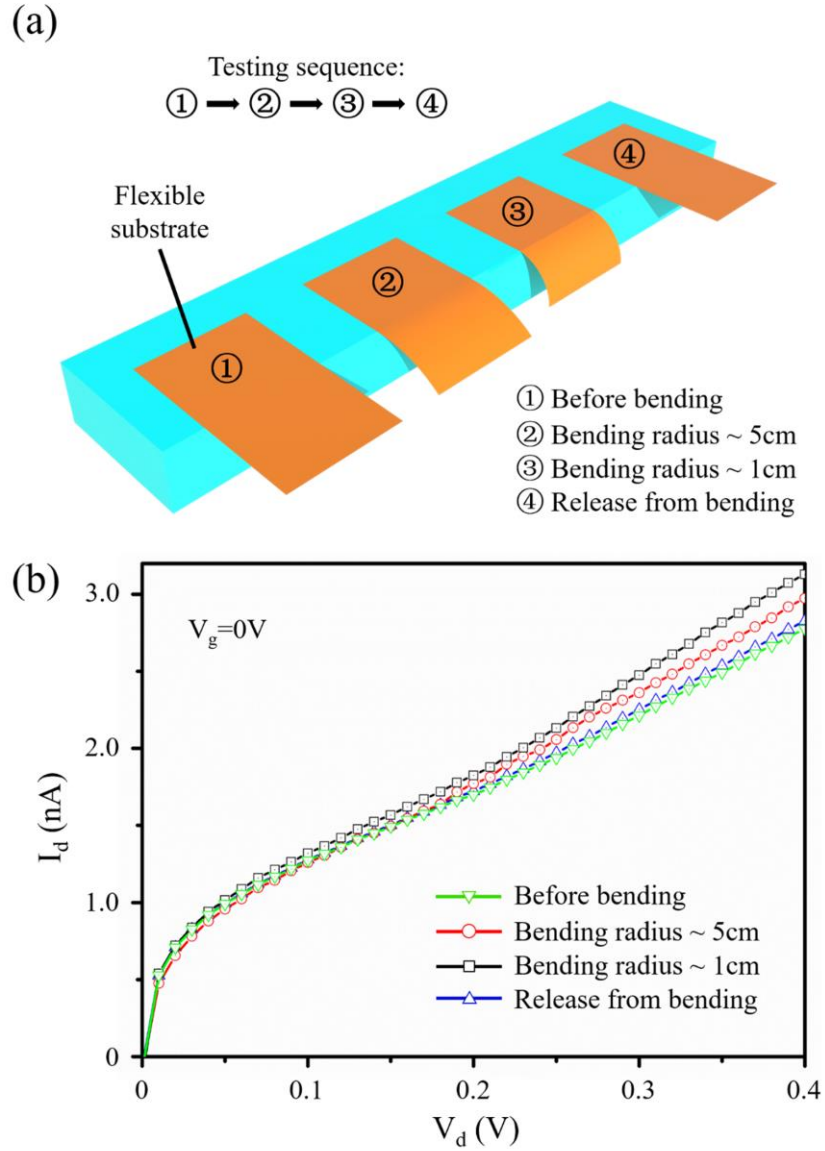


Figure 29. Device resistance measurements under bending conditions. (a) Illustration of the bending test sequence: first, the device was fixed at the edge of a step and measured under no bending condition; then the device was bent and measured with the bending radius around 5cm and 1cm, respectively; finally the device was released from bending. (b) V_d - I_d responses corresponding to four bending condition. V_g was fixed at 0V, and I_d was obtained by sweeping V_d from 0V to 0.4V. The current changes were small and proportional to the bending degree. This result proves the good compatibility of 2-D PANI nanostructure with flexible designs

One key feature for flexible devices is that they can work under deformation conditions such as bending or stretching without large signal variations. Since the performance of the 2-D PANI nanostructure biosensor highly relies on the conductivity of the PANI nanostructure, FET measurements were conducted when the PANI was under different bending conditions. To achieve this, a PI based biosensor device was attached on a thin copper film which can be bent to desired shape. The bottom part of the device that contains electrodes was fixed on the edge of a box to create enough space for device bending. The 2-D PANI nanostructure was covered with PBS 0.01X buffer solution during the test. As illustrated in figure 29a, the FET behavior was first recorded under no bending condition. Subsequently, the device was bent with different bending radius and the FET behaviors were measured respectively. Finally, the device was released from bending. Figure 29b shows the V_d - I_d behaviors (V_g was fixed at 0V) measured with probe station (Signatone s-1160) under four different conditions correspondingly to those in figure 29a. Notably, when the device was first bent with a bending radius around 5cm (red line), the drain current slightly increased compared with unbent condition (green line). As the bending radius further decreased to 1cm, larger drain current was observed (black line) which indicates that the conductivity of PANI nanostructure increases with the increase of surface tension created by the bending. Finally, when the device was released from the bending (blue line), the current returned to almost the same as original.

The mechanism behind this conductivity change can be briefly explained by the changing of molecular structures during bending. The bending shown in figure 29a creates tensile force on the PANI film, which makes the originally completely nonaligned molecule chains more aligned and elongated.¹³² Thus, the conductivity along the tensile direction can be enhanced.¹³³ We have

tested the device with bending radius up to 1cm due to the limitation of PDMS microfluidic bendability on the flexible substrate and obtained that the conductance of the 2-D PANI nanostructure varies up to 20% of the original conductance. However, this 20% variation may meet the requirement for flexible biosensor application, and further investigation of the conductance changes upon bending should be done for fully utilizing the device flexibility. More significantly, though the conductivity of the PANI film changes with bending, the current variation is highly dependent on the degree of bending which makes it easily controllable and predictable. Based on these results, we can conclude that the 2-D PANI nanostructures show excellent compatibility with flexible designs.

4.3.3 Fluorescence Tests of Functionalized PANI

It is always imperative to assure the successful surface functionalization before testing. However, it is difficult to observe fluorescence directly from PANI film on PET or PI substrates due to their strong autofluorescence property.¹³⁴ Therefore, fluorescent tests of PANI film synthesized on silicon wafer were used to verify the feasibility of the PANI functionalization method. Alexa Fluor™ 488 Conjugate aptamers (excitation at 495 nm and emission at 519 nm) were functionalized on PANI surface using the same method introduced before. Two filters (Filter 1: excitation spectrum from 450 nm to 500 nm, emission spectrum from 500 nm to 550nm; Filter 2: excitation spectrum from 540 nm to 560 nm, emission spectrum from 580 nm to 650nm) were used to examine the fluorescent results. Figure 30 shows three images taken using the same exposure time. As shown in figure 30a, clear green light which corresponds to 519 nm can be observed on the functionalized area using Filter 1, while no light was observed with the same area using Filter 2 (figure 30b). This result rules out the possibility that the light is from back

reflection. By further comparing with unfunctionalized area in figure 30c, we can confirm that the green light is the fluorescent emission from functionalized aptamers, which indicates the feasibility of the surface functionalization method.

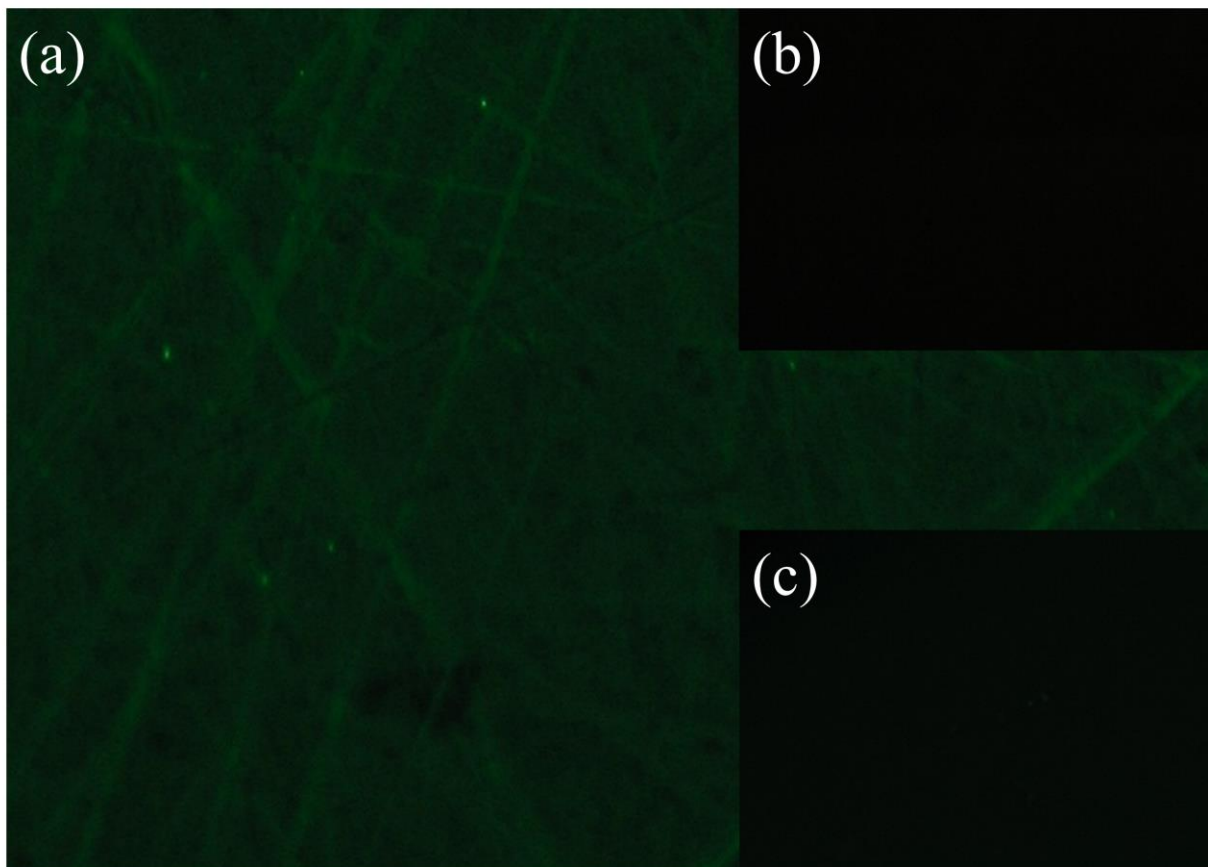


Figure 30. Fluorescent images taken by optical microscope under same exposure conditions. (a) Functionalized area using the correct filter, clear green light corresponding to the fluorescent wavelength was observed. (b) Functionalized area using the control filter, no notable fluorescent light observed (c) Unfunctionalized area using the correct filter, no notable fluorescent light observed

4.3.4 BNP Biomarker Detections

The proof-of-concept tests of flexible 2-D PANI nanostructure sensor were conducted using PI based sensor to detect BNP biomarkers. BNP biomarkers with concentrations ranging from

100pg/mL to 1ng/mL were used, and the specificity of the device was demonstrated with high concentration nonspecific targets (BSA, IgG). All biomarker solutions were prepared with phosphate buffered saline (PBS) 0.01X buffer solution to assure a same Debye length condition.³⁵ The test was initiated with the collection of background current response by pumping PBS 0.01X solution into the microfluidic channel via a syringe pump. I_d - V_d measurement was read three times using the linear sweeping method described previously. After a stable current signal was obtained, sample solutions containing BSA and IgG were pumped in and tested using the same condition. As shown in figure 31a, the current responses of PBS, BSA, and IgG are indistinguishable despite the high concentrations of the nonspecific targets. After that, samples containing different concentrations of BNP biomarkers were transferred into the device successively. Clear increases of the drain current read can be observed in figure 31a and the current increases corresponded to the increase of BNP concentrations from 100pg/mL to 1000pg/mL. These results are consistent with our previously reported results from the silicon wafer based biosensors,¹³⁵ which not only indicates that the 2-D PANI nanostructure biosensor is capable of specifically recognizing BNP biomarker, but also shows its potential ability of quantifying the different BNP concentrations.

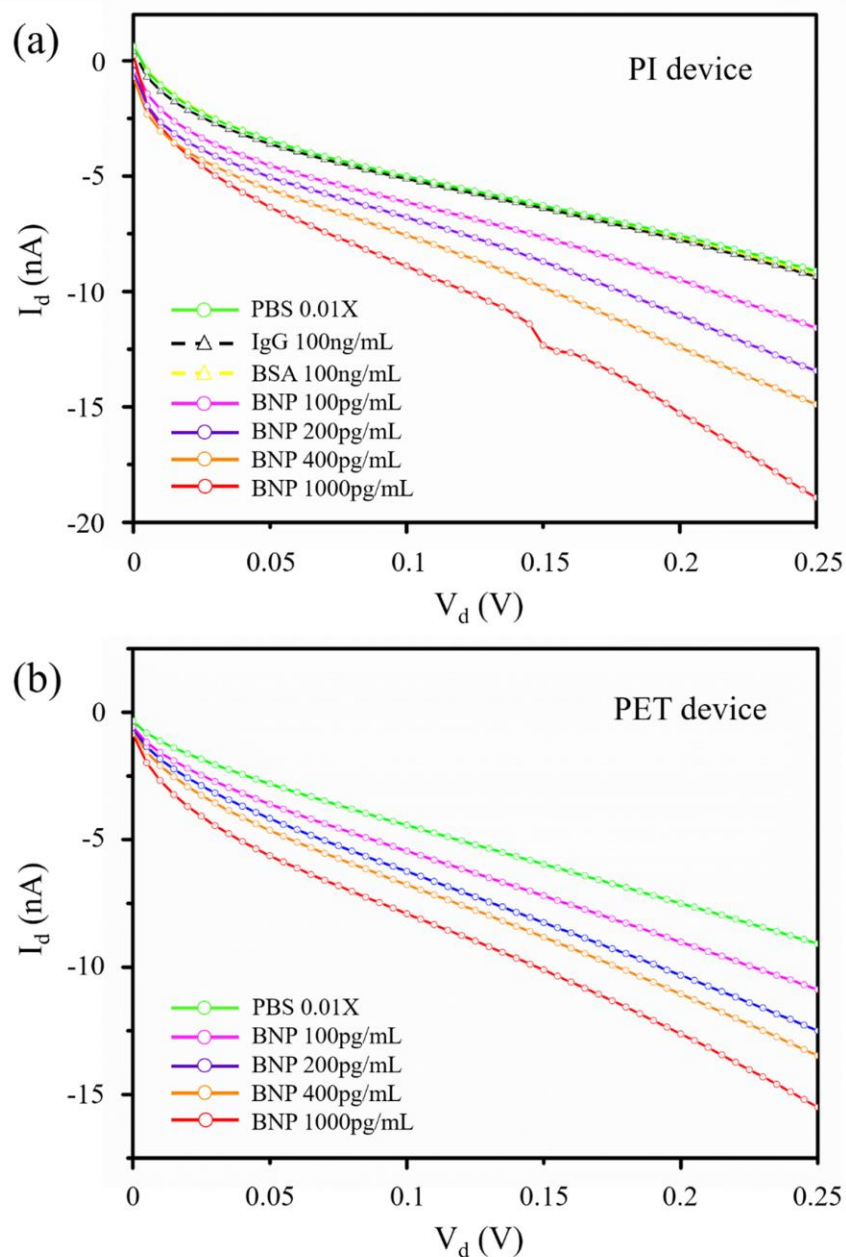


Figure 31. Device biomarker sensing results using PI (a) and PET (b). Biomarker and specificity test result of a 2-D PANI nanostructure on detection different concentration level of BNP among nonspecific targets (BSA and IgG). PBS buffer solutions that contained high concentration of BSA and IgG showed similar current responses as the PBS background sample. The drain current increased distinctly as sample solutions contained different concentrations of BNP were pumped in. The current changes were consistent with different BNP concentrations.

The detection using PET biosensor device was also performed and showed in figure 31b. The result currents and current changes are all at the same level as PI devices, which are similar compared with nonflexible devices as well. This result is expected since the sensing performance is mostly determined by the chemically synthesized PANI and its surface functionalization.

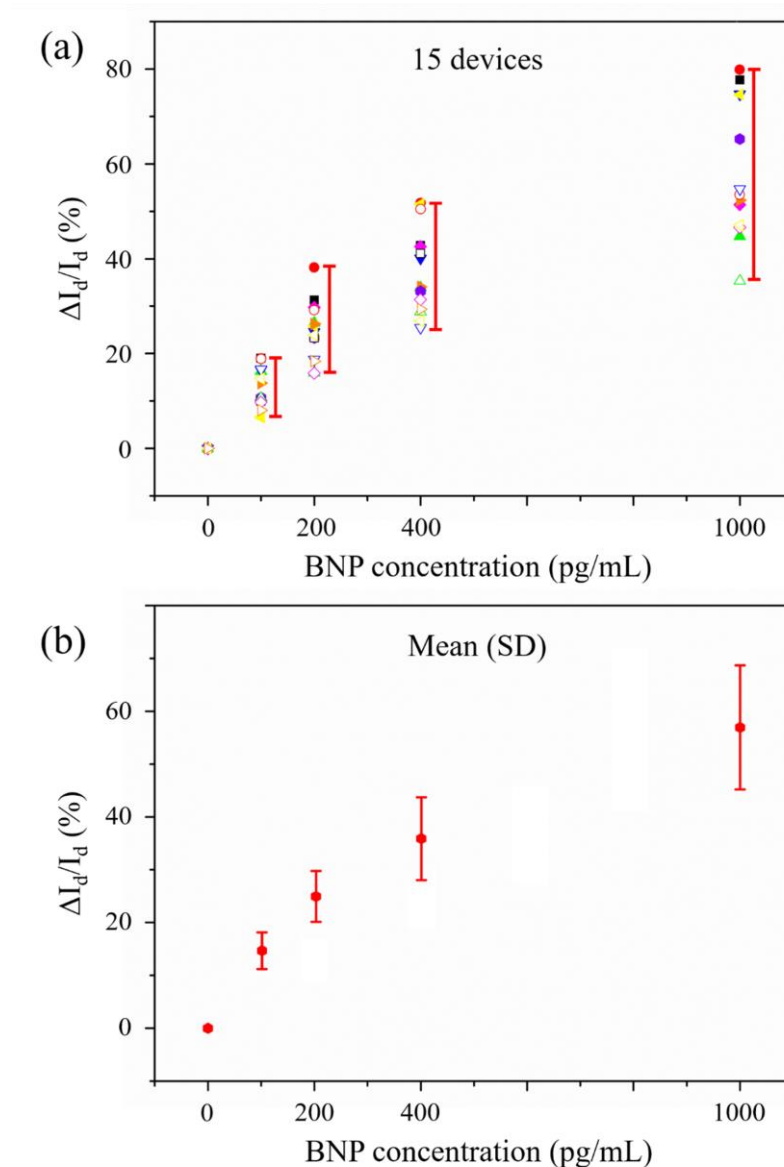


Figure 32. BNP biomarker statistic test results of 15 2-D PANI nanostructure biosensor devices. All devices showed current increase over the increase of BNP concentration. Useful information such as sensitivity can be extracted from these figures.

To investigate the reproducibility of the flexible design, 15 devices were tested one by one under the same condition with PBS 0.01X and BNP biomarkers with concentration ranging from 100pg/mL to 1000pg/mL. All the device performances are shown in figure 32a. The vertical axis represents the drain current response change with respect to the background current measured with PBS ($\Delta I/I$), and the horizontal axis represents different concentrations of BNP biomarkers. All 15 devices showed increase of drain current responses over increasing BNP concentrations which proves the reliability of the devices. Notably, higher concentration shows larger current signal variation. Such result is more distinct in the statistical analysis shown in figure 32b, where higher target concentration detections possess larger deviations. This result likely suggests that multi detections with one device would cause some of the antibodies to lose their activities. More importantly, the sensitivity of the biosensors can be extracted from these figures because of the nearly linear response.

In summary of the sensing results, we found that 2-D based PANI structure possessed excellent and comparable sensitivity with respect to the reported 1-D PANI structure. Similar to 1-D nanowire, the excellent sensing performance of 2-D PANI nanostructure is attributed to its extremely large SA/V ratio. There are two key features of the unique morphology on 2-D PANI nanostructure we believe that contribute to the boost of the sensing performance. First, the large surface area increased by the nanogranular structures provides more surface binding sites for BNP antibodies. According to the antigen-antibody interaction, under equilibrium condition, the concentration of antigen-antibody complex is proportional to the concentration of both antigen and antibody. Therefore, for a fixed antigen (target biomarker) condition, a higher concentration of antibody will increase the concentration of complex on surface, which leads to more charges gating the 2-D PANI nanostructure. Second, higher surface roughness also dramatically

increased the volume of the Debye sphere even under the same Debye length environment (same solution ion strength). Debye sphere describes the volume surrounding the PANI nanostructure outside which the surface bound charges will be screened out and cannot gate the PANI film.³⁵ Since the Debye length in PBS 0.01X at room temperature is $\sim 7.61\text{nm}$, which is much smaller compared to the roughness on PANI surface, this uneven surface also twisted and increased the volume of Debye sphere. Compared with a flat surface, the average distance between bound charges and PANI surface is reduced, i.e., more charges are included in the Debye sphere, thus leading to more charges gating the PANI nanostructure.

4.4 CONCLUSIONS

In this work, we presented a novel approach that combines top-down (microfabrication) and bottom-up (chemistry) techniques to enable the low cost and facile fabrication of two-dimensional PANI nanostructures onto flexible substrates with high throughput and uniformity. The chemical synthesis and following lift-off process facilitated the mass production of PANI nanostructures on large areas, while at the same time offering them with excellent electrical properties, high uniformity, and unique surface morphology. 2-D PANI nanostructure based flexible biosensors were then developed and their outstanding sensing performance was demonstrated by the detection of BNP biomarkers. The sensor devices exhibited high specificity and rapid responses to the target with a very low detection level of 100pg/mL . Electrical measurements under bending conditions showed both controllable conductance changes within 20% and good restorability which also confirmed that the 2-D PANI nanostructures have good compatibility with flexible designs. With more future works focusing on improving the

sensitivity and reliability, the demonstrated devices show great potential for wearable applications.

5.0 DEVELOPMENT OF PANI FILM/NANOTUBES HYBRID NANOSTRUCTURES

5.1 INTRODUCTION

Nanostructured materials have consistently been a popular field of research due to the fact that their high surface-area-to-volume (SA/V) ratio can enable plenty of unique physical and chemical properties including high molecular adsorption, large surface tension force, enhanced chemical and biological activities, and large catalytic effects.⁷⁴ Polyaniline (PANI), as one of the most studied conductive polymers, is also one of the few polymers that has the capability to adopt numerous different nanoscale shapes. In the past two decades, synthesis and characterizations of different PANI nanostructures such as nanofibers,¹³⁶ nanotubes,^{137,138} nanospheres,¹³⁹ and other fascinating nanostructures¹⁴⁰ have been continuously reported. Among them, PANI nanotubes are undoubtedly favored by many researchers because of their unique one-dimensional structure, chemical study merits, and excellent electrical properties which may eventually nourish practical application fields such as sensors and field-effect transistors (FETs).¹⁴¹

Chemically synthesis of PANI nanotubes is usually achieved by oxidizing aniline in acidic environment. In 1994, Parthasarathy and Martin, for the first time, demonstrated the synthesis of PANI microtubes by using a porous polycarbonate template membrane to guide the growth.¹⁴² These sorts of “hard template” methods were later improved and replaced by the so

called “soft template” methods, in which structure directors such as surfactants¹⁴³ or organic acid¹⁴⁴ are introduced. Though the soft template methods do not require a post-synthesis template removal process, it is rather difficult to control the morphology and tubular diameter.¹⁴⁵ In 2006, Trchová and co-workers demonstrated that PANI nanotubes can be synthesized in water with nothing but aniline and ammonium peroxydisulfate (APS).¹⁴⁶ This method limited the number of reagents to two, thus creating a much more simplified chemical reaction model for chemical mechanism study. In this simplified template-free method (STFM), aniline was oxidized and oligomeric products were formed in the first stage of the reaction when the pH is larger than 4. As time went on, the concentration of H₂SO₄, the byproduct from the oxidation, increased which brought the pH down below 4. Consequently, the reaction mechanism changed as aniline started to be protonated to anilinium cation, and large molecular weight PANI began to form. It is thought that the nucleated sites on oligomer crystallites were formed with the stack of the phenazine units. Created PANI chains then began to extend from them and continued to form nanotubular structures due to the hydrogen bonding and ionic interactions.¹³⁸

Despite of the study of the PANI nanotube synthesis is mature, the reported nanotubes were mostly nucleated and grew in the bulk solution for mechanism learning purpose, while direct synthesizing nanotubes on substrates were seldom studied.¹⁴⁶ This situation vastly limits the possibility of utilizing PANI nanotubes for device applications given the fact that directly manipulating nanotubes is rather difficult and always requires resource consuming technology such as electron beam lithography. Hence, it is of great interest to develop a facile and low cost way in order to make use of the excellent electrical and chemical properties of PANI nanotubes. Interestingly, it is noteworthy that during the late stage of the PANI nanotube synthesis (low pH media), PANI film was always forming on the surface where no “template” existed. This matter

of fact provides the possibility to create nanostructures that contain both PANI film and nanotubes. In light of this, herein, we present a facile and template-free method to synthesize a new thin film nanostructure: PANI film/nanotubes hybrid, which is a “pizza” like structure that consists of nanoscale thickness PANI film and PANI nanotubes. This method is a variant from the STFM, in which a typical single reaction is replaced with two separate ones. Less concentration of reagents are needed in this method compared with STFM and no surfactant or organic acid is required. The hybrid possesses unique surface morphology as well as excellent electrical characteristics. In this work, characterizations were first conducted to assure the successful forming of the nanotubular structures. Different synthesis conditions and a variety of substrates were then attempted for optimization purpose. Finally, a proof-of-concept FET device based upon PANI film/nanotubes hybrid was developed and characterized to demonstrate its potential capability in sensor applications.

5.2 EXPERIMENTAL

5.2.1 Chemical and Substrates Preparation

Aniline monomer, perchloric acid (70%), ammonium persulfate (APS) ($(\text{NH}_4)_2\text{S}_2\text{O}_8$) were purchased from Sigma Aldrich. Polyethylene terephthalate (PET) with thickness of 100 μm was purchased from Goodfellow. Gold substrates were fabricated by depositing 3 nm of Ti followed by 80 nm of Au on a SiO_2/Si wafer using an e-beam evaporator.

5.2.2 Synthesis Method

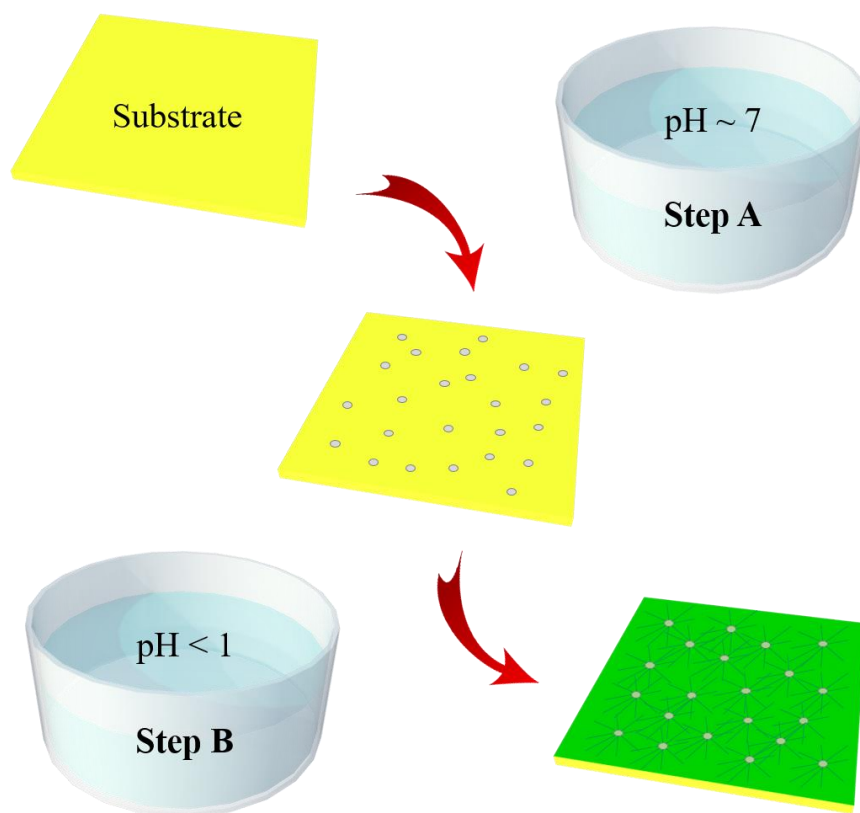


Figure 33. Illustration of the two-step synthesis process. Step A reaction has a starting pH of 7, while the pH in Step B reaction starts below 1.

PANI film/nanotubes hybrid was synthesized through a process of two separate reactions as illustrated in figure 33. Starting pH, as an essential parameter that distinguishes the two reactions, was set as 7 and below 1 for the first (Step A) and second (Step B) reactions, respectively. In the Step A reaction, 0.911 mL of aniline was added into a main beaker with 180 mL DI water and stirred for 30 min to form a uniform mixture in ice bath. Samples which are acting as the substrates for PANI film/nanotubes to grow on were cleaned with acetone followed by IPA and three times of DI water. The substrates were then mounted onto a clean wafer, fixed with scotch

tapes and immersed in the main beaker. In another beaker, 0.6845g APS was dissolved in 20 mL DI water and put in a freezer to cool down to 0~5 °C. The reaction was initiated by adding the APS solution into the main beaker and the temperature was kept at 0~5 °C under stirring condition (200 rpm). The mixed solution gradually turned brown soon after the initiation. In order to observe the formation of the PANI nanotubes and investigate how the reaction time in Step A affects the synthesis of PANI nanotubes, different reaction time ranging from 10 min to 4 hours was conducted. When the reaction was done, all samples were taken out, rinsed with DI water three times and dried with nitrogen.

To continue the synthesis, a dilute method^{110,111} was used which has been demonstrated and commonly used for uniform PANI film synthesis. The preparation of the Step B reaction was similar to the first one. The only difference is that 6 mL of perchloric acid was added into 180 mL of DI water together with aniline monomer to create low pH environment. The reaction was also conducted in ice bath with stirring. Under low pH environment, the mixture solution turned deep dark blue soon after the reaction was initiated which suggests the formation of long chain of PANI. After 4 hours, samples were rinsed with DI water, dried with nitrogen, and ready for characterizations.

5.3 RESULTS AND DISCUSSION

5.3.1 Characterization of PANI Nanotubes

Samples produced through one hour of Step A reaction and four hours of Step B reaction were characterized using both scanning electron microscope (SEM) (Quanta 600 FE-SEM) and

transmission electron microscope (TEM) (JEOL JEM-2000EX TEM) were utilized. Gold was used as the substrate for synthesizing in order to achieve better images with SEM due to its excellent conductivity.

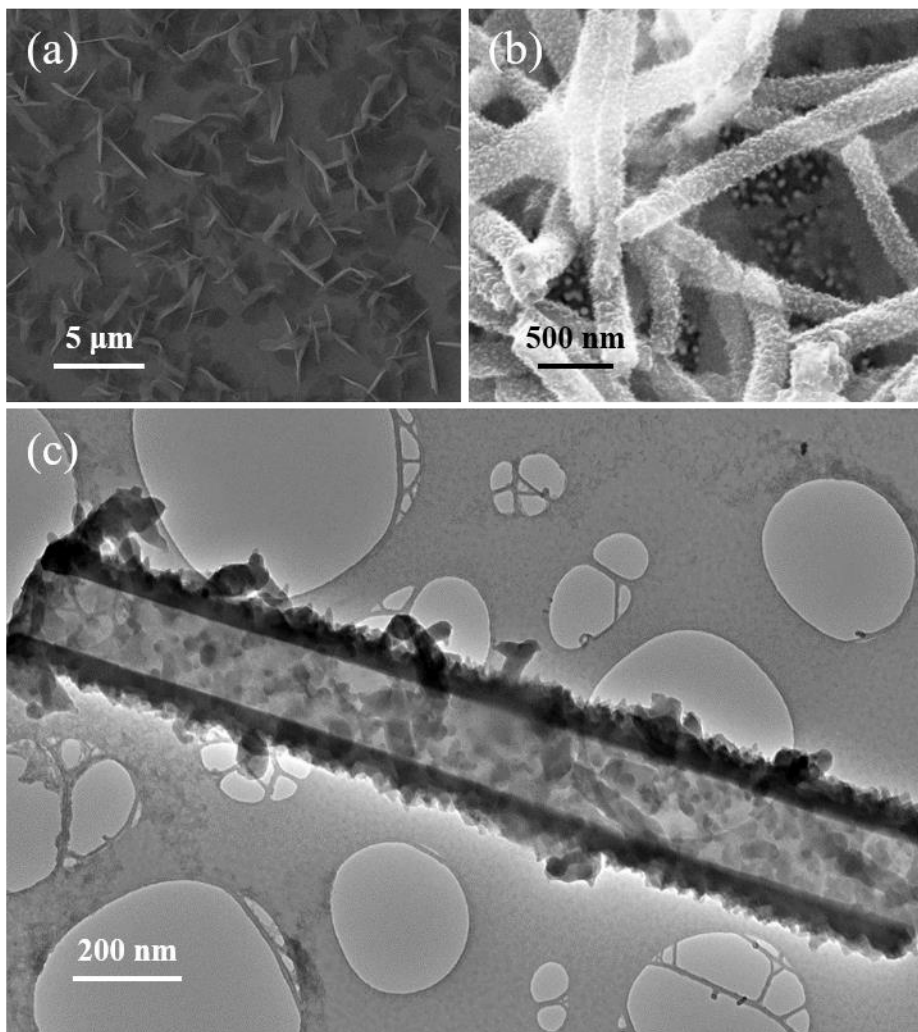


Figure 34. SEM and TEM images of aniline oligomers and PANI nanotubes grown on gold substrate. (a) SEM image of flake-like aniline oligomers formed in Step A. (b) SEM image of PANI nanotubes with a diameter of 300 nm formed after Step B. (c) TEM image of stripped-off PANI nanotube with inner diameter of 200 nm.

Figure 34 shows the characterization results after each reaction. After 1 hour of Step A reaction (figure 34a), flake-like oligomers were first formed on the gold substrate. The grown

oligomers are non-conducting, which was confirmed by the obvious surface charging during SEM. After another 4 hours of Step B reaction (figure 34b), clear high-density of cylinder-shaped nanostructures with an average diameter of 300 nm can be found on the substrate. The grown structures show extremely high surface roughness which is attributed to the nanogranular PANI structure formed in the late Step B reaction. In addition, hollow structures can also be observed on the end of some cylinder nanostructures. Further TEM image (figure 34c) verified the hollow structure with an inner diameter of 200 nm which indicates their nanotubular nature. This result confirms the successful forming of PANI nanotubes. Notably, Step B itself has been well-known and repeatedly demonstrated^{135,147} for large molecular weight PANI film synthesis. However, nanotubes were obtained after Step B instead of bare film with the existence of the oligomers formed in nonacidic media. This also proves that the oligomers formed in Step A reaction act as templates for guiding the growth of PANI nanotubes.

PANI nanotube formed in organic acid (acetic acid) was also conducted as a comparison. The synthesis condition is the same as Step B reaction, and the HClO_4 was replaced by the same concentration of acetic acid. The result SEM images of nanotubes synthesized in acetic acid are shown in figure 35a & b, and figure 35c & d show the nanotubes synthesized using our two steps method in perchloric acid. Two obvious differences can be found. First, strong acid formed nanotubes have extremely rough surface on the tubes, while in organic acid, nanotubes are much smoother. This feature makes strong acid formed nanotubes much useful in applications. Secondly, the size of nanotubes is more uniform in strong acid than in organic acid.

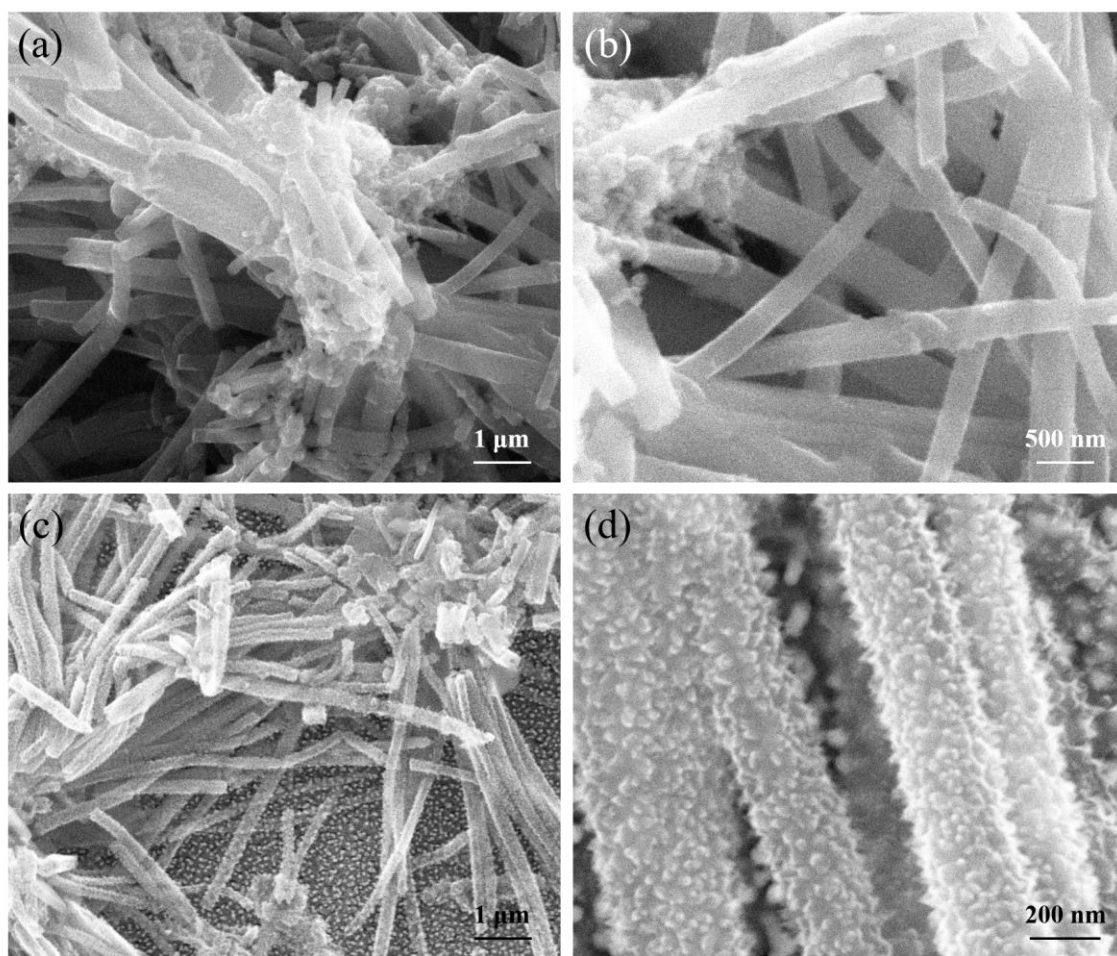


Figure 35. SEM images of PANI nanotubes synthesized in acetic acid (a & b) and perchloric acid (c & d).

5.3.2 Investigation of Synthesis Time in Step A

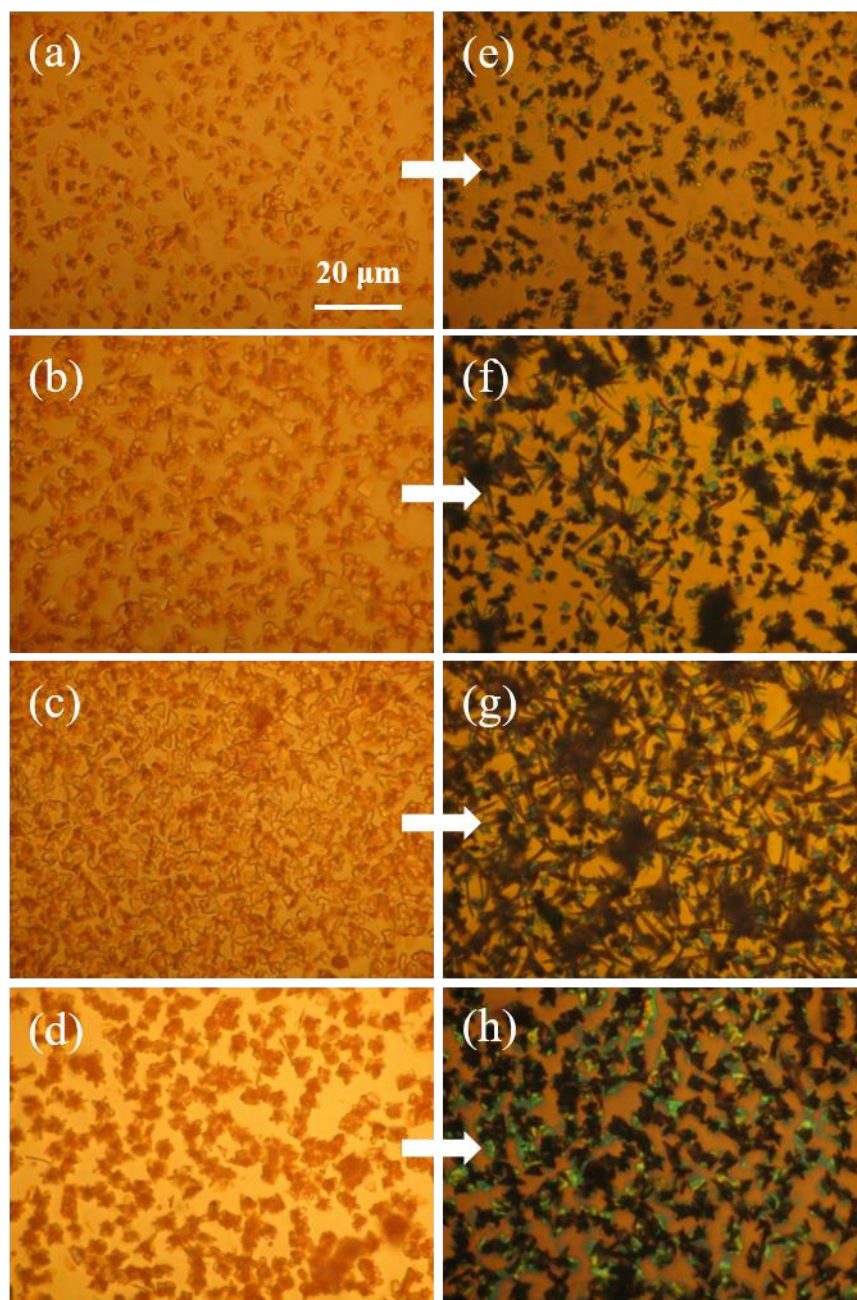


Figure 36. Optical images of synthesis condition optimization results. (a) 10 min in Step A. Small flake-like oligomers were formed. (b) 30 min in Step A. The density and size of oligomers were getting larger. Some oligomers started to evolve into clusters. (c) 1 hour in Step A. The density and size of oligomers kept increasing and reached to maximum. (d) 4 hours in Step A. All oligomers existed in the form of clusters. (e) 10 min in Step A and 4

hours in Step B. No nanotubes sighted. (f) 30 min in Step A and 4 hours in Step B. Some nanotube was found. (g) 1 hour in Step A and 4 hours in Step B. High density of nanotubes were observed (h) 4 hours in Step A and 4 hours in Step B. No nanotube was found.

It is essential to study the condition of PANI nanotube synthesis in order to gain better understanding of the chemical reactions as well as to optimize the synthesis process. In a typical STFM reaction, one key factor for triggering the growth of PANI nanotubes is the drop of pH due to the byproduct H_2SO_4 generated throughout the reaction. The reaction can thus transit naturally from “template forming stage” to “PANI synthesis stage” as the time goes on. However, our method deliberately separates those two stages which requires optimizing the synthesis time in Step A reaction while maintaining the same Step B reaction time. To investigate this, a set of experiments were conducted with different synthesis times in Step A reaction (10 min, 30 min, 1 hour, 4 hours) followed by the same synthesis time in Step B reaction (4 hours). Gold was used as the substrate and images were taken with an optical microscope for all samples after each reaction. As shown in figure 36a-d, aniline oligomers were formed on the gold surface during Step A. With the increased reaction time, both the density and the average size of the oligomers became larger and larger due to the increased oligomer affinity (from figure 36a to c). In addition, some of the oligomers evolved from a two-dimensional flake-like structure into a three-dimensional cluster. However, the oligomers were all turned into the cluster structures after 4 hours of Step A process as shown in figure 36d. The obvious decrease in oligomer density compared with figure 36c may suggest that a long time in Step A reaction could alter the surface affinity to the oligomer from hydrophilicity to hydrophobicity which eventually caused some of them to detach from the substrate. No change can be observed when the reaction time further increased which is different from a typical STFM. This is because of the utilization of the diluted

concentration of both aniline and APS which cannot produce sufficient of H_2SO_4 to trigger the PANI synthesis. Figure 36e-h shows the results of the four samples after completing another 4 hours of Step B. In figure 36e, no nanotube can be sighted on the sample with 10 min of Step A and 4 hours of Step B reactions. Nanotubes began to form when 30 min of Step A was employed (figure 36e), and the largest density of nanotubes was achieved after Step B reaction when 1 hour of Step A was used (figure 36f). It is clear that the nanotubes generated from the oligomers and extended out in every direction. This result agrees with the growing model developed with the STFM.¹³⁸ Surprisingly, however, no nanotube was observed on the sample with 4 hours in Step A (figure 36h). Detailed SEM images of this sample after each reaction were shown in figure 37. Instead of guiding the growth of PANI nanotubes, the oligomers lost their functions as soft templates, and were covered uniformly by large molecular weight PANI formed in Step B reaction. One possible hypothesis is that the three-dimensional clusters of oligomers formed in nonacidic media for a decent amount of time cannot act as templates for PANI nanotubes to grow on. Therefore, based on these results, we can conclude that the forming of the oligomer templates requires optimal time in Step A reaction, which, in our case, is around 1 hour.

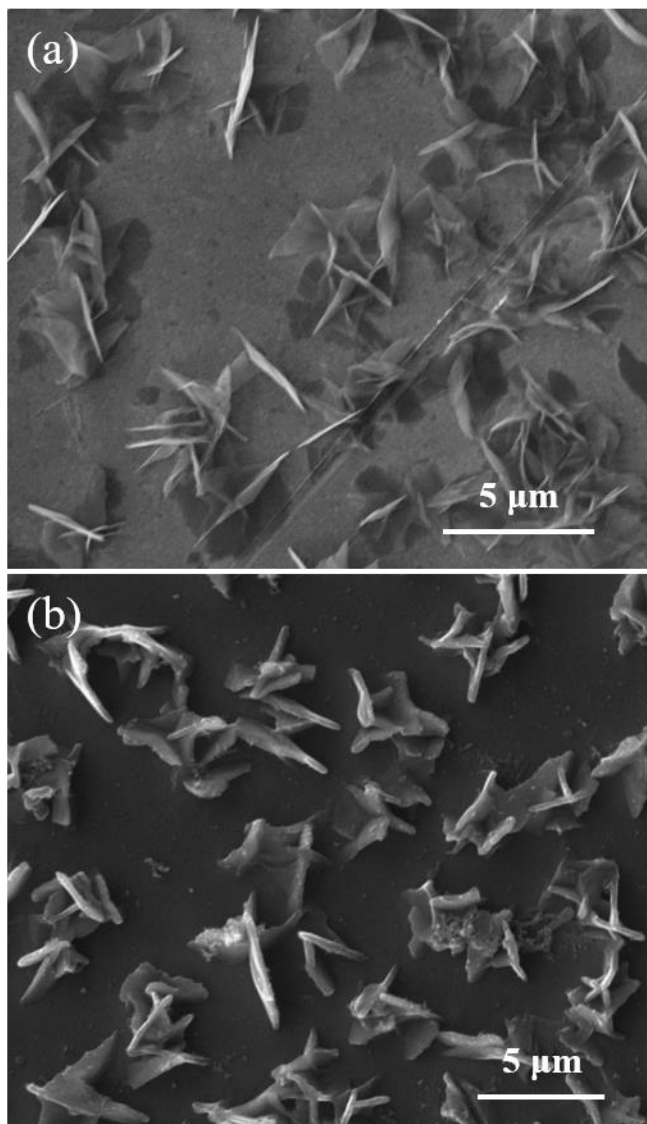


Figure 37. SEM images of the sample with 4 hours of Step A before and after Step B. (a) Oligomer clusters before Step B. (b) PANI film covered oligomer clusters after Step B.

5.3.3 Importance of Protonated Aniline

In the previous part, a reaction time of 1 hour was found to be optimal for Step A reaction before switching to low pH Step B reaction. However, pH can be tuned easily by simply adding acid in Step A reaction. Therefore, the Step B reaction seems to be redundant if the pH dropping is the

only reason that causes the forming of PANI. To investigate this, another set of experiment was conducted. Instead of two reactions, only Step A was used this time, and 6 mL was added directly into the Step A reaction after 1 hour (oligomers that could template the growth of PANI nanotubes were formed). After another 4 hours, the reaction was stopped and the sample was cleaned and dried. Figure 38 shows the SEM image of this sample. It is obvious that no nanotubes can be found. The most possible explanation for this result is that the aniline concentration was extremely low after 1 hour of Step A, which results in little aniline being protonated by the acid. This result not only confirms that the protonated aniline is the key for reaction mechanism transition in STFM, but also indicates the significance of the Step B reaction in forming the nanotubes.

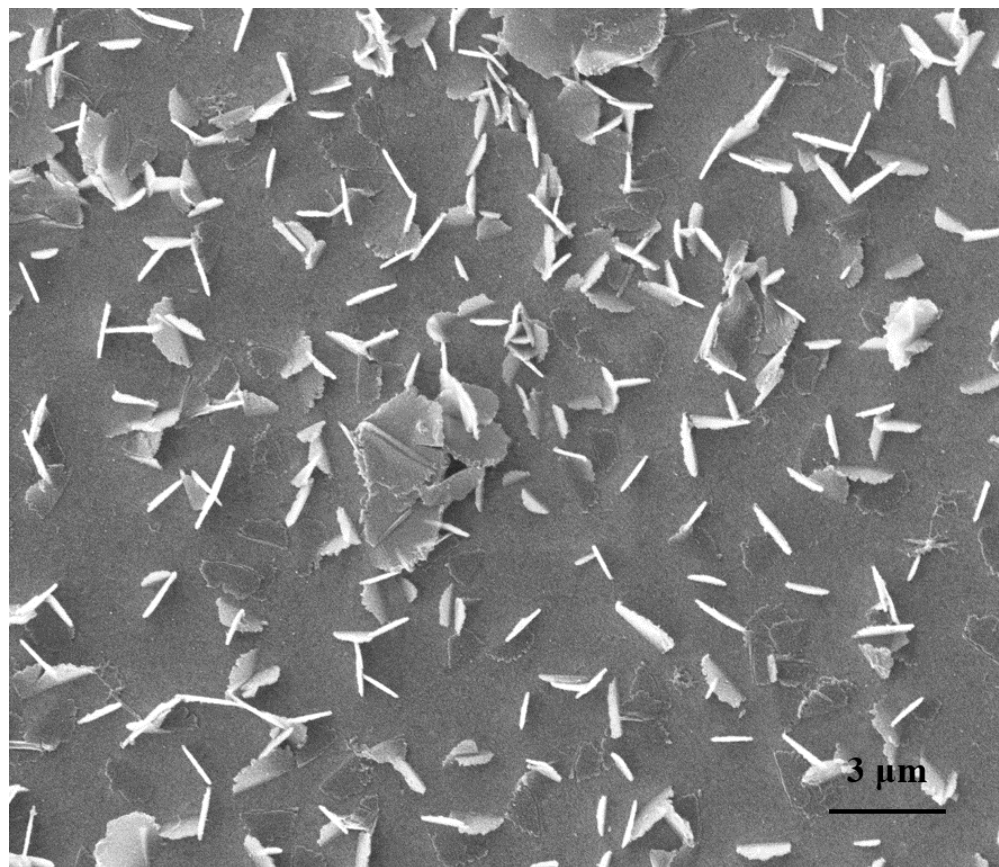


Figure 38. SEM image of the sample after 4 hours of Step A reaction with pH tuned after 1 hour.

5.3.4 Synthesis of the PANI Film/Nanotubes Hybrid Nanostructures on Substrates

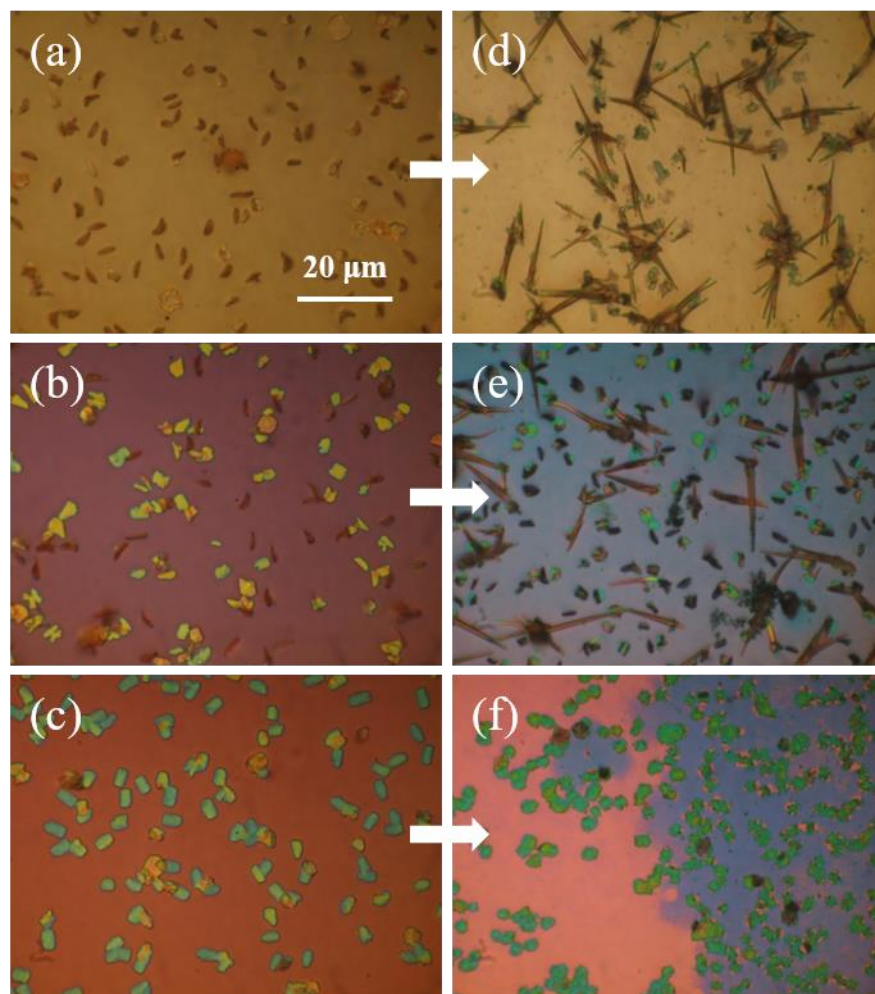


Figure 39. Optical images of PANI film/nanotubes hybrid on different of substrates. (a) PET after Step A, most oligomers grew vertically to the surface. (b) SiO₂ after Step A, half of oligomers were vertical while the other half were parallel to the surface. (c) HF-dipped SiO₂ after Step A, all oligomers were parallel to the surface. (d) PET after Step A and Step B, nanotubes were found. (e) SiO₂ after Step A and Step B, less density of nanotubes were found compared with it on PET. (f) HF-dipped after Step A and Step B, no nanotube was found.

With the aim of developing PANI film/nanotubes hybrid structure for FET device applications, commonly used substrates must be tested. However, it is noteworthy that different surface water

affinities may strongly affect the nucleation that occurs on the interface, thus determining the formation of the nanotubes. Therefore, in this work, three commonly used substrates with different water affinities were used. They are PET (hydrophobic), SiO₂ (hydrophilic) and HF-dipped SiO₂ (extremely hydrophilic due to the hydroxyl groups).¹⁴⁸

A combination of one hour Step A and four hours Step B reactions were used for hybrid synthesis. In order to have accurate optical images, transparent PET film was fixed on the holding wafer with the edges sealed so that no reaction would occur on the backside of the film, while the other two substrates were prepared as described in the synthesis method part. All three substrates were characterized by optical microscopy after each reaction. Figure 39a-c shows the substrates after only Step A reaction. Flake-like oligomers were observed on all three samples. The densities of the oligomers were similar which were much lower compared with it on gold substrate, and almost no three-dimensional oligomer was found. However, the oligomers appeared differently according to the substrates: on PET, all of the oligomers were “standing” vertically to the surface; on SiO₂, half of the oligomers were parallel to the surface with one side facing up; on HF-dipped SiO₂, all oligomers were parallel to the surface. Figure 39d-f shows the three substrates after Step B reaction in addition to Step A. We observed needle-like nanotubes on both PET and SiO₂ substrates that clearly came from the oligomers. On the contrary, no nanotube was observed on HF-dipped SiO₂ substrate. Instead, a thin PANI film grew directly on top of the oligomers which generated a distinct color difference between figure 39c and figure 39f. Similar PANI film covered oligomers can also be seen in figure 39e. These results likely suggest that the parallel-to-the-surface-grown oligomers that are attributed to the more hydrophilic substrate surface cannot act as templates for guiding the PANI nanotubes, while the vertically formed ones can. More future chemical studies need to be done to confirm this

hypothesis. Notably, the relatively low density of oligomers on PET and SiO₂ substrates created larger space for PANI film to grow on compared with gold substrate, which can also be seen between figure 39d and figure 39e as color difference. This indicates the successful formation of the PANI film/nanotubes hybrid.

5.3.5 PANI Film/Nanotubes Hybrid FET

In order to further verify the structure as well as the functionality of the PANI film/nanotubes hybrid, an FET device based upon the hybrid was developed on SiO₂ substrate using the combination of one hour Step A and four hours Step B reactions. Detailed description of device fabrication processes can be found in Chapter 2. An ordinary PANI film based FET device was also made and the film was synthesized together with the hybrid in Step B reaction. Figure 40a, b shows the optical microscope images of both hybrid (figure 40a) and bare film (figure 40b) FETs. Clearly, despite being covered uniformly with nanotubes, the hybrid presents the same color as the film, which not only confirms the existence of PANI film in the hybrid structure, but also suggests that they have similar thickness and oxidation state. Further surface topological results measured by atomic force microscope (AFM) (Solver Next AFM) on both FETs are shown in figure 40c-e. The nanotubes that grew along the surface have an average diameter around 300 ~ 400 nm. Due to some overlapping, the highest point detected is 627 nm from the film surface. This value is within the nanometer scale, which implies that the hybrid as a whole is still technically a two-dimensional thin film structure. In addition, high magnification topological results of the film area on hybrid (figure 40e) and bare film (figure 40d) reveal that they have the same nanogranular surface. Therefore, we confirmed that, structure-wise, the hybrid in this study is a two-dimensional thin film structure that consists of ordinary PANI film and PANI nanotubes.

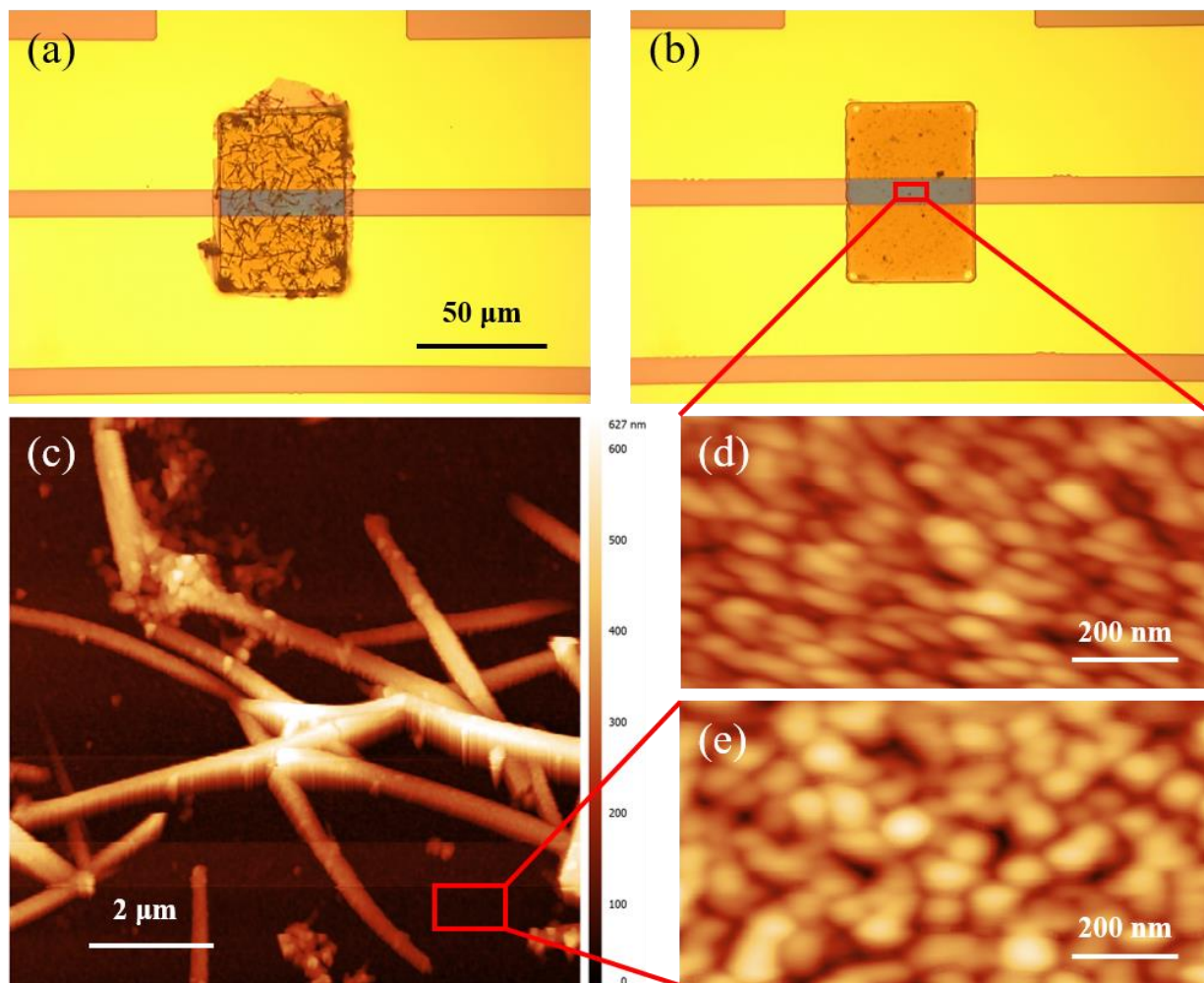


Figure 40. Optical and AFM images of PANI film/nanotubes hybrid FET and bare film FET. (a) Hybrid FET. (b) Bare film FET. (c) Surface topography of the hybrid. (d) High magnification of bare film surface measured by AFM. (e) High magnification of the dark area in (c).

5.3.6 Quantitatively Evaluating SA/V Ratio of the Hybrid Nanostructure

Surface-to-volume (SA/V) ratio is one of the most useful characteristics that can determine the functionality of micro or nano structures. With a fixed volume, the higher the SA/V is, the larger surface area a structure can offer. A larger surface area allows more sites for chemical or biological reactions. In this work, the proposed PANI film/nanotubes hybrid

structure is believed to possess larger surface area and a higher SA/V ratio than PANI bare film. The detailed calculation is provided below.

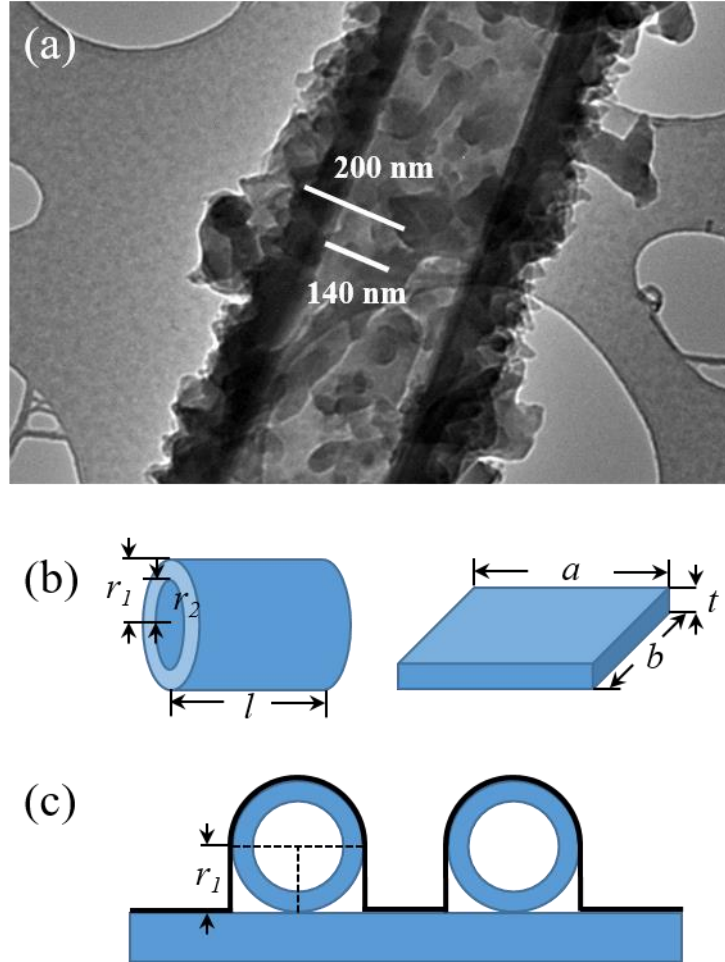


Figure 41. (a) TEM picture of a PANI nanotube. (b) Simplified structure of nanotubes and thin film. (c) Cross section view of the hybrid structure.

To calculate how much the surface area and SA/V ratio are increased, a simplified mathematic model needs to be created given with several presumptions: first, assume the nanotubes are uniformly constructed and are the same size, and that the distribution of the nanotubes on the hybrid structure is homogeneous; second, ignore the overlapping of the nanotubes and the surface roughness of PANI on both film and nanotubes; third, ignore the side

face area when calculating the total surface area. Figure 41a shows a TEM image of a nanotube. The inner and outer radii of the tube were measured around 140 nm and 200 nm, respectively. Figure 41b illustrates the ideal structures of both nanotube and bare film. r_1 and r_2 represent the outer and inner radii of the nanotube and l is the average length of the nanotubes; a and b represent the length and width of the film, with t as the thickness of the film, which is measured as 100 nm. With these information, we can roughly calculate the SA/V of a nanotube and a piece of film:

$$\text{Nanotube: } \frac{2\pi r_1 l}{(\pi r_1^2 - \pi r_2^2)l} = \frac{2r_1}{(r_1 + r_2)(r_1 - r_2)} = \frac{1}{51} \text{ nm}^{-1}$$

$$\text{Film: } \frac{ab}{abt} = \frac{1}{t} = \frac{1}{100} \text{ nm}^{-1}$$

The results show that the SA/V ratio of a nanotube is approximately twice the SA/V ratio of a thin film. It is noteworthy that the real SA/V ratios of nanotubes and film should be much higher than these simplified calculation values. This is due to the natural rough surface of PANI. This rough surface was ignored since it contributes similarly to the SA/V ratios for both bare film and nanotubes.

The next step of the calculation is to estimate the density of the nanotubes on PANI film surfaces. By analyzing the AFM result from figure 40c, it was observed that the surface area is increased by 25.4% ($25.4 \mu\text{m}^2$) compared with a same size ($10 \mu\text{m} \times 10 \mu\text{m}$) bare film. However, the surface area measured by AFM is not accurate enough due to the undercut area created by the nanotubes. Instead, the black line on the cross section view of the hybrid structure (figure 41c) is the actual surface measured by AFM. Therefore, we can estimate the actual increase of the surface area caused by nanotubes and the amount of the nanotubes within a $10 \mu\text{m} \times 10 \mu\text{m}$ size

window. Assume n is the total numbers of the nanotubes and the average length of these nanotubes is l . We have:

$$25.4 \mu m^2 = n(\pi r_1 + 2r_1 - 2r_1)l$$

$$nl = 40.4 \mu m$$

nl here represents the amount (total length) the nanotubes. The actual surface area increase is then:

$$S_{increase} = nl2\pi r_1 = 50.7 \mu m^2$$

Thus, the surface area increase from bare film to hybrid structure is about 50.7%. The total volume of the hybrid structure in figure 40c is:

$$V_{hybrid} = 10 \mu m \times 10 \mu m \times 100 nm + nl(\pi r_1^2 - \pi r_2^2) = 12.6 \mu m^3$$

The S/A ratio of the hybrid structure is:

$$S/V_{hybrid} = \frac{100 \mu m^2 + 50.7 \mu m^2}{12.6 \mu m^3} = 12.0 \mu m^{-1} = 0.012 nm^{-1}$$

Therefore, the SA/V ratio increase from bare film to hybrid structure is about 20%.

5.3.7 FET Characterizations

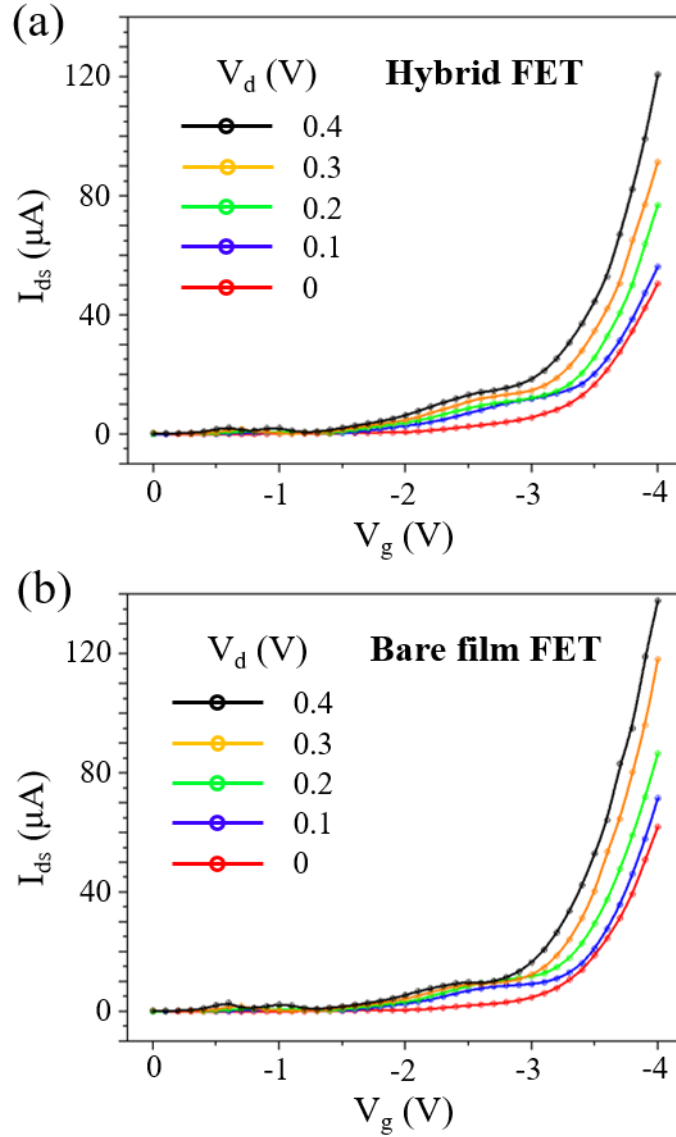


Figure 42. FET characterization of the hybrid FET (a) and bare film FET (b). The I_d - V_g characteristic was obtained by sweeping V_g from 0 to -4 V while keeping V_d staying at different potential level from 0 to 0.4 V.

Electrical characterization of both FETs was performed using a typical electrolyte-gate configuration.^{149,150} As shown in figure 40a, b, the rectangular patterns have a size of 50 μm by

100 μm with a thickness around 100 nm. They are located across the drain and source electrodes with a 10 μm gap in between, while the gate electrode is located near the source. Phosphate-buffered saline (PBS) solution (0.1X) was dropped onto the FETs and the drain current (I_d) versus gate voltage (V_g) characteristics as the function of different drain voltages (V_d) were obtained by a probe station (Signatone s-1160) shown in figure 42. During the measurement, V_g was constantly decreased from 0 to -4 V while V_d was fixed at different values ranging from 0 to 0.4 V. Notably, the two FETs have nearly identical characteristics: I_{ds} increased upon decreasing of V_g due to PANI's p-type nature; The threshold voltage was around -1.5 V after which I_{ds} started to rise exponentially; as V_g became more negative than -3.5 V, I_{ds} became linear. These results indicate that the hybrid behaves the same as PANI film formed in the same conditions in terms of surface charge transportation.

One promising application for PANI film/nanotubes hybrid is in the development of FET biosensors. A desired design of an FET biosensor requires a semiconductor FET transducer with the ability of being chemically functionalized with bio-receptors such as antibodies and enzymes. When the bio-receptors catch the targets, the charged target molecules start to gate the transducer, thus causing measurable current changes. PANI, as a p-type semiconductor, is capable of being directly functionalized with the presence of crosslinkers such as glutaraldehyde.¹⁵¹ Well controlled two-dimensional (2-D) PANI layer has been successfully demonstrated in biosensor applications. The high sensitivity is attributed to PANI's good p-type semiconducting property and high SA/V ratio. As an improvement, the hybrid structure developed in this work possesses approximately 50.7% increase of the surface area and 20% larger SA/V ratio given by the embedded nanotubes, which offers more surface sites for bio-receptors/targets complexes. Undoubtedly, with such superiority, PANI film/nanotubes hybrid can be the next generation

conductive polymer based two-dimensional thin film towards the design of facile and low cost point-of-care biosensors.

5.4 CONCLUSIONS

In conclusion, we developed a facile method for PANI film/nanotubes hybrid synthesis on substrate by splitting the STFM into two reactions: an oligomer templates synthesis reaction (Step A) and a PANI synthesis reaction (Step B). This template free method requires no organic participant other than aniline as well as less concentration of the reagents. The successful formation of the PANI nanotubes was confirmed by both SEM and TEM, and oligomers that formed in Step A were proved to serve as templates. The reaction time in Step A reaction was then optimized and PANI film/nanotubes hybrid was successfully synthesized on commonly used substrates such as SiO₂ and PET. By analyzing the microscope images, a hypothesis was proposed: the fully evolved three-dimensional oligomer clusters generated in nonacidic media and parallel-grown flake-like oligomers due to the hydrophilic substrate cannot act as templates for PANI nanotubes to grow on, which requires further in-depth study. Finally, an FET device was developed based on PANI film/nanotubes hybrid. FET characterization and AFM scanning not only verified the structure of the hybrid, but also revealed that the hybrid exhibits excellent p-type semiconductor property similar to the ordinary PANI film while at the same time possesses 50.7% larger surface area. This superiority promises the hybrid a great potential in future sensor researches and makes it an ideal substitute of PANI film in thin film related applications.

6.0 SUMMARY

In summary, the achievements of this work are presented as follow:

1. Microfluidics integrated 2-D PANI layers based biosensors were developed on SiO₂ substrates. The chemical synthesis of PANI was optimized to achieve suitable conductivity and well-controlled rough surface. The developed biosensors have good specificity and a lowest detection limit of 100 pg/mL with a response time less than 1 min.
2. Au electrodes and PANI layers were successfully patterned and optimized on PET substrates using a low temperature bilayer lift-off method combined with a sandwich-like baking process to overcome the PET's low thermal stability. With the help of this method, complex microscale structures can be easily built on PET or other flexible substrate using conventional CMOS compatible microfabrication techniques.
3. A facile method of high temperature imidizing polyamic acid in N₂ environment was demonstrated to achieve polyimide film with desired thickness. The polyimide film not only features good mechanical strength and flexibility, but also shows the capability to stay on a wafer during device fabrication processes due to the plasma pre-treatment, which vastly lowers the fabrication difficulty and improves yields. A debonding process can be easily done in water, and the wafer can be reused.
4. Microfluidics integrated 2-D PANI layers based biosensors were developed on PET and polyimide substrates. Both the PET and PI devices exhibit excellent sensitivity in the

detections of BNP biomarkers with a detection limit as low as 100 pg/mL. The conductivity changes of PANI layers upon stretching (substrate bending) was studied, which is not significant compared with the changes during detections. Device reproducibility was also investigated using 15 different devices.

5. A facile method of using two steps of reactions to synthesize 2-D PANI film/nanotubes hybrid structures were developed. The hybrid structures features extremely large SA/V ratio due to the embedded nanotubes, and similar FET characteristics to PANI bare film, which make the hybrid structures ideal substitutes for PANI bare film in FET biosensor designs.
6. The role of aniline oligomers as templates for guiding the growth of PANI nanotubes was studied. A hypothesis was proposed: the fully evolved three-dimensional oligomer clusters generated in nonacidic media and parallel-grown flake-like oligomers due to the hydrophilic substrate cannot act as templates for PANI nanotubes to grow on. Further in-depth study is needed to gain fully understanding.

6.1 LIST OF PUBLICATIONS

1. **Liu, P.**, Zhu, Y., Lee, S. H., Yun, M. (2017). Facile and template-free method towards chemical synthesis of two-dimensional polyaniline hybrid structures. *J. Polym. Sci. A Polym. Chem.*, submitted.
2. **Liu, P.**, Zhu, Y., Lee, S. H., & Yun, M. (2016). Two-dimensional polyaniline nanostructure to the development of microfluidic integrated flexible biosensors for biomarker detection. *Biomedical microdevices*, 18(6), 113.

3. **Liu, P.**, Huang, J., Sanchez, D. V., Schwartzman, D., Lee, S. H., & Yun, M. (2016). High yield two-dimensional (2-D) polyaniline layer and its application in detection of B-type natriuretic peptide in human serum. *Sensors and Actuators B: Chemical*, 230, 184-190.

7.0 FUTURE WORK

In this thesis, two major approaches to improve the functions of PANI based FET biosensors have been presented: one is to upgrade the substrate from conventional nonflexible SiO_2 to flexible substrates such as PET and PI; the other is to develop PANI film/nanotubes hybrid nanostructures to replace PANI bare films. Though the flexible biosensors show excellent sensing performances, more future works still need to be done to realize the implantation of PANI hybrid nanostructures in biosensor designs.

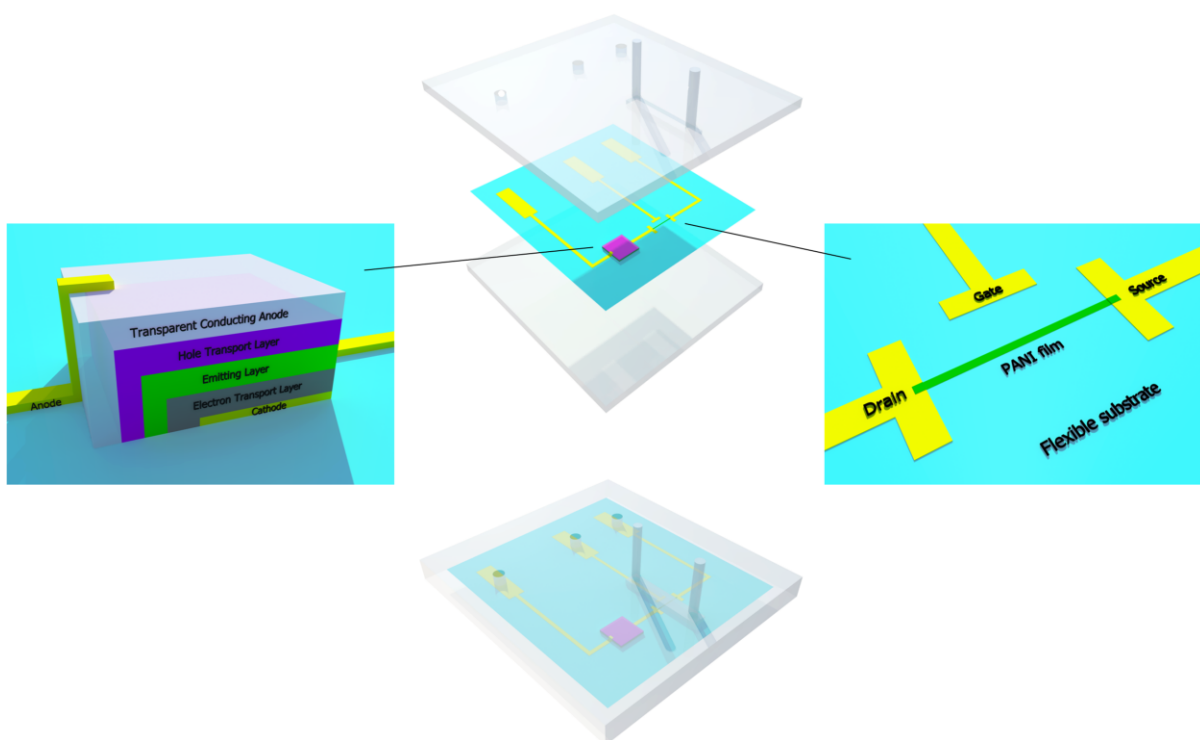


Figure 43. Preliminary design of microfluidic integrated PANI/QLED biosensor.

In addition to sensing materials and substrates, data acquiring is another part of the biosensor that we can improve. Current electrical transducers (bio-signals transduced into electrical signals) based biosensors usually require sophisticated instruments such as potentiostat or probstation to assure accuracy of the detections. This limits their applications in daily monitoring. One possible improvement is to apply current or voltage control LEDs to further transduce electrical signals into directly visible light emissions. Quantum dot LEDs (QLEDs), due to their low power consumption, low-cost manufacture, ultrathin and transparent features, can be an excellent candidate for this project. Figure 7.1 illustrates the preliminary design. During detection, the conductivity of PANI film will increase upon antibodies-antigens interactions. With proper designs, QLEDs can show on/off responses to abnormal/normal samples, which is much easier.

BIBLIOGRAPHY

- [1]. Kato, Y., Iba, S., Teramoto, R., Sekitani, T., Someya, T., Kawaguchi, H., & Sakurai, T. (2004). High mobility of pentacene field-effect transistors with polyimide gate dielectric layers. *Applied physics letters*, 84(19), 3789-3791.
- [2]. Sekitani, T., Kato, Y., Iba, S., Shinaoka, H., Someya, T., Sakurai, T., & Takagi, S. (2005). Bending experiment on pentacene field-effect transistors on plastic films. *Applied Physics Letters*, 86(7), 73511-74100.
- [3]. Klauk, H., Zschieschang, U., Pflaum, J., & Halik, M. (2007). Ultralow-power organic complementary circuits. *Nature*, 445(7129), 745-748.
- [4]. Lacour, S. P., Tsay, C., & Wagner, S. (2004). An elastically stretchable TFT circuit. *Electron Device Letters, IEEE*, 25(12), 792-794.
- [5]. Park, S. K., Mourey, D., Subramanian, S., Anthony, J. E., & Jackson, T. N. (2008). Polymeric substrate spin-cast diF-TESADT OTFT circuits. *Electron Device Letters, IEEE*, 29(9), 1004-1006.
- [6]. Jin, D. U., Lee, J. S., Kim, T. W., An, S. G., Straykhilev, D., Pyo, Y. S. & Chung, H. K. (2009, June). 65.2: Distinguished Paper: World-Largest (6.5”) Flexible Full Color Top Emission AMOLED Display on Plastic Film and Its Bending Properties. In *SID Symposium Digest of Technical Papers* (Vol. 40, No. 1, pp. 983-985). Blackwell Publishing Ltd.
- [7]. Sakurai, R., Ohno, S., Kita, S. I., Masuda, Y., & Hattori, R. (2006, June). 68.2: Color and Flexible Electronic Paper Display using QR-LPD® Technology. In *SID Symposium Digest of Technical Papers* (Vol. 37, No. 1, pp. 1922-1925). Blackwell Publishing Ltd.
- [8]. Zhou, L., Wanga, A., Wu, S. C., Sun, J., Park, S., & Jackson, T. N. (2006). All-organic active matrix flexible display. *Applied Physics Letters*, 88(8), 3502.
- [9]. Pagliaro, M., Ciriminna, R., & Palmisano, G. (2008). Flexible solar cells. *ChemSusChem*, 1(11), 880-891.

- [10]. Axisa, F., Schmitt, P. M., Gehin, C., Delhomme, G., McAdams, E., & Dittmar, A. (2005). Flexible technologies and smart clothing for citizen medicine, home healthcare, and disease prevention. *Information Technology in Biomedicine, IEEE Transactions on*, 9(3), 325-336.
- [11]. Istepanian, R. S., Jovanov, E., & Zhang, Y. T. (2004). Guest editorial introduction to the special section on m-health: Beyond seamless mobility and global wireless health-care connectivity. *Information Technology in Biomedicine, IEEE Transactions on*, 8(4), 405-414.
- [12]. Lane, S. S., Kuppermann, B. D., Fine, I. H., Hamill, M. B., Gordon, J. F., Chuck, R. S., Hoffman, R. S., Packer, M. & Koch, D. D. (2004). A prospective multicenter clinical trial to evaluate the safety and effectiveness of the implantable miniature telescope. *American journal of ophthalmology*, 137(6), 993-1001.
- [13]. Turner, C. W., Gantz, B. J., Vidal, C., Behrens, A., & Henry, B. A. (2004). Speech recognition in noise for cochlear implant listeners: benefits of residual acoustic hearing. *The Journal of the Acoustical Society of America*, 115(4), 1729-1735.
- [14]. Homola, J. (2003). Present and future of surface plasmon resonance biosensors. *Analytical and bioanalytical chemistry*, 377(3), 528-539.
- [15]. Mulvaney, S. P. (2011). Biosensors: Magnets tackle kinetic questions. *Nature nanotechnology*, 6(5), 266-267.
- [16]. Anker, J. N., Hall, W. P., Lyandres, O., Shah, N. C., Zhao, J., & Van Duyne, R. P. (2008). Biosensing with plasmonic nanosensors. *Nature materials*, 7(6), 442-453.
- [17]. Endo, T., Kerman, K., Nagatani, N., Hiepa, H. M., Kim, D. K., Yonezawa, Y., Nakano, K. & Tamiya, E. (2006). Multiple label-free detection of antigen-antibody reaction using localized surface plasmon resonance-based core-shell structured nanoparticle layer nanochip. *Analytical chemistry*, 78(18), 6465-6475.
- [18]. Nie, S., & Emory, S. R. (1997). Probing single molecules and single nanoparticles by surface-enhanced Raman scattering. *Science*, 275(5303), 1102-1106.
- [19]. Qian, X. M., & Nie, S. M. (2008). Single-molecule and single-nanoparticle SERS: from fundamental mechanisms to biomedical applications. *Chemical Society Reviews*, 37(5), 912-920.
- [20]. Qian, X., Peng, X. H., Ansari, D. O., Yin-Goen, Q., Chen, G. Z., Shin, D. M., Yang, L., Young, A. N., Wang, M. D. & Nie, S. (2008). In vivo tumor targeting and spectroscopic detection with surface-enhanced Raman nanoparticle tags. *Nature biotechnology*, 26(1), 83-90.
- [21]. Yang, Y. T., Callegari, C., Feng, X. L., Ekinici, K. L., & Roukes, M. L. (2006). Zeptogram-scale nanomechanical mass sensing. *Nano letters*, 6(4), 583-586.

- [22]. Burg, T. P., Godin, M., Knudsen, S. M., Shen, W., Carlson, G., Foster, J. S., Babcock, K. & Manalis, S. R. (2007). Weighing of biomolecules, single cells and single nanoparticles in fluid. *Nature*, 446(7139), 1066-1069.
- [23]. Cheng, M. M. C., Cuda, G., Bunimovich, Y. L., Gaspari, M., Heath, J. R., Hill, H. D., Mirkin, C. A., Nijdam, A. J., Terracciano, R., Thundat, T. & Ferrari, M. (2006). Nanotechnologies for biomolecular detection and medical diagnostics. *Current opinion in chemical biology*, 10(1), 11-19.
- [24]. Kong, J., Franklin, N. R., Zhou, C., Chapline, M. G., Peng, S., Cho, K., & Dai, H. (2000). Nanotube molecular wires as chemical sensors. *Science*, 287(5453), 622-625.
- [25]. Elfström, N., Karlström, A. E., & Linnros, J. (2008). Silicon nanoribbons for electrical detection of biomolecules. *Nano letters*, 8(3), 945-949.
- [26]. Cui, Y., Wei, Q., Park, H., & Lieber, C. M. (2001). Nanowire nanosensors for highly sensitive and selective detection of biological and chemical species. *Science*, 293(5533), 1289-1292.
- [27]. Patolsky, F., Zheng, G., Hayden, O., Lakadamyali, M., Zhuang, X., & Lieber, C. M. (2004). Electrical detection of single viruses. *Proceedings of the National Academy of Sciences of the United States of America*, 101(39), 14017-14022.
- [28]. Zheng, G., Patolsky, F., Cui, Y., Wang, W. U., & Lieber, C. M. (2005). Multiplexed electrical detection of cancer markers with nanowire sensor arrays. *Nature biotechnology*, 23(10), 1294-1301.
- [29]. Star, A., Tu, E., Niemann, J., Gabriel, J. C. P., Joiner, C. S., & Valcke, C. (2006). Label-free detection of DNA hybridization using carbon nanotube network field-effect transistors. *Proceedings of the National Academy of Sciences of the United States of America*, 103(4), 921-926.
- [30]. Cai, D., Ren, L., Zhao, H., Xu, C., Zhang, L., Yu, Y., Wang, H., Lan, Y., Roberts, M. F., Chuang, J. H., Naughton, M. J., Ren, Z. & Chiles, T. C. (2010). A molecular-imprint nanosensor for ultrasensitive detection of proteins. *Nature nanotechnology*, 5(8), 597-601.
- [31]. Stern, E., Vacic, A., Rajan, N. K., Criscione, J. M., Park, J., Ilic, B. R., Mooney, D. J., Reed, M. A. & Fahmy, T. M. (2010). Label-free biomarker detection from whole blood. *Nature nanotechnology*, 5(2), 138-142.
- [32]. Bergveld, P. (1970). Development of an ion-sensitive solid-state device for neurophysiological measurements. *IEEE Transactions on Biomedical Engineering*, 1(BME-17), 70-71.
- [33]. Janata, J., & Moss, S. D. (1976). Chemically sensitive field-effect transistors. *Biomedical engineering*, 11(7), 241.

- [34]. Schöning, M. J., & Poghossian, A. (2002). Recent advances in biologically sensitive field-effect transistors (BioFETs). *Analyst*, 127(9), 1137-1151.
- [35]. Stern, E., Wagner, R., Sigworth, F. J., Breaker, R., Fahmy, T. M., & Reed, M. A. (2007). Importance of the Debye screening length on nanowire field effect transistor sensors. *Nano letters*, 7(11), 3405-3409.
- [36]. Gao, X. P., Zheng, G., & Lieber, C. M. (2009). Subthreshold regime has the optimal sensitivity for nanowire FET biosensors. *Nano letters*, 10(2), 547-552.
- [37]. Kudo, H., Sawada, T., Kazawa, E., Yoshida, H., Iwasaki, Y., & Mitsubayashi, K. (2006). A flexible and wearable glucose sensor based on functional polymers with Soft-MEMS techniques. *Biosensors and Bioelectronics*, 22(4), 558-562.
- [38]. Iguchi, S., Kudo, H., Saito, T., Ogawa, M., Saito, H., Otsuka, K., Funakubo, A. & Mitsubayashi, K. (2007). A flexible and wearable biosensor for tear glucose measurement. *Biomedical microdevices*, 9(4), 603-609.
- [39]. Park, S. J., Kwon, O. S., Lee, S. H., Song, H. S., Park, T. H., & Jang, J. (2012). Ultrasensitive flexible graphene based field-effect transistor (FET)-type bioelectronic nose. *Nano letters*, 12(10), 5082-5090.
- [40]. Xu, S., Zhang, Y., Jia, L., Mathewson, K. E., Jang, K. I., Kim, J., Fu, H., Huang, X., Chava, P., Wang, R., Bhole, S., Wang, L., Na, Y. J., Guan, Y., Flavin, M., Han, Z., Huang, Y. & Rogers, J. A. (2014). Soft microfluidic assemblies of sensors, circuits, and radios for the skin. *Science*, 344(6179), 70-74.
- [41]. Rex, W. J., & Tennant, D. J. (1949). *U.S. Patent No. 2,465,319*. Washington, DC: U.S. Patent and Trademark Office.
- [42]. Winther-Jensen, B., & Krebs, F. C. (2006). High-conductivity large-area semi-transparent electrodes for polymer photovoltaics by silk screen printing and vapour-phase deposition. *Solar Energy Materials and Solar Cells*, 90(2), 123-132.
- [43]. Gomez De Arco, L., Zhang, Y., Schlenker, C. W., Ryu, K., Thompson, M. E., & Zhou, C. (2010). Continuous, highly flexible, and transparent graphene films by chemical vapor deposition for organic photovoltaics. *ACS nano*, 4(5), 2865-2873.
- [44]. MacDonald, W. A. (2004). Engineered films for display technologies. *Journal of Materials Chemistry*, 14(1), 4-10.
- [45]. Ju, S., Facchetti, A., Xuan, Y., Liu, J., Ishikawa, F., Ye, P., Zhou, C., Marks, T. J. & Janes, D. B. (2007). Fabrication of fully transparent nanowire transistors for transparent and flexible electronics. *Nature nanotechnology*, 2(6), 378-384.
- [46]. Nomura, K., Ohta, H., Takagi, A., Kamiya, T., Hirano, M., & Hosono, H. (2004). Room-temperature fabrication of transparent flexible thin-film transistors using amorphous oxide semiconductors. *Nature*, 432(7016), 488-492.

- [47]. Wong, W. S., & Salleo, A. (Eds.). (2009). *Flexible electronics: materials and applications* (Vol. 11). Springer Science & Business Media.
- [48]. Zhang, B., & Cui, T. (2011). An ultrasensitive and low-cost graphene sensor based on layer-by-layer nano self-assembly. *Applied Physics Letters*, 98(7), 073116.
- [49]. Ohya, H., Kudryavsev, V. V., & Semenova, S. I. (1997). *Polyimide membranes: applications, fabrications and properties*. CRC Press.
- [50]. Lim, J. W., Cho, D. Y., Eun, K., Choa, S. H., Na, S. I., Kim, J., & Kim, H. K. (2012). Mechanical integrity of flexible Ag nanowire network electrodes coated on colorless PI substrates for flexible organic solar cells. *Solar Energy Materials and Solar Cells*, 105, 69-76.
- [51]. Xia, Y., & Whitesides, G. M. (1998). Soft lithography. *Annual review of materials science*, 28(1), 153-184.
- [52]. Kim, D. H., & Rogers, J. A. (2008). Stretchable electronics: materials strategies and devices. *Advanced Materials*, 20(24), 4887-4892.
- [53]. Larmagnac, A., Eggenberger, S., Janossy, H., & Vörös, J. (2014). Stretchable electronics based on Ag-PDMS composites. *Scientific reports*, 4.
- [54]. Plichta, A., Weber, A., & Habeck, A. (2003, January). Ultra thin flexible glass substrates. In *MRS Proceedings* (Vol. 769, pp. H9-1). Cambridge University Press.
- [55]. Kang, M. G., Park, N. G., Ryu, K. S., Chang, S. H., & Kim, K. J. (2006). A 4.2% efficient flexible dye-sensitized TiO₂ solar cells using stainless steel substrate. *Solar Energy Materials and Solar Cells*, 90(5), 574-581.
- [56]. Shah, A., Torres, P., Tscharnner, R., Wyrsh, N., & Keppner, H. (1999). Photovoltaic technology: the case for thin-film solar cells. *Science*, 285(5428), 692-698.
- [57]. Lee, I., Luo, X., Huang, J., Cui, X. T., & Yun, M. (2012). Detection of cardiac biomarkers using single polyaniline nanowire-based conductometric biosensors. *Biosensors*, 2(2), 205-220.
- [58]. Inzelt, G. (2012). *Conducting polymers: a new era in electrochemistry*. Springer Science & Business Media.
- [59]. Chiang, C. K., Fincher Jr, C. R., Park, Y. W., Heeger, A. J., Shirakawa, H., Louis, E. J., Gau, S. C. & MacDiarmid, A. G. (1977). Electrical conductivity in doped polyacetylene. *Physical Review Letters*, 39(17), 1098.
- [60]. Gerard, M., Chaubey, A., & Malhotra, B. D. (2002). Application of conducting polymers to biosensors. *Biosensors and Bioelectronics*, 17(5), 345-359.

- [61]. Ekanayake, E. M., Preethichandra, D. M., & Kaneto, K. (2007). Polypyrrole nanotube array sensor for enhanced adsorption of glucose oxidase in glucose biosensors. *Biosensors and Bioelectronics*, 23(1), 107-113.
- [62]. Shimano, J. Y., & MacDiarmid, A. G. (2001). Polyaniline, a dynamic block copolymer: key to attaining its intrinsic conductivity. *Synthetic Metals*, 123(2), 251-262.
- [63]. Dhand, C., Das, M., Datta, M., & Malhotra, B. D. (2011). Recent advances in polyaniline based biosensors. *Biosensors and Bioelectronics*, 26(6), 2811-2821.
- [64]. De Albuquerque, J. E., Mattoso, L. H. C., Faria, R. M., Masters, J. G., & MacDiarmid, A. G. (2004). Study of the interconversion of polyaniline oxidation states by optical absorption spectroscopy. *Synthetic Metals*, 146(1), 1-10.
- [65]. Bhadra, S., Chattopadhyay, S., Singha, N. K., & Khastgir, D. (2008). Improvement of conductivity of electrochemically synthesized polyaniline. *Journal of applied polymer science*, 108(1), 57-64.
- [66]. Stafström, S., Bredas, J. L., Epstein, A. J., Woo, H. S., Tanner, D. B., Huang, W. S., & MacDiarmid, A. G. (1987). Polaron lattice in highly conducting polyaniline: theoretical and optical studies. *Physical Review Letters*, 59(13), 1464.
- [67]. Skotheim, T. A. (Ed.). (1997). *Handbook of conducting polymers*. CRC press.
- [68]. Wallace, G. G., Teasdale, P. R., Spinks, G. M., & Kane-Maguire, L. A. (2008). *Conductive electroactive polymers: intelligent polymer systems*. CRC press.
- [69]. Zotti, G., Cattarin, S., & Comisso, N. (1988). Cyclic potential sweep electropolymerization of aniline: The role of anions in the polymerization mechanism. *Journal of electroanalytical chemistry and interfacial electrochemistry*, 239(1), 387-396.
- [70]. Maser, W. K., Sainz, R., Martínez, M. T., & Benito, A. M. (2008). Electroactive polymer-carbon nanotube composites: smart organic materials for optoelectronic applications. *Contributions to science*, 4(2), 187-192.
- [71]. Dong, B., He, B. L., Xu, C. L., & Li, H. L. (2007). Preparation and electrochemical characterization of polyaniline/multi-walled carbon nanotubes composites for supercapacitor. *Materials Science and Engineering: B*, 143(1), 7-13.
- [72]. Xia, Y., Yang, P., Sun, Y., Wu, Y., Mayers, B., Gates, B., Yin, Y., Kim, F. & Yan, H. (2003). One-dimensional nanostructures: synthesis, characterization, and applications. *Advanced materials*, 15(5), 353-389.
- [73]. Yin, Y., & Alivisatos, A. P. (2005). Colloidal nanocrystal synthesis and the organic-inorganic interface. *Nature*, 437(7059), 664-670.

- [74]. Roduner, E. (2006). Size matters: why nanomaterials are different. *Chemical Society Reviews*, 35(7), 583-592.
- [75]. Huang, W. S., Humphrey, B. D., & MacDiarmid, A. G. (1986). Polyaniline, a novel conducting polymer. Morphology and chemistry of its oxidation and reduction in aqueous electrolytes. *Journal of the Chemical Society, Faraday Transactions 1: Physical Chemistry in Condensed Phases*, 82(8), 2385-2400.
- [76]. Weng, S., Lin, Z., Chen, L., & Zhou, J. (2010). Electrochemical synthesis and optical properties of helical polyaniline nanofibers. *Electrochimica Acta*, 55(8), 2727-2733.
- [77]. Anderson, R. E., Ostrowski, A. D., Gran, D. E., Fowler, J. D., Hopkins, A. R., & Villahermosa, R. M. (2008). Diameter-controlled synthesis of polyaniline nanofibers. *Polymer bulletin*, 61(5), 563-568.
- [78]. Wan, M. (2008). A template-free method towards conducting polymer nanostructures. *Advanced Materials*, 20(15), 2926-2932.
- [79]. Li, J., Jia, Q., Zhu, J., & Zheng, M. (2008). Interfacial polymerization of morphologically modified polyaniline: from hollow microspheres to nanowires. *Polymer International*, 57(2), 337-341.
- [80]. Li, G., & Zhang, Z. (2004). Synthesis of dendritic polyaniline nanofibers in a surfactant gel. *Macromolecules*, 37(8), 2683-2685.
- [81]. Liu, P., & Zhang, L. (2009). Hollow nanostructured polyaniline: Preparation, properties and applications. *Critical Reviews in Solid State and Materials Sciences*, 34(1-2), 75-87.
- [82]. Park, H. W., Kim, T., Huh, J., Kang, M., Lee, J. E., & Yoon, H. (2012). Anisotropic growth control of polyaniline nanostructures and their morphology-dependent electrochemical characteristics. *ACS nano*, 6(9), 7624-7633.
- [83]. Fan, H., Wang, H., Yu, X., Zhao, N., Zhang, X., & Xu, J. (2012). Synthesis and electrochemical properties of various dimensional polyaniline micro/nanostructures: Microdisks, nanospheres and nanofibers. *Materials Letters*, 71, 70-73.
- [84]. Tran, H. D., Li, D., & Kaner, R. B. (2009). One-Dimensional Conducting Polymer Nanostructures: Bulk Synthesis and Applications. *Advanced Materials*, 21(14-15), 1487-1499.
- [85]. Martin, C. R. (1995). Template synthesis of electronically conductive polymer nanostructures. *Accounts of chemical research*, 28(2), 61-68.
- [86]. Zhang, L., Long, Y., Chen, Z., & Wan, M. (2004). The Effect of Hydrogen Bonding on Self-Assembled Polyaniline Nanostructures. *Advanced Functional Materials*, 14(7), 693-698.

- [87]. Stejskal, J., Sapurina, I., Trchová, M., & Konyushenko, E. N. (2008). Oxidation of aniline: Polyaniline granules, nanotubes, and oligoaniline microspheres. *Macromolecules*, 41(10), 3530-3536.
- [88]. Luo, X., Vidal, G. D., Killard, A. J., Morrin, A., & Smyth, M. R. (2007). Nanocauliflowers: a nanostructured polyaniline-modified screen-printed electrode with a self-assembled polystyrene template and its application in an amperometric enzyme biosensor. *Electroanalysis*, 19(7-8), 876-883.
- [89]. Zhu, Y., Li, J., Wan, M., Jiang, L., & Wei, Y. (2007). A New Route for the Preparation of Brain-Like Nanostructured Polyaniline. *Macromolecular rapid communications*, 28(12), 1339-1344.
- [90]. Flickinger, M. C., & Drew, S. W. (1999). *Encyclopedia of bioprocess technology*. John Wiley.
- [91]. Jegannathan, K. R., Abang, S., Poncelet, D., Chan, E. S., & Ravindra, P. (2008). Production of biodiesel using immobilized lipase—a critical review. *Critical Reviews in Biotechnology*, 28(4), 253-264.
- [92]. Kumar, N., Bhardwaj, L. M., Sharma, A. L., & Singh, D. P. (2009). *Studies of glucose oxidase immobilized carbon nanotube-polyaniline composites* (Doctoral dissertation).
- [93]. Guisan, J. M. (2006). Immobilization of enzymes as the 21st Century begins: an already solved problem or still an exciting challenge?. *Immobilization of enzymes and cells*, 1-13.
- [94]. Bucur, B., Danet, A. F., & Marty, J. L. (2004). Versatile method of cholinesterase immobilisation via affinity bonds using Concanavalin A applied to the construction of a screen-printed biosensor. *Biosensors and Bioelectronics*, 20(2), 217-225.
- [95]. Subramanian, A., Kennel, S. J., Oden, P. I., Jacobson, K. B., Woodward, J., & Doktycz, M. J. (1999). Comparison of techniques for enzyme immobilization on silicon supports. *Enzyme and Microbial Technology*, 24(1), 26-34.
- [96]. Chiang, C. J., Hsiau, L. T., & Lee, W. C. (1997). Immobilization of cell-associated enzymes by entrapment in polymethacrylamide beads. *Biotechnology techniques*, 11(2), 121-125.
- [97]. Klotzbach, T. L., Watt, M., Ansari, Y., & Minteer, S. D. (2008). Improving the microenvironment for enzyme immobilization at electrodes by hydrophobically modifying chitosan and Nafion® polymers. *Journal of Membrane Science*, 311(1), 81-88.
- [98]. Shen, Q., Yang, R., Hua, X., Ye, F., Zhang, W., & Zhao, W. (2011). Gelatin-templated biomimetic calcification for β -galactosidase immobilization. *Process Biochemistry*, 46(8), 1565-1571.
- [99]. Prabhakar, N., Arora, K., Singh, H., & Malhotra, B. D. (2008). Polyaniline based nucleic acid sensor. *The Journal of Physical Chemistry B*, 112(15), 4808-4816.

- [100]. Lim, S. Y., Chung, W. Y., Lee, H. K., Park, M. S., & Park, H. G. (2008). Direct and nondestructive verification of PNA immobilization using click chemistry. *Biochemical and biophysical research communications*, 376(4), 633-636.
- [101]. Vetter, D., Tate, E. M., & Gallop, M. A. (1995). Strategies for the synthesis and screening of glycoconjugates. 2. Covalent immobilization for flow cytometry. *Bioconjugate chemistry*, 6(3), 319-322.
- [102]. Anisfeld, S. T., & Lansbury Jr, P. T. (1990). A convergent approach to the chemical synthesis of asparagine-linked glycopeptides. *The Journal of Organic Chemistry*, 55(21), 5560-5562.
- [103]. Huang, J., Luo, X., Lee, I., Hu, Y., Cui, X. T., & Yun, M. (2011). Rapid real-time electrical detection of proteins using single conducting polymer nanowire-based microfluidic aptasensor. *Biosensors and Bioelectronics*, 30(1), 306-309.
- [104]. Lee, I., Luo, X., Cui, X. T., & Yun, M. (2011). Highly sensitive single polyaniline nanowire biosensor for the detection of immunoglobulin G and myoglobin. *Biosensors and Bioelectronics*, 26(7), 3297-3302.
- [105]. Yan, H., Yang, Y., Fu, Z., Yang, B., Xia, L., Fu, S., & Li, F. (2005). Fabrication of 2D and 3D ordered porous ZnO films using 3D opal templates by electrodeposition. *Electrochemistry Communications*, 7(11), 1117-1121.
- [106]. Gunawidjaja, R., Jiang, C., Peleshanko, S., Ornatska, M., Singamaneni, S., & Tsukruk, V. V. (2006). Flexible and Robust 2D Arrays of Silver Nanowires Encapsulated within Freestanding Layer-by-Layer Films. *Advanced Functional Materials*, 16(15), 2024-2034.
- [107]. Yang, W., Ratinac, K. R., Ringer, S. P., Thordarson, P., Gooding, J. J., & Braet, F. (2010). Carbon nanomaterials in biosensors: should you use nanotubes or graphene?. *Angewandte Chemie International Edition*, 49(12), 2114-2138.
- [108]. Maisel, A. S., Krishnaswamy, P., Nowak, R. M., McCord, J., Hollander, J. E., Duc, P., Omland, T., Storrow, A. B., Abraham, W. T., Wu, A. H. B., Clopton, P., Steg, P. G., Westheim, A., Knudsen, C. W., Perez, A., Kazanegra, R. H., Herrmann, C., & McCullough, P. A. (2002). Rapid measurement of B-type natriuretic peptide in the emergency diagnosis of heart failure. *New England Journal of Medicine*, 347(3), 161-167.
- [109]. Sapurina, I., Riede, A., & Stejskal, J. (2001). In-situ polymerized polyaniline films: 3. Film formation. *Synthetic Metals*, 123(3), 503-507.
- [110]. Chiou, N. R., Lu, C., Guan, J., Lee, L. J., & Epstein, A. J. (2007). Growth and alignment of polyaniline nanofibres with superhydrophobic, superhydrophilic and other properties. *Nature nanotechnology*, 2(6), 354-357.
- [111]. Xu, J., Wang, K., Zu, S. Z., Han, B. H., & Wei, Z. (2010). Hierarchical nanocomposites of polyaniline nanowire arrays on graphene oxide sheets with synergistic effect for energy storage. *ACS nano*, 4(9), 5019-5026.

- [112]. Haeberle, S., & Zengerle, R. (2007). Microfluidic platforms for lab-on-a-chip applications. *Lab on a Chip*, 7(9), 1094-1110.
- [113]. Choi, S., Goryll, M., Sin, L. Y. M., Wong, P. K., & Chae, J. (2011). Microfluidic-based biosensors toward point-of-care detection of nucleic acids and proteins. *Microfluidics and Nanofluidics*, 10(2), 231-247.
- [114]. Aran, K., Fok, A., Sasso, L. A., Kamdar, N., Guan, Y., Sun, Q., Ündar, A. & Zahn, J. D. (2011). Microfiltration platform for continuous blood plasma protein extraction from whole blood during cardiac surgery. *Lab on a Chip*, 11(17), 2858-2868.
- [115]. Dimov, I. K., Basabe-Desmonts, L., Garcia-Cordero, J. L., Ross, B. M., Ricco, A. J., & Lee, L. P. (2011). Stand-alone self-powered integrated microfluidic blood analysis system (SIMBAS). *Lab on a Chip*, 11(5), 845-850.
- [116]. Haeberle, S., Brenner, T., Zengerle, R., & Duccré, J. (2006). Centrifugal extraction of plasma from whole blood on a rotating disk. *Lab on a Chip*, 6(6), 776-781.
- [117]. Yang, S., Ündar, A., & Zahn, J. D. (2006). A microfluidic device for continuous, real time blood plasma separation. *Lab on a Chip*, 6(7), 871-880.
- [118]. Stejskal, J., Sapurina, I., Prokeš, J., & Zemek, J. (1999). In-situ polymerized polyaniline films. *Synthetic Metals*, 105(3), 195-202.
- [119]. Gundry, R. L., & Van Eyk, J. E. (2007). Unraveling the complexity of circulating forms of brain natriuretic peptide.
- [120]. Jung, M., Kim, J., Noh, J., Lim, N., Lim, C., Lee, G., Kim, J., Kang, H., Jung, K., Lenonard, A. D., Tour, J. M., & Cho, G. (2010). All-printed and roll-to-roll-printable 13.56-MHz-operated 1-bit RF tag on plastic foils. *IEEE Transactions on Electron Devices*, 57(3), 571-580.
- [121]. Gelinck, G. H., Huitema, H. E. A., van Veenendaal, E., Cantatore, E., Schrijnemakers, L., van der Putten, Geuns, T. C. T., Beenhakkers, M., Giesbers, J. B., Huisman, B., Meijer, E. J., Benito, E. M., Touwslager, F. J., Marsman, A. W., van Rens, B. J. E., & de Leeuw, D. M. (2004). Flexible active-matrix displays and shift registers based on solution-processed organic transistors. *Nature materials*, 3(2), 106-110.
- [122]. Rogers, J. A., Bao, Z., Baldwin, K., Dodabalapur, A., Crone, B., Raju, V. R., Kuck, V., Katz, H., Amundson, K., Ewing, J., & Drzaic, P. (2001). Paper-like electronic displays: Large-area rubber-stamped plastic sheets of electronics and microencapsulated electrophoretic inks. *Proceedings of the National Academy of Sciences*, 98(9), 4835-4840.
- [123]. Lipomi, D. J., Tee, B. C. K., Vosgueritchian, M., & Bao, Z. (2011). Stretchable organic solar cells. *Advanced Materials*, 23(15), 1771-1775.
- [124]. Lipomi, D. J., & Bao, Z. (2011). Stretchable, elastic materials and devices for solar energy conversion. *Energy & Environmental Science*, 4(9), 3314-3328.

- [125]. Kwon, O. S., Park, S. J., Hong, J. Y., Han, A. R., Lee, J. S., Lee, J. S., Oh, J. H., & Jang, J. (2012). Flexible FET-type VEGF aptasensor based on nitrogen-doped graphene converted from conducting polymer. *ACS nano*, 6(2), 1486-1493.
- [126]. Janata, J., & Josowicz, M. (2003). Conducting polymers in electronic chemical sensors. *Nature materials*, 2(1), 19-24.
- [127]. Malinauskas, A. (2001). Chemical deposition of conducting polymers. *polymer*, 42(9), 3957-3972.
- [128]. Bandom, D. K., & Wilkes, G. L. (1994). Study of the multiple melting behaviour of the aromatic polyimide LaRC CPI-2. *Polymer*, 35(26), 5672-5677.
- [129]. Brink, M. H., Bandom, D. K., Wilkes, G. L., & McGrath, J. E. (1994). Synthesis and characterization of a novel '3F'-based fluorinated monomer for fluorine-containing polyimides. *Polymer*, 35(23), 5018-5023.
- [130]. Woodard, M. H., Rogers, M. E., Bandom, D. K., Wilkes, G. L., & McGrath, J. E. (1992). Synthetic investigations of high Tg fluorinated polyimides. *Polymer Preprints(USA)*, 33(2), 333-334.
- [131]. Chen, J., Ho, J. C., Chen, G., & Lee, C. C. (2012, June). 20.2: Invited Paper: Reliability Improvement of Flexible AMOLED Based on Auxiliary Functional Film Technology. In *SID Symposium Digest of Technical Papers* (Vol. 43, No. 1, pp. 264-267). Blackwell Publishing Ltd.
- [132]. Fischer, J. E., Zhu, Q., Tang, X., Scherr, E. M., MacDiarmid, A. G., & Cajipe, V. B. (1994). Polyaniline fibers, films, and powders: X-ray studies of crystallinity and stress-induced preferred orientation. *Macromolecules*, 27(18), 5094-5101.
- [133]. Abell, L., Adams, P. N., & Monkman, A. P. (1996). Electrical conductivity enhancement of predoped polyaniline by stretch orientation. *Polymer*, 37(26), 5927-5931.
- [134]. Piruska, A., Nikcevic, I., Lee, S. H., Ahn, C., Heineman, W. R., Limbach, P. A., & Seliskar, C. J. (2005). The autofluorescence of plastic materials and chips measured under laser irradiation. *Lab on a Chip*, 5(12), 1348-1354.
- [135]. Liu, P., Huang, J., Sanchez, D. V., Schwartzman, D., Lee, S. H., & Yun, M. (2016). High yield two-dimensional (2-D) polyaniline layer and its application in detection of B-type natriuretic peptide in human serum. *Sensors and Actuators B: Chemical*, 230, 184-190.
- [136]. Huang, J., Virji, S., Weiller, B. H., & Kaner, R. B. (2003). Polyaniline nanofibers: facile synthesis and chemical sensors. *Journal of the American Chemical Society*, 125(2), 314-315.
- [137]. Qiu, H., Wan, M., Matthews, B., & Dai, L. (2001). Conducting polyaniline nanotubes by template-free polymerization. *Macromolecules*, 34(4), 675-677.

- [138]. Stejskal, J., Sapurina, I., Trchová, M., Konyushenko, E. N., & Holler, P. (2006). The genesis of polyaniline nanotubes. *Polymer*, 47(25), 8253-8262.
- [139]. Venancio, E. C., Wang, P. C., & MacDiarmid, A. G. (2006). The azanes: A class of material incorporating nano/micro self-assembled hollow spheres obtained by aqueous oxidative polymerization of aniline. *Synthetic Metals*, 156(5), 357-369.
- [140]. Stejskal, J., Sapurina, I., & Trchová, M. (2010). Polyaniline nanostructures and the role of aniline oligomers in their formation. *Progress in Polymer Science*, 35(12), 1420-1481.
- [141]. Aleshin, A. N. (2006). Polymer nanofibers and nanotubes: Charge transport and device applications. *Advanced materials*, 18(1), 17-27.
- [142]. Parthasarathy, R. V., & Martin, C. R. (1994). Template-synthesized polyaniline microtubules. *Chemistry of Materials*, 6(10), 1627-1632.
- [143]. Zhang, X., & Manohar, S. K. (2004). Polyaniline nanofibers: chemical synthesis using surfactants. *Chemical communications*, (20), 2360-2361.
- [144]. Pillalamarri, S. K., Blum, F. D., Tokuhito, A. T., Story, J. G., & Bertino, M. F. (2005). Radiolytic synthesis of polyaniline nanofibers: a new templateless pathway. *Chemistry of materials*, 17(2), 227-229.
- [145]. Ding, H., Shen, J., Wan, M., & Chen, Z. (2008). Formation Mechanism of Polyaniline Nanotubes by a Simplified Template-Free Method. *Macromolecular Chemistry and Physics*, 209(8), 864-871.
- [146]. Trchová, M., Šeděnková, I., Konyushenko, E. N., Stejskal, J., Holler, P., & Ćirić-Marjanović, G. (2006). Evolution of polyaniline nanotubes: the oxidation of aniline in water. *The Journal of Physical Chemistry B*, 110(19), 9461-9468.
- [147]. Liu, P., Zhu, Y., Lee, S. H., & Yun, M. (2016). Two-dimensional polyaniline nanostructure to the development of microfluidic integrated flexible biosensors for biomarker detection. *Biomedical microdevices*, 18(6), 113.
- [148]. Kang, J. K., & Musgrave, C. B. (2002). The mechanism of HF/H₂O chemical etching of SiO₂. *The Journal of chemical physics*, 116(1), 275-280.
- [149]. Dhoot, A. S., Yuen, J. D., Heeney, M., McCulloch, I., Moses, D., & Heeger, A. J. (2006). Beyond the metal-insulator transition in polymer electrolyte gated polymer field-effect transistors. *Proceedings of the National Academy of Sciences*, 103(32), 11834-11837.
- [150]. Alam, M. M., Wang, J., Guo, Y., Lee, S. P., & Tseng, H. R. (2005). Electrolyte-gated transistors based on conducting polymer nanowire junction arrays. *The Journal of Physical Chemistry B*, 109(26), 12777-12784.

- [151]. Sai, V. V. R., Mahajan, S., Contractor, A. Q., & Mukherji, S. (2006). Immobilization of antibodies on polyaniline films and its application in a piezoelectric immunosensor. *Analytical chemistry*, 78(24), 8368-8373.